



Geostatistical estimates for intertidal shellfish monitoring in the northern North Island region, 2019–20

New Zealand Fisheries Assessment Report 2021/77

L. Tremblay-Boyer,
P. Neubauer,
K. Berkenbusch,
D. Damodaran

ISSN 1179-5352 (online)
ISBN 978-1-99-102602-6 (online)

December 2021



Requests for further copies should be directed to:

Publications Logistics Officer
Ministry for Primary Industries
PO Box 2526
WELLINGTON 6140

Email: brand@mpi.govt.nz
Telephone: 0800 00 83 33
Facsimile: 04-894 0300

This publication is also available on the Ministry for Primary Industries websites at:
<http://www.mpi.govt.nz/news-and-resources/publications>
<http://fs.fish.govt.nz> go to Document library/Research reports

© Crown Copyright - Fisheries New Zealand

TABLE OF CONTENTS

EXECUTIVE SUMMARY	1
1 INTRODUCTION	3
2 METHODS	4
2.1 Model-based estimators of abundance	5
2.1.1 Performance metrics	5
2.1.2 Mesh configurations	6
2.2 Sampling-based estimators of abundance	9
3 RESULTS	10
3.1 Sensitivity and optimisation of mesh configuration	10
3.2 Matérn covariance relationship	12
3.3 Temporal models based on multiple years	14
3.4 Comparison between the highest-ranked models and sampling-based estimator	18
3.5 Multiple models for distanced strata	18
4 DISCUSSION	20
5 ACKNOWLEDGMENTS	22
6 REFERENCES	22
APPENDIX A SINGLE-YEAR MODELS—MESH SCENARIOS	24
A.1 Bowentown Beach	24
A.2 Cockle Bay	26
A.3 Eastern Beach	28
A.4 Grahams Beach	30
A.5 Little Waihi Estuary	32
A.6 Pataua Estuary	34
A.7 Raglan Harbour	36
A.8 Tairua Harbour	38
A.9 Umupuia Beach	40
A.10 Waiotahe Estuary	42
A.11 Whangateau Harbour	44
A.12 Whitianga Harbour	46
APPENDIX B SPATIO-TEMPORAL MODELS	48
B.1 Bowentown Beach	48
B.2 Cockle Bay	49
B.3 Eastern Beach	50
B.4 Grahams Beach	51
B.5 Little Waihi Estuary	52
B.6 Pataua Estuary	53
B.7 Raglan Harbour	54
B.8 Tairua Harbour	55
B.9 Umupuia Beach	56
B.10 Waiotahe Estuary	57
B.11 Whangateau Harbour	58
B.12 Whitianga Harbour	59
APPENDIX C SPLIT MODELS BY SITE	60
C.1 Bowentown Beach	60

C.2	Raglan Harbour	61
C.3	Whangateau Harbour	64

EXECUTIVE SUMMARY

Tremblay-Boyer, L.¹; Neubauer, P.¹; Berkenbusch, K.¹; Damodaran, D.¹ (2021). Geostatistical estimates for the intertidal shellfish monitoring in the northern North Island region, 2019–20.

New Zealand Fisheries Assessment Report 2021/77. 66 p.

Fishery surveys are aimed at collecting information about target species, such as the population abundance, density, and size structure. The analyses of these data are dependent on the sampling design and type and amount of data collected, with the assessments generally focused on providing robust and reliable population estimates. For longer-term monitoring series, survey data also allow the assessment of population trends over time when the data collection methods have been consistent between surveys.

Across northern North Island, regular (usually annual) surveys of intertidal bivalves (cockle or littleneck clam, tuangi *Austrovenus stutchburyi* and pipi *Paphies australis*) were initiated in the early 1990s, prompted by concerns about the potential impact of recreational and customary fisheries. The surveys are commissioned by Fisheries New Zealand (and its predecessors) and encompass a diverse range of coastal habitats in the wider Auckland, Northland, Waikato and Bay of Plenty regions. Across the northern region, the surveys focus on twelve sites each year, with the sampling at each site surveying bivalve beds that are considered to be targeted in non-commercial fisheries.

From the survey data, the population abundance at each site is derived from a sampling-based estimator by extrapolating local density (individuals per square metre), calculated from the number of individuals per sampling unit to the stratum size. Nevertheless, recent data have documented the presence of high-density cockle patches that seemed to shift unpredictably between surveys, resulting in population estimates with relatively high uncertainty. This high uncertainty suggested that fixed stratification and the survey-based estimation may not be the most appropriate approach for providing population estimates. For this reason, the current study explored a model-based geostatistical approach, which may be more suitable for inference of abundance than survey-based estimators at sites with high variability. Model-based geostatistical estimators interpolate between observations to generate site-wide predictions, also accounting for the correlation between observations as the distance increases between them. This feature may result in more accurate site-wide estimates of abundance than the sampling-based estimator, which implicitly assumes that the un-sampled areas share the same density as the nearest observation.

Geostatistical models have been used for the northern bivalve surveys since 2015–16 to design the optimal shape and location of strata at each site prior to the field sampling. The current study was aimed at extending this approach, by deriving model-based geostatistical estimates for all 12 sites of the 2019–20 survey, and comparing them with survey-based estimates. The model exploration was focused on providing an understanding of situations when the model-based estimators may be more suitable than sampling-based estimators, including the precision of estimates. The model exploration was limited to cockle populations, because pipi populations may extend into subtidal areas that are not accessible during the intertidal field sampling. In addition to comparing estimates from the two different approaches, two operational components necessary to conduct geostatistical models were explored: first, the design of the triangulated “mesh” that is required as part of the Stochastic Partial Differential Equations (SPDE) approach that was used for the geostatistical modelling, and for which a spatial effect is estimated for each vertex; and second, the use of performance metrics to inform model selection. For each site, models were run using the most recent survey data, and also with the addition of a temporal correlation structure, allowing the inclusion of multiple years of survey data.

Owing to the diversity in the spatial configuration of survey sites, a set of general rules was trialled to define a mesh design framework that could be applied across sampling locations. These rules focused on the spatial resolution of the mesh as a function of the 5th quantile of the distribution of the smallest distance between samples, how tightly the shape of the inner mesh area should be constrained by the overall sampling strata shape, and how much buffer around each stratum should be included as part

¹Dragonfly Data Science, New Zealand.

of the inner mesh. No universal framework was ascertained for the mesh design that resulted in the highest-ranked model for each site. Instead, model performance for some sites appeared to be robust to mesh configuration; most mesh configurations resulted in realistic predictions of site-wide abundance with coefficient of variation (CV) values below or close to the 20% threshold of the target CV for the sampling-based estimates. For other sites, only specific mesh configurations achieved a similar result, with the best-performing mesh configuration varying amongst those sites.

Because there is no “true” measure of site-wide abundance, the estimates from the two different approaches were compared using precision only. This comparison showed that the highest-ranked geostatistical model selected for each site resulted in more precise estimates of population abundance for most sites. Nevertheless, the results could be sensitive to model configuration, and some models appeared to predict implausible results. For this reason, a set of criteria was defined for model selection, which accounted for model performance under traditional metrics, and discarded models that failed to meet specific standards for predictions and diagnostics. In general, for the same mesh configuration, the spatio-temporal model using all surveyed years tended to result in more stable square-metre and site-wide predictions, despite increased model complexity.

For most site-mesh combinations, the three performance metrics included in this study did not always select against models making unrealistic predictions at the fine-scale level. Nevertheless, once unrealistic models were omitted, all three performance metrics tended to select the same highest-ranked model, which was usually the model with the closest fit to the observations. Mesh complexity did not appear to be penalised by model selection, and the selected models often had finer mesh configurations.

In summary, the current study found that although geostatistical models can provide population estimates with greater precision than sampling-based estimators, results can be sensitive to model configuration. Model selection needs to account for factors beyond performance metrics, and for site configuration. In general, it is recommended that spatio-temporal models are favoured because they were more robust to mesh configuration, and yielded more precise population estimates for most sites. Single-year models should still be used for sites with high inter-annual variability in cockle bed locations.

1. INTRODUCTION

Intertidal populations of littleneck clam (cockle, tuangi/tuaki; *Austrovenus stutchburyi*) and pipi (*Paphies australis*) are frequently targeted in recreational and customary fisheries throughout New Zealand (Hartill et al. 2005, King & Lake 2013). In northern North Island, both species are part of a monitoring programme by Fisheries New Zealand (and its predecessors) that regularly surveys their populations across a range of coastal habitats in the wider Auckland, Northland, Waikato and Bay of Plenty regions (Fisheries Management Areas 1 and 9)(see most recent survey findings given by Berkenbusch & Neubauer 2020). Across the northern region, the surveys focus on twelve sites each year (most recently in 2019–20), sampling particular areas and bivalve beds that are considered to be targeted in recreational and customary fisheries.

The monitoring programme was initiated in the early 1990s, and survey methods have been relatively consistent since 1999–2000; they are based on a sampling protocol that combines a systematic design with a two-phase stratified random design (Akroyd et al. 2000, Pawley & Ford 2007). The intertidal areas sampled are identified based on existing information and input from local communities and stakeholders, and pre-survey reconnaissance. Similarly, the stratification is based on existing information and accounts for spatial variation along and down the shore at each site.

Data from the survey are used in subsequent analyses to provide information about the abundance, density and size structure of cockle and pipi populations at each site. Population abundances are derived by estimating abundance within the sampled strata by extrapolating local density (individuals per square metre), calculated from the number of individuals per sampling unit to the stratum size. To derive total population estimates for each species, the sum of total abundance within each stratum, is estimated by multiplying the density within each stratum by the stratum area. The target coefficient of variation (CV) for the total population estimate of each species is $\leq 20\%$.

Since 2013–14, the field sampling has included the use of global positioning system (GPS) to determine the accurate position of each sampling point. Prior to the 2015–16 survey, the GPS-referenced samples were used in preliminary analyses of cockle density data from the preceding surveys (2013–14 and 2014–15) to assess the stratification of areas that predominantly sample cockles. These analyses indicated that the previous stratification at individual sites rarely delimited areas of similar characteristics (e.g., homogenous densities) and, therefore, did not necessarily lead to reductions in variance in the estimation of cockle population sizes and densities. For this reason, the high-resolution spatial data from the previous surveys were used within geostatistical models of cockle densities to re-define cockle strata based on the spatial distribution and variability of previous samples (see Berkenbusch & Neubauer 2016). The model-based geostatistical estimators have been used since 2015–16 for re-stratification; however, population estimates continue to be derived from sampling-based estimators to ensure comparability of population data throughout the survey series.

At a number of sites, recent survey data documented the presence of high-density cockle patches that seemed to shift unpredictably between surveys. At these sites, re-stratification did not achieve reductions in the uncertainty associated with the estimates, indicating that fixed stratification may not be the most suitable approach for providing population estimates. Instead, model-based geostatistical estimators may be more suitable for inference of abundance than survey-based estimators at sites with high variability. In addition, model-based geostatistical estimators interpolate between observations to generate site-wide predictions, also accounting for the correlation between observations as the distance increases between them. This feature may result in more accurate site-wide estimates of abundance than the sampling-based estimator which implicitly assumes that the un-sampled areas share the same density as the nearest observation.

Based on this notion, the present study was aimed at providing model-based geostatistical estimates, including a comparison with previously-used sampling-based estimates of cockle abundance. The model exploration was focused on providing an understanding of situations when the model-based estimators may be more suitable than sampling-based estimators, including the precision of estimates. The model exploration was limited to cockle populations, because pipi populations may extend into subtidal areas

that are not accessible during the intertidal field sampling. The modelling approach was designed to address questions relevant to the application of geostatistical estimators to survey data of intertidal species such as cockles, with consideration of their wider application to other species also.

2. METHODS

The current comparison of abundance estimation methods focused on data collected during the 2019–20 field survey (see Berkenbusch & Neubauer 2020). The northern sites included in this survey were Bowentown Beach, Cockle Bay, Eastern Beach, Grahams Beach, Little Waihi Estuary, Pataua Estuary, Raglan Harbour, Tairua Harbour, Umupuia Beach, Waiotahē Estuary, Whangateau Harbour and Whitianga Harbour (Figure 1). These sites represent a diversity of coastal soft-sediment habitats inhabited by infaunal bivalves, including sheltered beaches, estuaries and semi-enclosed bays.

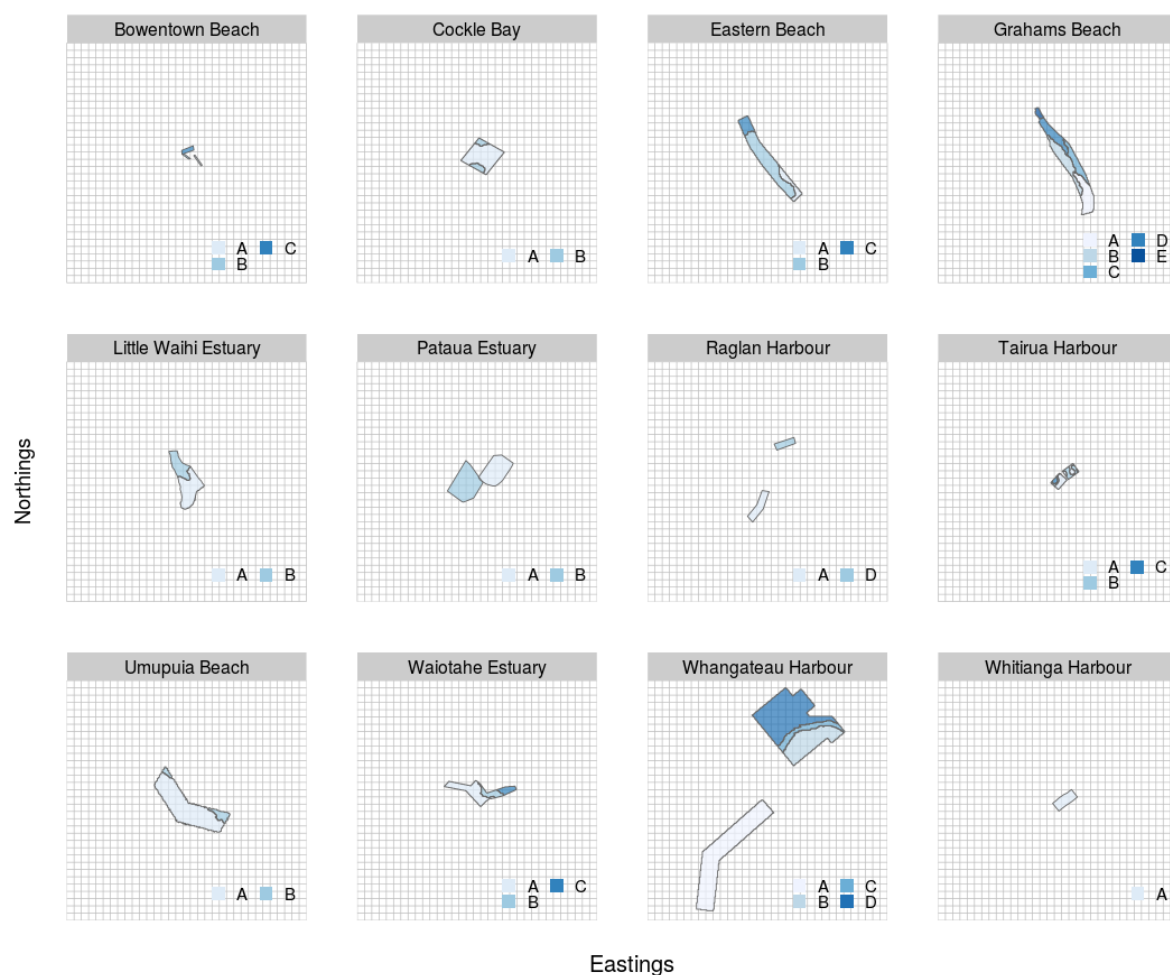


Figure 1: Outline of the twelve sites included in this analysis, with survey strata identified by individual letters and shown in shades of blue. Only cockle strata were included. Each grid square represents 100 m², with the same spatial scale used across all sites.

Model-based cockle abundance estimates (and CV) were generated by strata and site, and then compared with corresponding estimates from a standard sampling-based method for the same sites. The comparison considered the scale and variability of the estimates. The overall objectives of the current study also included the identification of a robust model selection strategy that would result in a model that could be applied to a range of different sites (of varying strata layouts and interannual variability). In addition, the model exploration process investigated the sensitivity of model-based predictions of abundance to key model settings, and surveyed key aspects of model configuration likely to affect the modelling results.

Input data for model-based abundance estimates were the observed cockle density by sampling site and the geographical location of each sample (determined by GPS units).

2.1 Model-based estimators of abundance

The current spatial modelling followed the approach developed to re-stratify sites between surveys (see Berkenbusch & Neubauer 2016). This approach was expanded to generate estimates of total cockle abundance by strata and site, and estimates of variability (variance and CV).

A geostatistical model was used to predict cockle density in space for each site based on observations. The model assumed that cockle density is distributed in space according to a Gaussian Random Field (GRF), defined by a covariance function which describes how the correlation between observations changes as the distance between them increases. The model can otherwise be viewed as a generalised linear mixed model with a Poisson response and a spatial random effect term. The model can be written hierarchically as:

$$y_i \sim \text{Poisson}(\lambda_i), \quad (1)$$

$$\log(\lambda_i) = \mu + S_i, \quad (2)$$

for bivalve counts y at sampling location i . The scale parameter λ_i is linked to a linear predictor through the log-link function; the parameter μ is the overall mean on the log-scale, and S is a Gaussian random field so that $S \sim MVN(0, \Sigma)$, where Σ is a covariance matrix. The covariance between measurements y_i and y_j is determined by their distance in space via a stationary, isotropic Matérn correlation function. Thus $Cov(y_i, y_j) = Matérn(d(y_i, y_j))$, where d specifies the distance in space. The total cockle abundance for a single-year analysis is thus $\sum_s y_s/a$, with a the quadrat area and s locations on a square-metre grid.

A negative binomial response was also trialled, but diagnostics were poor compared with diagnostics based on the Poisson response.

The geostatistical model was implemented using the Integrated Nested Laplace Approximation (INLA) algorithm which performs a Bayesian estimation of the GRF by approximating the solution to a stochastic partial differential equation (SPDE; see Lindgren et al. 2011). The estimates of the spatial field were obtained on a triangulated-mesh representation of the sampling extent, allowing predictions to any point z_s on a square-metre grid within the original sampling extent (Lindgren & Rue 2015). The model was implemented in R (R Core Team 2021) using the packages *R-INLA* (Blangiardo et al. 2013, Lindgren & Rue 2015) and *inlabru* (Bachl et al. 2019).

Because the model was implemented in a Bayesian framework, the variability was estimated by drawing 5000 samples (n) from the posterior distribution for each square-metre prediction, calculating the total abundance for the strata or site under each draw, and generating variability metrics (standard deviation σ and variance σ^2) based on the 5000 draws. For comparison with the sampling-based estimates, 95% confidence intervals were generated under the frequentist approach as $\mu \pm 1.96 \times SE$, where the standard error SE is approximated as the standard deviation of the posterior distribution.

2.1.1 Performance metrics

Three metrics were examined for selecting a “preferred” (or highest-ranked) model when comparing models using different configurations: the Deviance Information Criteria (DIC), the Watanabe-Akaike information criterion (WAIC), and the log conditional predictive ordinate (CPO). The DIC is a generalisation of the Akaike information criterion, which weights improved fit against increased model complexity. The WAIC is an extension of the AIC for Bayesian models. In comparison, the CPO is a cross-validation metric that estimates the leave-one-out predictive distribution for each observation,

from which an overall score can be obtained (the log CPO). The CPO does not down-rank model complexity, unlike the two other metrics.

The three metrics are provided as part of the *R-INLA* package output. For the CPO, the metric was recalculated for each observation using the *inla.cpo* function, which minimises failure rate with the computation in the original INLA algorithm. The logCPO score over all observations was then calculated as:

$$\log CPO = -\frac{1}{N} \sum_{i=1}^N \log(CPO_i), \quad (3)$$

where N is the number of observations in the model.

All three performance metrics are optimised at smaller values; that is, the highest-ranked model under a given metric was the model with the minimum value of this metric. The highest-ranking model for a site amongst the candidate pool of models was, therefore, selected based on the highest number of minima across DIC, WAIC and logCPO values, pending no other limitations with model fit. When the metrics differed in their higher-ranked model, logCPO was prioritised, because it has been shown previously to be the most robust performance metric (Vehtari et al. 2017 but see also Piironen & Vehtari 2017). Limitations that were considered included a high CV ($>100\%$) in the population abundance estimate, a 95% confidence interval in population abundance that overlapped with zero, an irregularity in the computation of any performance metric (e.g., overly high values) and implausible predictions at the square-metre scale. Predictions were deemed implausible when the 97.5th quantile exceeded the threshold of five times the maximum observed field density over all sites surveyed since 2013–2014 (i.e., $5 \times 8102 \text{ individuals/m}^2 = 40\,510 \text{ individuals/m}^2$). The number of square-metre cells exceeding this threshold was counted for each model and, other conditions equal, models with a lower number of cells with implausible predictions were deemed to perform better. When the top model according to the three performance metrics had to be discarded based on these considerations, the next-ranked model was similarly assessed until a “preferred” (highest-ranked) model was selected (hereafter the “selected” model).

2.1.2 Mesh configurations

The triangulated mesh is a series of interconnected triangles spanning the spatial domain of the data. It is required by INLA to fit a GRF using the SPDE approximation. A spatial effect is only fitted for each mesh vertex; predictions for locations between vertices are interpolated from the three closest vertices. The mesh can be defined to be dense or sparse, and should extend to an outer boundary surrounding the observations to prevent edge effects. The mesh is user-defined based on a few settings, including: the maximum edge length for the inner and outer regions, the minimum edge length (“cut-off”) for the inner and outer regions, and the extent of the outer region (see Figure 2 for examples of meshes produced by varying key settings). By default, the inner region is calculated as the convex hull containing all observations; however, it is also possible to define an inner region based on a non-convex hull.

Because there are no clear guidelines on how an optimal mesh should be designed, a series of mesh configuration scenarios was trialled to identify settings sensitive to model predictions (see Table 1). To generate mesh scenarios that were comparable across sites, mesh settings were defined based on multiples of the 5th quantile of the distribution of nearest observations (“nearest neighbours”) between sampling units for the site examined. The nearest neighbour to each observation was determined by computing the distance between each possible pair of observations and minimising it. Three types of range settings were explored: the length of the maximum edge of the inner region, the definition of the inner region based on a convex hull or a non-convex hull, and, for the non-convex hull, the extension and minimal concave curvature radius (EMCCR). The EMCCR determines the extent of the inner region from the observations, and the smoothness of the inner boundary.

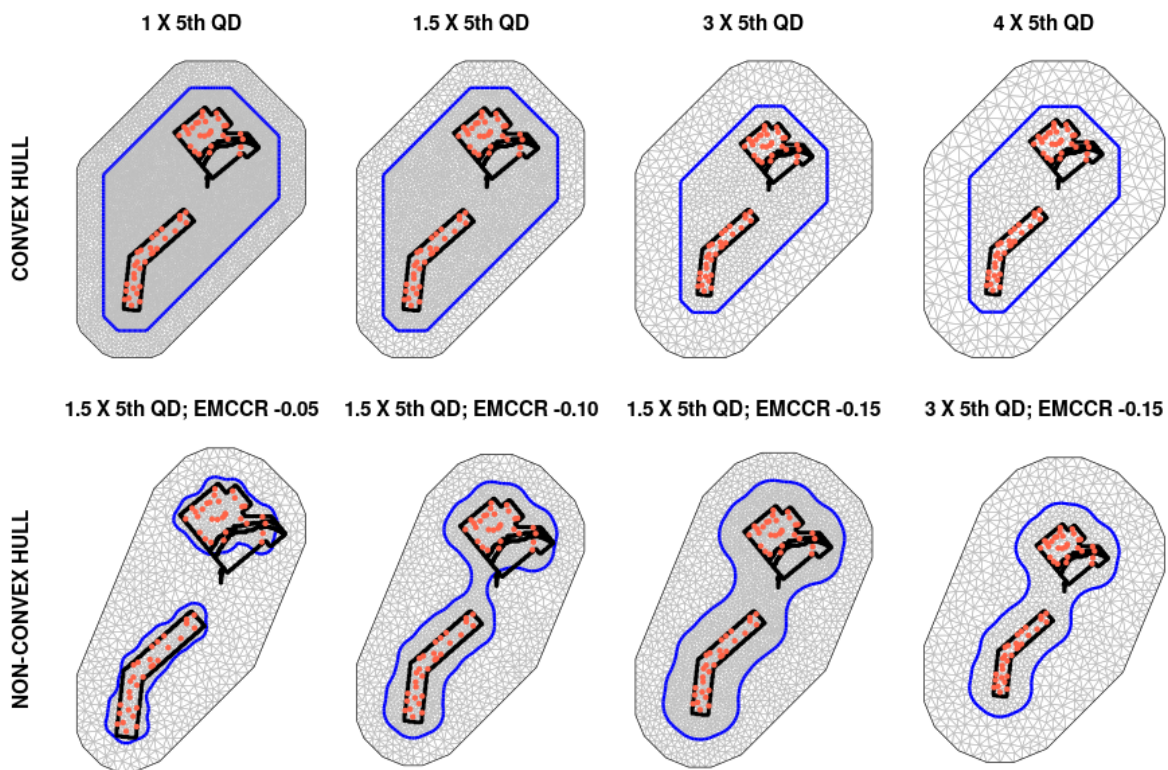


Figure 2: Mesh configuration for a survey site (here, Whangateau Harbour) that results from changing key settings: the type of hull, convex (top row) and non-convex (bottom row), the maximum edge length for the inner region as a multiple of the 5th quantile of the distribution of the distance between nearest observations (neighbours), and the extension and minimal concave curvature radius (EMCCR) for the non-convex hull. The mesh is shown in grey and the inner region is highlighted in blue. Cockle observations for the most recent survey are shown in red.

Table 1: Mesh scenarios used for the selection of a geospatial model to predict cockle density across northern North Island survey sites (MD, mean distance; NCH, non-convex hull; EMCCR, extension and minimal concave curvature radius).

Mesh configuration	Label	Description
5th quantile × 1	5Q × 1	Maximum inner edge is 1 × the length of the 5th quantile of the distance between nearest observations; convex hull.
5th quantile × 1.5	5Q × 1.5	Maximum inner edge is 1.5 × the length of the 5th quantile of the distance between nearest observations; convex hull.
5th quantile × 3	5Q × 3	Maximum inner edge is 3 × the length of the 5th quantile of the distance between nearest observations; convex hull.
5th quantile × 1.5; Non-convex hull -0.05	5Q × 1.5; NCH -0.05	Maximum inner edge is 1.5 × the length of the 5th quantile of the distance between nearest observations; non-convex hull with EMCCR = -0.05.
5th quantile × 1.5; Non-convex hull -0.10	5Q × 1.5; NCH -0.10	Maximum inner edge is 1.5 × the length of the 5th quantile of the distance between nearest observations; non-convex hull with EMCCR = -0.10.
5th quantile × 1.5; Non-convex hull -0.15	5Q × 1.5; NCH -0.15	Maximum inner edge is 1.5 × the length of the 5th quantile of the distance between nearest observations; non-convex hull with EMCCR = -0.15.
5th quantile × 3; Non-convex hull -0.15	5Q × 3; NCH -0.15	Maximum inner edge is 3 × the length of the 5th quantile of the distance between nearest observations; non-convex hull with EMCCR = -0.15.

At some sites, some individual strata are designated to primarily sample pipi beds, and these strata generally show little overlap with cockle beds. For these pipi strata, the assumption that observations are correlated in space in the same way as primary cockle habitat is tenuous. For this reason, these strata were excluded from the model domain; they were in Pataua Estuary (stratum D in 2019–20), Raglan Harbour (stratum C), Tairua Harbour (strata D and E), Whangateau Harbour (stratum E) and Whitianga Harbour (stratum B).

Some sites included multiple cockle beds that were sampled across separate strata. For these sites, the separate strata were modelled using either a single model encompassing all strata, or multiple models centred on spatially-adjacent strata only. For each site, either modelling approach was selected based on whether non-plausible square-metre predictions were produced, and by comparing the range parameter estimated for the Matérn covariance function. If the ranges differed significantly (no overlap in the 95% credible interval), it was assumed that cockle abundance varied spatially in a different manner across the distant strata, so that a customised model for each area was more appropriate. All investigations of multiple models per site were performed using the “5th quantile × 1.5; convex hull“ mesh configuration.

For sites that have been surveyed across multiple years, the model can be expanded to include a temporal component. If locations within the spatial field for the survey site are correlated among years, information can be gained by considering the spatial field of the previous survey when estimating abundance for the current survey. This information is based on the assumption that differences in the spatial fields over time are related to the time-lag between surveys. That is, spatial fields are more likely to be similar for surveys that occurred closer to each other in time.

The model in Equations 1 and 2 then becomes:

$$y_{i,t} \sim \text{Poisson}(\lambda_{i,t}), \quad (4)$$

$$\log(\lambda_{i,t}) = \mu + \Omega_{i,t}, \quad (5)$$

$$\Omega_{i,t} = \rho\Omega_{i,t-1} + S_{i,t}, \quad (6)$$

where $\Omega_{i,t}$ is a realisation of the spatio-temporal state process, with $S_{i,t}$ representing the change to the random field at time t defined as above, and ρ the autocorrelation among random fields over time under a second-order stationarity assumption.

Predictions of total abundance by strata and site were performed in the same way as for the single-year model, except for indexing with the survey year. Comparisons with the sampling-based estimates were made for all years in which surveys were conducted. Given computational limitations, the fitting of the spatio-temporal model was attempted with three different mesh configurations only: one configuration was the “5% quantile \times 1.5; convex hull”; the second configuration was the “5% quantile \times 3; convex hull”; the third configuration was the “5% quantile \times 1.5; non-convex hull” using -0.10 for the extension and minimal concave curvature radius (i.e., the middle point of the values trialled for this parameter).

Performance metrics were computed for the temporal models similarly to the single-year model, except for the logCPO metric; this latter metric was not included for computational reasons. The best temporal model was thus selected based on the DIC and WAIC metrics only, but also took into account the same aspects for model fit listed above.

2.2 Sampling-based estimators of abundance

For comparison with past and current methods for estimating cockle abundance by survey site, abundance was also estimated by stratum and site using sampling-based estimators, following the approach initially described by Berkenbusch et al. (2015) and recently reported by Berkenbusch & Neubauer (2020). Bivalve abundance within the sampled strata at each site was estimated by extrapolating local density (individuals per square metre), calculated from the number of individuals per sampling unit, to the stratum size:

$$\hat{y}_k = \frac{1}{S_k} \sum_{s=1}^S \frac{n_{s,k}}{0.035}, \quad (7a)$$

$$\hat{N} = \sum_{k=1}^K A_k \hat{y}_k, \quad (7b)$$

where $n_{s,k}$ is the number of individuals in sample s within stratum k , S_k is the total number of samples processed in stratum k , and \hat{y}_k is the estimated density of cockles (individuals per square metre) within the stratum. The total number \hat{N} of cockles at each site is then the sum of total abundance within each stratum, estimated by multiplying the density within each stratum by the stratum area A_k .

The variance $\sigma_{\hat{N}}^2$ of the total abundance was estimated as

$$\hat{\sigma}_{\hat{N}}^2 = \sum_{k=1}^K \frac{A_k^2 \sigma_{\hat{y}_k}^2}{S_k}, \quad (8)$$

where $\sigma_{\hat{y}_k}^2$ is the variance of the estimated density per sample. The corresponding coefficient of variation (CV, in %) is then

$$CV = 100 \times \frac{\sigma_{\hat{N}}}{\hat{N}}. \quad (9)$$

3. RESULTS

3.1 Sensitivity and optimisation of mesh configuration

Spatial models were able to predict observed densities for all sites when applied to a single year of data, often with high accuracy (see Appendix A, Figures A-1 to A-24). Finer meshes also tended to result in improved fits to observations. In some instances, predictions at the square-metre scale were implausible for some cells within sites, with upper bounds of the predicted uncertainty range considerably higher than densities observed in the field. Also, population-estimates for some scenarios had high variability with CV values exceeding 40% (Table 2).

The occurrence of non-plausible density estimates was sensitive to mesh configuration for all sites, with some mesh settings resulting in more stable predictions than others. There was no clear pattern in the mesh configurations that resulted in non-plausible density estimates. Predictions for Bowentown Beach, Grahams Beach and Waiotahe Estuary were robust to mesh configuration, with all configurations resulting in realistic predictions, but high variability in site-wide predictions in abundance still remaining for some models. Cockle Bay, Little Waihi Estuary, Raglan Harbour, Tairua Harbour and Whitianga Harbour had some scenarios with implausible predictions, but for less than 5 square-metre cells each. In contrast, none of the mesh configurations that were trialled resulted in realistic predictions for all square-metre cells in the sampled strata for Pataua Estuary and Whangateau Harbour. For Eastern Beach, only the finer meshes (“5th quantile \times 1” and “5th quantile \times 1.5”) resulted in realistic predictions for all square-metre cells.

Table 2: Key performance metrics for each mesh configuration trialled by site using single-year models, including the coefficient of variation (CV, %) of the population estimate, whether non-plausible predictions were generated at the square-metre scale, and the number of square-metre cells with non-plausible predictions. QD, quantile of the distance between nearest observations; NCH, non-convex hull; CPO, conditional predictive ordinate; WAIC, Watanabe-Akaike information criterion; DIC, Deviance Information Criteria. Asterisks indicate the highest-ranked model for the site under each performance metric.

Site	Mesh configuration	logCPO	WAIC	DIC	CV	Non-plausible	No. of cells
Bowentown Beach	5th QD x 1	4.69	680.50	687.43	6.37		
	5th QD x 1.5	4.68	679.32*	686.93*	6.40		
	5th QD x 3	4.87	719.54	709.95	6.26		
	5th QD x 1.5; NCH -0.05	4.68	681.06	688.05	6.19		
	5th QD x 1.5; NCH -0.1	4.67*	680.71	687.64	6.21		
	5th QD x 1.5; NCH -0.15	4.68	680.47	687.50	6.26		
	5th QD x 3; NCH -0.1	4.85	714.93	707.18	6.10		
Cockle Bay	5th QD x 1	3.14*	328.71*	335.13*	23.00		
	5th QD x 1.5	3.33	343.26	342.97	26.24		
	5th QD x 3	3.60	377.74	362.39	29.90	×	1
	5th QD x 1.5; NCH -0.05	3.24	335.51	338.83	25.59		
	5th QD x 1.5; NCH -0.1	3.31	345.28	344.17	26.44		
	5th QD x 1.5; NCH -0.15	3.29	343.35	343.14	24.55		
	5th QD x 3; NCH -0.1	3.59	376.01	361.16	32.78	×	1
Eastern Beach	5th QD x 1	3.15*	379.74*	389.58*	19.96		
	5th QD x 1.5	3.17	381.17	390.00	21.08		
	5th QD x 3	3.73	427.14	414.04	63.74	×	64
	5th QD x 1.5; NCH -0.05	3.17	381.55	390.38	21.15		
	5th QD x 1.5; NCH -0.1	3.19	381.40	390.32	21.48		
	5th QD x 1.5; NCH -0.15	3.18	381.37	390.18	21.60		
	5th QD x 3; NCH -0.1	4.27	500.94	461.87	31.84	×	18

(Continued on next page)

Table 2: (continued)

Site	Mesh configuration	logCPO	WAIC	DIC	CV	Non-plausible	No. of cells
Grahams Beach	5th QD x 1	1.61	236.91	241.71	17.86		
	5th QD x 1.5	1.60*	235.53	240.88	17.63		
	5th QD x 3	1.60*	239.05	243.10	15.32		
	5th QD x 1.5; NCH -0.05	1.60*	236.54	241.49	17.45		
	5th QD x 1.5; NCH -0.1	1.60*	235.50*	240.75*	17.38		
	5th QD x 1.5; NCH -0.15	1.60*	236.44	241.43	17.77		
	5th QD x 3; NCH -0.1	1.60*	238.96	243.02	15.06		
Little Waihi Estuary	5th QD x 1	2.67	694.84	715.26	18.68		
	5th QD x 1.5	2.65*	694.55	714.69	19.87		
	5th QD x 3	2.74	702.96	717.49	20.86	×	1
	5th QD x 1.5; NCH -0.05	2.66	694.06*	714.38*	17.03		
	5th QD x 1.5; NCH -0.1	2.66	694.69	714.72	17.20		
	5th QD x 1.5; NCH -0.15	2.67	694.20	714.49	17.05		
	5th QD x 3; NCH -0.1	2.75	701.26	716.80	17.36	×	2
Pataua Estuary	5th QD x 1	4.80	368.87	373.68	40.92	×	195
	5th QD x 1.5	4.87	368.99	373.43	44.15	×	152
	5th QD x 3	4.87	370.31	372.98*	55.49	×	96
	5th QD x 1.5; NCH -0.05	4.82	368.98	373.38	38.69	×	141
	5th QD x 1.5; NCH -0.1	4.78	368.94	373.38	36.25	×	133
	5th QD x 1.5; NCH -0.15	4.74*	368.82*	373.56	37.28	×	118
	5th QD x 3; NCH -0.1	5.04	370.33	373.18	50.36	×	87
Raglan Harbour	5th QD x 1	5.07	456.44	464.96	8.55		
	5th QD x 1.5	5.04*	454.26*	463.63*	8.84		
	5th QD x 3	5.37	466.89	467.82	8.66	×	2
	5th QD x 1.5; NCH -0.05	5.30	462.91	468.45	8.98		
	5th QD x 1.5; NCH -0.1	5.18	459.09	466.26	8.64		
	5th QD x 1.5; NCH -0.15	5.18	458.66	466.05	8.85		
	5th QD x 3; NCH -0.1	5.40	460.29	463.70	8.79	×	1
Tairua Harbour	5th QD x 1	4.96*	349.73*	356.97*	23.17	×	2
	5th QD x 1.5	5.14	353.74	359.24	18.77		
	5th QD x 3	5.23	376.46	365.44	27.19	×	2
	5th QD x 1.5; NCH -0.05	5.08	353.19	358.70	20.39		
	5th QD x 1.5; NCH -0.1	5.04	351.47	357.85	21.73		
	5th QD x 1.5; NCH -0.15	5.09	353.09	358.65	20.03		
	5th QD x 3; NCH -0.1	8.93	625.95	548.66	17.28	×	2
Umupuia Beach	5th QD x 1	2.75*	373.88*	383.12*	17.31		
	5th QD x 1.5	2.78	377.57	385.17	16.85		
	5th QD x 3	3.27	457.02	427.23	12.25		
	5th QD x 1.5; NCH -0.05	2.75*	376.57	384.43	16.66		
	5th QD x 1.5; NCH -0.1	2.76	376.76	384.49	16.62		
	5th QD x 1.5; NCH -0.15	2.76	376.63	384.48	17.29		
	5th QD x 3; NCH -0.1	3.26	457.09	427.17	12.37		
Waiotahē Estuary	5th QD x 1	2.31*	583.70*	588.46*	13.64		
	5th QD x 1.5	2.32	585.16	588.96	13.97		
	5th QD x 3	2.67	690.63	649.49	10.08		
	5th QD x 1.5; NCH -0.05	2.32	585.91	589.41	13.53		
	5th QD x 1.5; NCH -0.1	2.31*	585.68	588.93	13.39		
	5th QD x 1.5; NCH -0.15	2.32	586.16	589.47	14.17		
	5th QD x 3; NCH -0.1	2.63	681.38	644.24	11.31		
Whangateau Harbour	5th QD x 1	4.56	377.08	383.36	31.56	×	90
	5th QD x 1.5	4.56	376.57	383.00	29.53	×	30
	5th QD x 3	4.52*	378.86	381.99*	29.30	×	34
	5th QD x 1.5; NCH -0.05	4.56	376.51*	382.94	30.12	×	39
	5th QD x 1.5; NCH -0.1	4.54	376.59	382.82	29.02	×	89
	5th QD x 1.5; NCH -0.15	4.57	376.91	383.11	28.19	×	83
	5th QD x 3; NCH -0.1	4.58	380.22	382.75	43.09	×	315

(Continued on next page)

Table 2: (continued)

Site	Mesh configuration	logCPO	WAIC	DIC	CV	Non-plausible	No. of cells
Whitianga Harbour	5th QD x 1	4.36	285.44	293.72	6.88		
	5th QD x 1.5	4.34*	285.38	293.14	6.65		
	5th QD x 3	6.17	403.31	363.61	3.99		
	5th QD x 1.5; NCH -0.05	4.36	286.50	293.68	6.76		
	5th QD x 1.5; NCH -0.1	4.38	287.02	294.04	6.78		
	5th QD x 1.5; NCH -0.15	4.34*	284.76*	292.91*	6.58		
	5th QD x 3; NCH -0.1	5.07	324.19	311.87	6.81	x	1

The three metrics that were trialled as an indicator of model performance, logCPO, DIC and WAIC, tended to select the same mesh configuration for each site (Table 2), or the highest-ranked model was within one rank difference of the model selected by the other metrics. Some scenarios had little contrast in the scores assigned by the performance metrics; for example, five of the mesh scenarios for Bowentown Beach were within 0.01 logCPO score of each other. In addition, none of the metrics appeared to prevent the selection of a model generating unrealistically high predictions; for example, the highest-ranked model according to all three metrics for Tairua Harbour made unrealistic predictions for 4 square-metre cells, whereas alternative mesh scenarios without unrealistic predictions ranked more poorly.

3.2 Matérn covariance relationship

The Matérn covariance relationship predicts the correlation between observations as a function of the distance between them. The estimated range (the distance at which correlation between observations becomes small, typically <0.1) varied between sites and mesh scenarios (Figure 3). Sites with smaller ranges (125 m or less) estimated across multiple mesh scenarios included Bowentown Beach, Little Waihi Estuary, Raglan Harbour, Tairua Harbour and Whitianga Harbour. Sites with longer ranges (250 m or more for most scenarios) included Eastern Beach, Grahams Beach, Pataua Estuary, Umupuia Beach and Whangateau Harbour. For most sites, there was little variability in the shape of the Matérn covariance relationship predicted between scenarios. For Eastern Beach and Whangateau Harbour, the coarser mesh scenarios (“5th quantile × 3”) resulted in a smaller estimated range. Pataua Estuary and Whangateau Harbour, the two sites where all scenarios produced a high number of implausible square-metre predictions, also had greater estimated ranges compared with other sites.

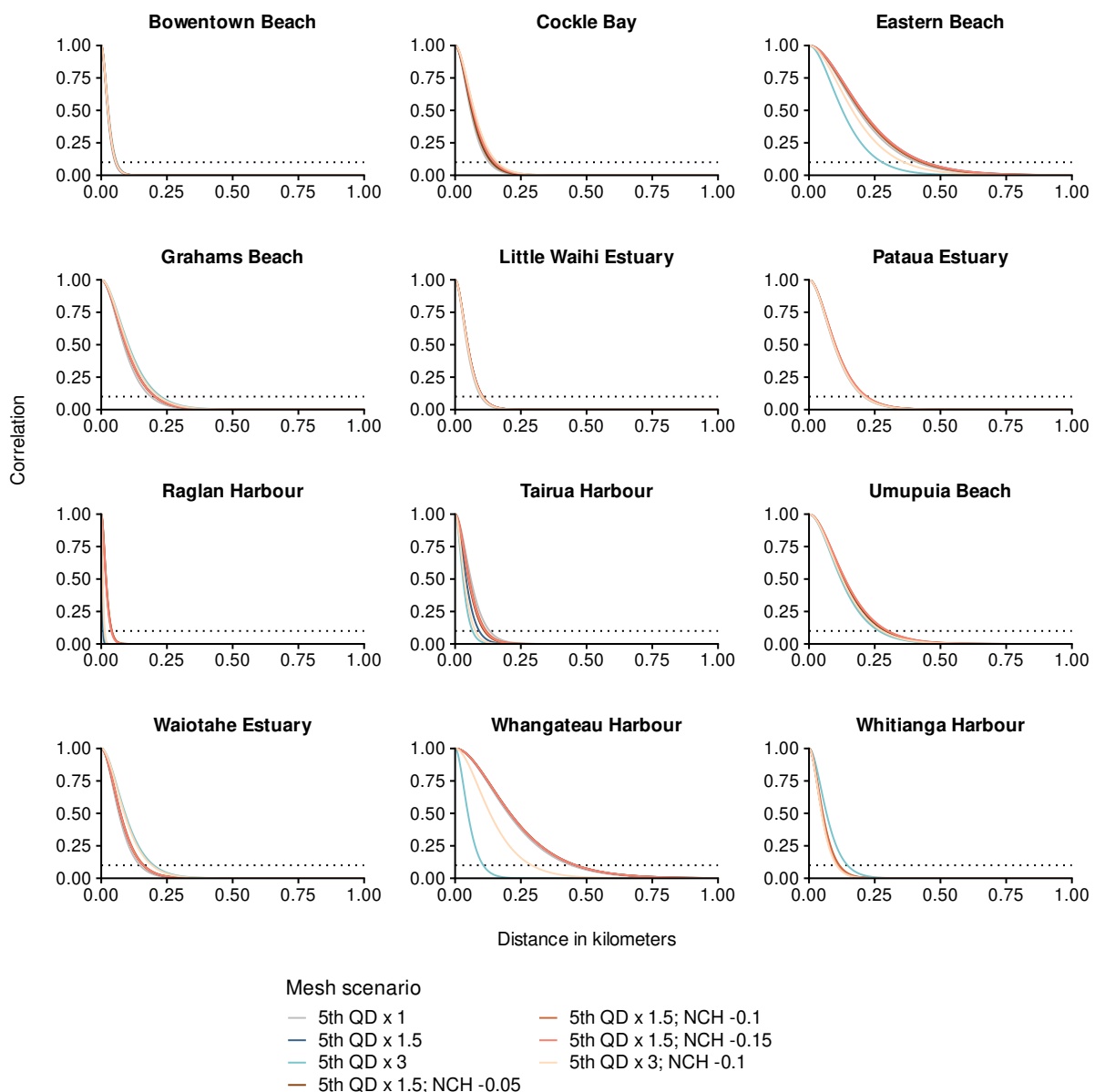


Figure 3: Matérn covariance function estimated for each mesh scenario by site (QD, quantile of the distance between nearest observations; NCH, non-convex hull). Dotted line at $\rho = 0.1$ indicates the range of the estimated relationship, i.e., the distance at which the correlation between observations becomes small.

3.3 Temporal models based on multiple years

Spatio-temporal models predicting cockle abundance were fitted for all sites using both the convex and non-convex hull for the “5th quantile $\times 1.5$ ” mesh scenario (with the non-convex hull using the median value for the EMCCR parameter, i.e. -0.10), as well as a third scenario using the “5th quantile $\times 3$ ” convex hull mesh (Appendix B). Spatio-temporal models tended to produce more stable results for most sites (Table 3). That is, site-wide predictions with a CV of less than 50% were produced for all sites and mesh scenarios but one, including some mesh scenarios where the corresponding single-year scenario failed to result in stable predictions (e.g., Cockle Bay, Eastern Beach, Pataua Estuary, and Whangateau Harbour) (Figure 4). Although some scenarios still resulted in non-plausible predictions at the square-metre scale, the number of impacted cells was smaller than for the corresponding single-year model for most site and scenario combinations (Tables 2 and 3). In addition, a number of sites with non-plausible values predicted under the single-year model had no non-plausible predictions under the temporal model. In most instances, the CV for the estimate of site-wide abundance was smaller for the temporal model than the single-year model (Figure 4). Exceptions included Grahams Beach, Tairua Harbour, and Waiotahe Estuary. For many combinations of sites and mesh scenarios, the mean site-wide abundance and its 95% confidence interval fell within the range predicted using the sampling-based estimator. The mean site-wide abundance under both scenarios was almost always slightly larger than the corresponding sampling-based estimator, except for Cockle Bay and Whangateau Harbour, where means were slightly lower.

Table 3: Key performance metrics for each mesh configuration trialled by site using spatio-temporal models, including the coefficient of variation (CV, %) of the population estimate, whether non-plausible predictions were generated at the square-metre scale, and the number of square-metre cells with non-plausible predictions. QD, 5th quantile of the distance between nearest observations; NCH, non-convex hull; CPO, conditional predictive ordinate; WAIC, Watanabe-Akaike information criterion; DIC, Deviance Information Criteria. Asterisks indicate the highest-ranked model for the site under each performance metric.

Site	Mesh configuration	WAIC	DIC	CV	Non-plausible	No. of cells
Bowentown Beach	5th quantile x 1.5	2171.29*	2179.20*	4.32		
	5th quantile x 3	2211.19	2198.95	4.02		
	5th quantile x 1.5; NCH -0.10	2191.15	2191.72	4.33		
Cockle Bay	5th quantile x 1.5	1464.19*	1471.27*	9.92		
	5th quantile x 3	1506.42	1493.23	11.38		
	5th quantile x 1.5; NCH -0.10	1466.86	1473.66	9.88		
Eastern Beach	5th quantile x 1.5	> 10000	1670.58	17.88		
	5th quantile x 3	8483.92*	1886.42	13.96		
	5th quantile x 1.5; NCH -0.10	> 10000	1669.69*	16.84		
Grahams Beach	5th quantile x 1.5	882.37	898.85	26.64		
	5th quantile x 3	974.07	947.18	45.92		
	5th quantile x 1.5; NCH -0.10	880.48*	897.77*	28.48		
Little Waihi Estuary	5th quantile x 1.5	2139.83	2188.00	21.23		
	5th quantile x 3	2170.32	2202.10	19.76		
	5th quantile x 1.5; NCH -0.10	2139.49*	2187.71*	23.04		
Pataua Estuary	5th quantile x 1.5	3118.89*	3138.68*	10.88	×	6
	5th quantile x 3	6135.14	5156.15	32.14	×	99
	5th quantile x 1.5; NCH -0.10	3121.22	3140.56	10.86	×	7
Raglan Harbour	5th quantile x 1.5	1915.28	1939.59	6.36		
	5th quantile x 3	2297.35	2162.33	7.28		
	5th quantile x 1.5; NCH -0.10	1913.65*	1938.97*	6.29		
Tairua Harbour	5th quantile x 1.5	2229.21*	2220.15*	24.33	×	4
	5th quantile x 3	5524.80	4333.10	55.88	×	17
	5th quantile x 1.5; NCH -0.10	2245.51	2227.41	24.69	×	8
Umupuia Beach	5th quantile x 1.5	2038.93	2031.91	12.27		
	5th quantile x 3	3208.93	2747.62	15.52	×	1
	5th quantile x 1.5; NCH -0.10	2038.51*	2031.28*	11.68		
Waiotahē Estuary	5th quantile x 1.5	1708.88*	1716.46*	11.68		
	5th quantile x 3	1912.11	1834.40	25.04	×	2
	5th quantile x 1.5; NCH -0.10	1712.82	1718.74	11.48		
Whangateau Harbour	5th quantile x 1.5	3346.90	3322.82	13.16	×	14
	5th quantile x 3	4884.82	4339.10	34.30	×	314
	5th quantile x 1.5; NCH -0.10	3300.60*	3293.92*	13.64	×	9
Whitianga Harbour	5th quantile x 1.5	981.95*	998.43*	5.92		
	5th quantile x 3	1332.13	1202.37	4.31		
	5th quantile x 1.5; NCH -0.10	992.82	1004.13	5.96		

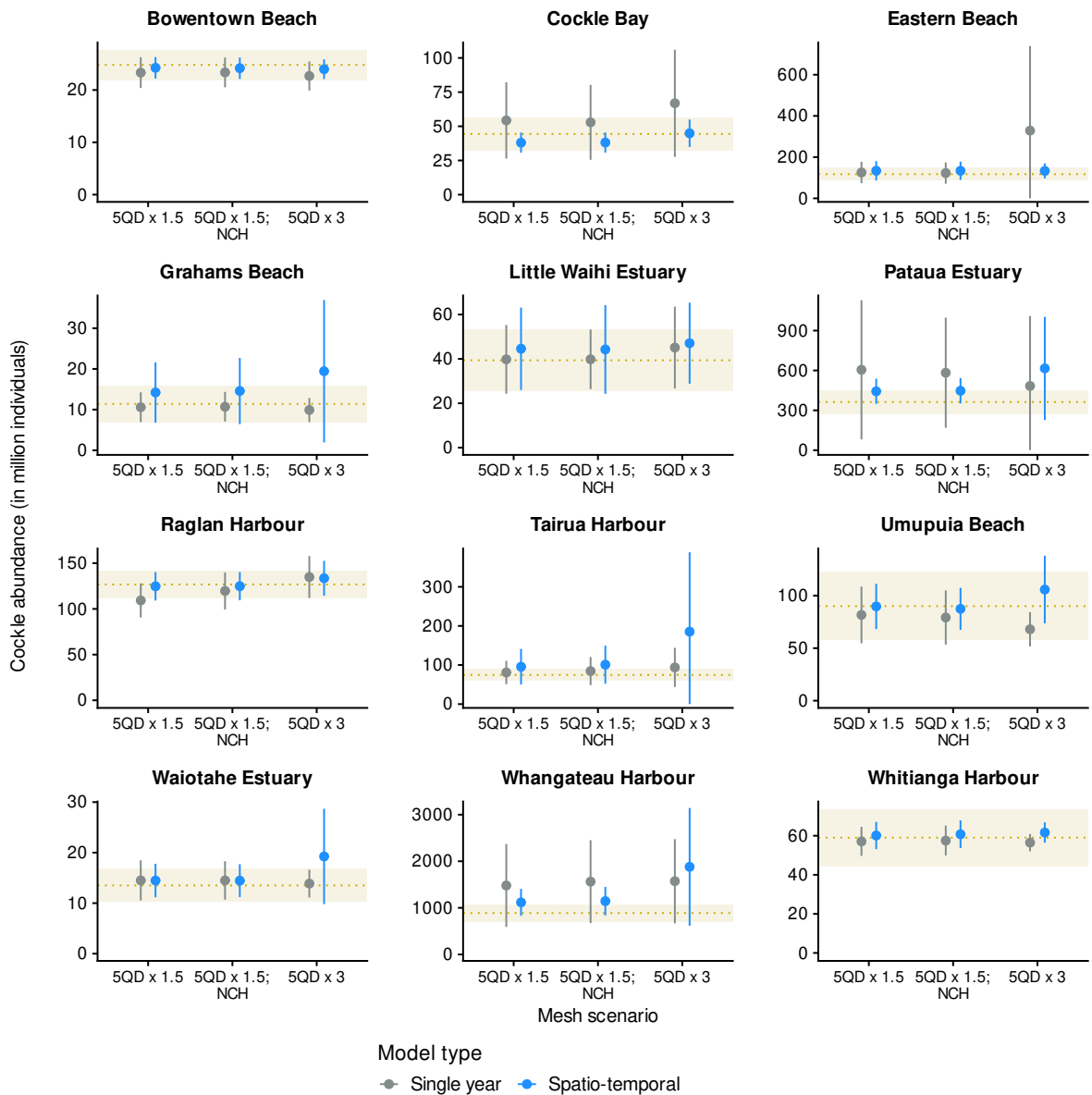


Figure 4: Comparison of predictions for site-wide abundance between single-year (grey) and spatio-temporal models (blue) for northern North Island survey sites with predicted model estimates with a coefficient of variation (CV) of less than 75%. Shown are three mesh scenarios: 1.5 × 5th quantile of the distance (QD) between nearest observations, convex hull; 1.5 × 5th QD between nearest observations, non-convex hull (NCH, extension and minimal concave curvature radius = -0.10); and 3 × 5th QD between nearest observations, convex hull. Yellow band highlights the prediction from the sampling-based estimator (mean, dotted line; 95% confidence interval, band).

The distribution of the AR-1 ρ (interannual correlation) parameter varied across sites and between mesh configurations (Figure 5). The value of ρ by site was generally higher under the coarser mesh scenario, “5th quantile $\times 3$ ”, compared with the finer mesh scenarios. Nevertheless, the relative distribution of ρ amongst sites within a single mesh scenario was preserved, i.e., most sites that tended to have a low value of ρ compared with other sites did so under all scenarios. For example, Cockle Bay, Grahams Beach, Little Waihi Estuary and Whitianga Harbour had lower estimates of ρ compared with other sites across all scenarios, whereas Pataua Estuary had the highest estimate of ρ . Some sites with a lower value of ρ had more variable site-wide estimates of abundance (Grahams Beach and Tairua Harbour), whereas other sites did not (Cockle Bay, Little Waihi Estuary) (Figure 4). Particularly for Tairua Harbour, the one scenario resulting in a high population CV (“5th quantile $\times 3$ ”) also had a considerably lower estimate of ρ compared with other scenarios.

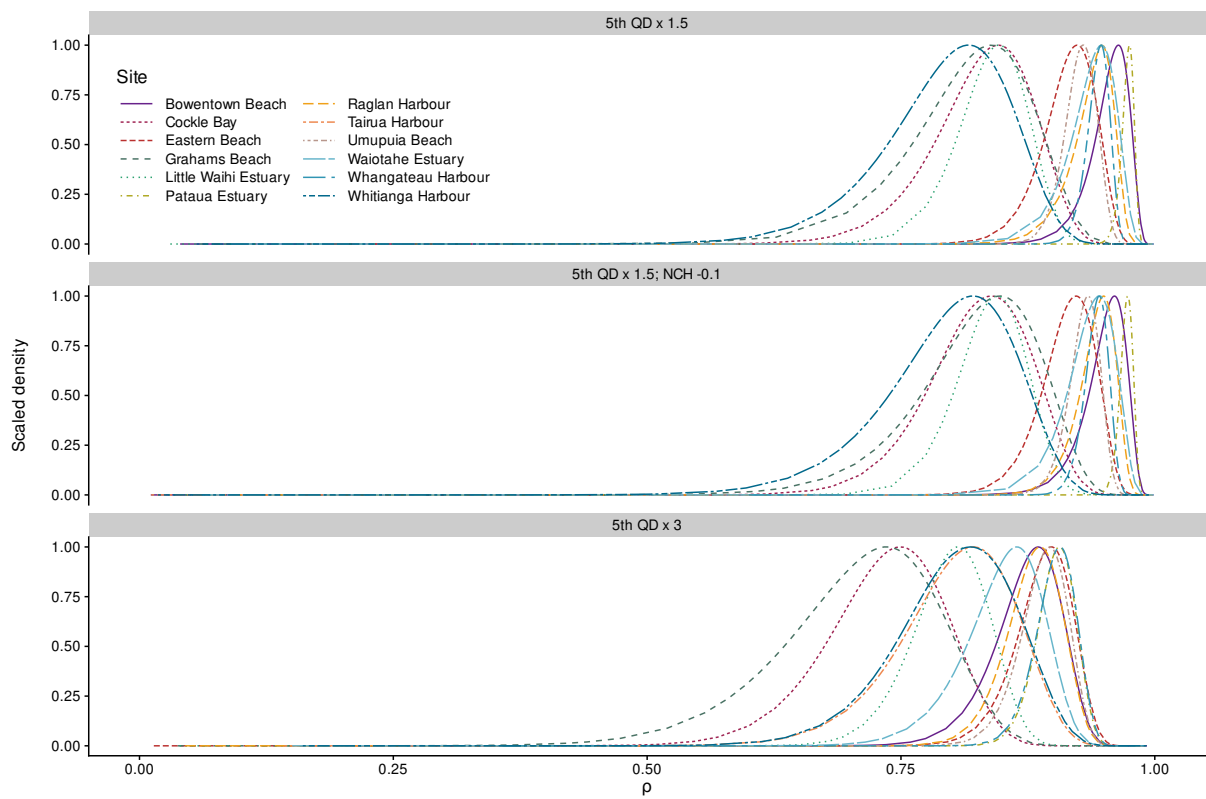


Figure 5: Posterior distribution for the AR-1 correlation parameter fitted in the spatio-temporal model to each site under three scenarios: $1.5 \times$ 5th quantile of the distance (QD) between nearest observations, convex hull; $1.5 \times$ 5th QD between nearest observations, non-convex hull (NCH, extension and minimal concave curvature radius = -0.10); and $3 \times$ 5th QD between nearest observations, convex hull.

3.4 Comparison between the highest-ranked models and sampling-based estimator

The highest-ranked model for each site and modelling approach (single-year versus temporal) was selected by considering the relative ranking of models according to the logCPO, DIC, and WAIC metrics (Table 4). Models with high discrepancies in model fit or diagnostics (e.g., a higher number of implausible predictions at the square-metre scale) were discarded. For the single-year modelling approach, the mesh configurations most often selected were the finer meshes, either “5th quantile $\times 1$ ” or “5th quantile $\times 1.5$ ”. These mesh configurations often resulted in a close fit to observations (Figures A-1 to A-23). Similarly, the finer mesh configurations also yielded more precise and realistic population-wide estimates under the temporal modelling approach (“5th quantile $\times 1$ ” convex hull and non-convex hull), with the coarser mesh scenario only ranked higher for Eastern Beach. No high-ranked model met all fit and diagnostic criteria under the single-year approach for Pataua Estuary or Whangateau Harbour; the model outputs improved for sites under the temporal modelling approach, with more precise CV and population-wide estimates overlapping (or close to) the 95% confidence interval from the sampling-based estimator. In both instances the finer meshes were selected: the “5th quantile $\times 1.5$ ” convex hull model was highest-ranked for Pataua Estuary, and the “5th quantile $\times 1.5$ ” non-convex hull model was highest-ranked for Whangateau Harbour.

For six of the twelve sites, the CV of the population abundance estimate was smaller under the selected temporal model than with the sampling-based estimator; for another three sites it was equivalent (Figure 6). The mean population estimate for the highest-ranked model was consistently contained within the 95% confidence interval from the sampling-based estimator, except at Pataua Estuary and at Tairua Harbour. There was no clear trend in its relative value compared with the mean population estimate from the sampling-based estimator. Exceptions of considerably higher CV values from the temporal model than from the sampling-based estimator included Grahams Beach, Little Waihi Estuary, and Tairua Harbour. Results from the single-year model were less conclusive, and most CV values for population estimates were higher than values obtained from the sampling-based estimator. Sites with particularly precise estimates of population abundance included Bowentown Beach, Grahams Beach, Raglan Harbour, Umupuia Beach, Waiotahe Estuary, and Whitianga Harbour.

Table 4: Highest-ranked model for each site under the single-year and temporal modelling approaches (QD, quantile nearest neighbour distance).

Site	Single year	Temporal
Bowentown Beach	5th QD $\times 1.5$; Non-convex hull -0.1	5th QD $\times 1.5$
Cockle Bay	5th QD $\times 1$	5th QD $\times 1.5$
Eastern Beach	5th QD $\times 1$	5th QD $\times 3$
Grahams Beach	5th QD $\times 1.5$	5th QD $\times 1.5$; Non-convex hull -0.1
Little Waihi Estuary	5th QD $\times 1.5$; Non-convex hull -0.05	5th QD $\times 1.5$; Non-convex hull -0.1
Pataua Estuary	No highest-ranked model	5th QD $\times 1.5$
Raglan Harbour	5th QD $\times 1.5$	5th QD $\times 1.5$; Non-convex hull -0.1
Tairua Harbour	5th QD $\times 1.5$; Non-convex hull -0.05	5th QD $\times 1.5$
Umupuia Beach	5th QD $\times 1$	5th QD $\times 1.5$; Non-convex hull -0.1
Waiotahe Estuary	5th QD $\times 1$	5th QD $\times 1.5$
Whangateau Harbour	No highest-ranked model	5th QD $\times 1.5$; Non-convex hull -0.1
Whitianga Harbour	5th QD $\times 1.5$; Non-convex-hull -0.15	5th QD $\times 1.5$

3.5 Multiple models for distanced strata

There were three sites with separate strata: Bowentown Beach, Raglan Harbour and Whangateau Harbour. For these sites, the strata were divided into two areas (some areas had multiple strata that were immediately adjacent to each other). Independent geostatistical models were fitted to each stratum (or group of strata if they were immediately adjacent), and results were compared with findings from the single spatial domain approach.

For Bowentown Beach, by-strata and site-wide predictions of total abundance were comparable under both approaches, with a slightly lower CV under the multiple-model approach (Appendix C, Figure C-1).

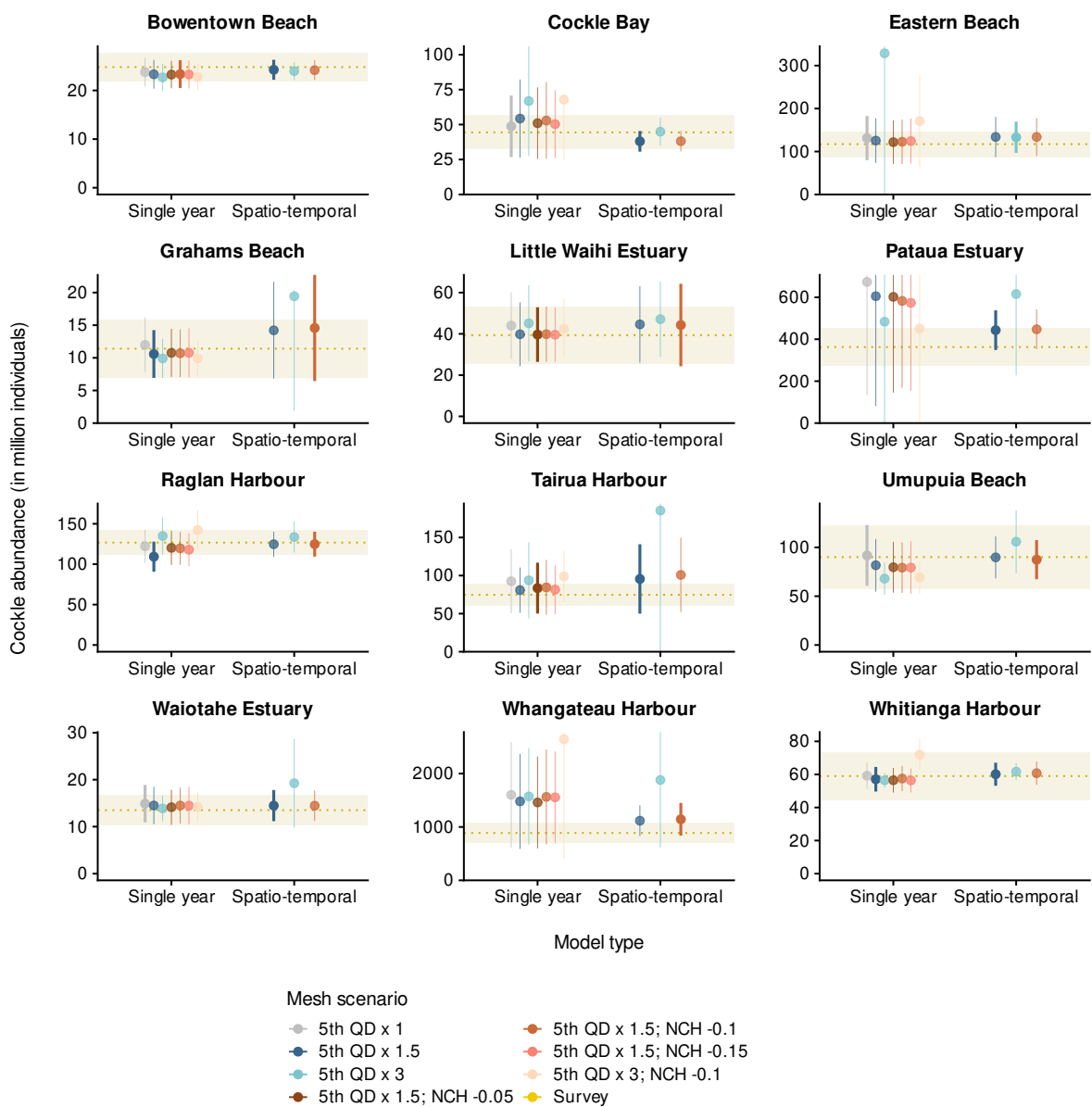


Figure 6: Comparison of predictions for site-wide abundance between all single-year mesh scenarios and spatio-temporal models (QD, quantile of the distance between nearest observations; NCH, non-convex hull). The highest-ranked model for each category is shown in bold. For clarity, the upper limits on wide confidence intervals were bounded. Yellow band highlights the prediction from the sampling-based estimator (mean, dotted line; 95% confidence interval, band).

The fine-scale predictions per metre square were also similar, but the single-model approach predicted higher localised densities for some cells (Figure C-2). The estimated covariance relationship was similar for strata B and C (i.e., the strata determining most of the overall site abundance), but differed for stratum A. For this stratum, the range predicted from the strata-specific model was about a third of the range predicted by the single model (Figure C-3).

For Raglan Harbour, the site-wide predictions of total abundance were comparable, but stratum-specific predictions differed, with the multiple mesh approach estimating a higher abundance for stratum A, and a lower abundance for stratum B. In both instances, the multiple mesh estimates were closer to the survey-based abundance estimates than for the single-model approach. The stratum-specific CV was lower under the single-model approach, but comparable at the population-level. Cockle density was distributed slightly differently within strata, with the single-model predicting even density across all strata, whereas the multiple mesh approach had different mean densities across strata (but distributed evenly within the stratum, with some high-density “hotspots”) (Figure C-2). The estimated covariance relationships were similar, with the multiple mesh approach predicting slightly greater ranges for both strata, compared with the single model (Figure C-3).

For Whangateau Harbour, the multiple-model strategy led to similar predictions of abundance to the single model approach for all strata, with a higher CV for stratum A, and a lower CV for stratum D (Figure C-7). The CV values at the population level were similar for both approaches. The median value of high-density areas were generally higher under the multiple model strategy, especially in stratum A (Figure C-8). The estimated covariance relationship compared with the single-model approach was different for both strata groups: stratum A showed a markedly lower range, and strata B, C, and D (modelled jointly) showed a markedly greater range (Figure C-9). This difference was also reflected in the greater spread of high-density areas in the fine-scale predictions (Figure C-8).

4. DISCUSSION

This research explored strategies for fitting geostatistical models to survey data within the INLA framework, with the goal to produce cockle population estimates with high accuracy and precision for the surveyed sites. The resulting estimates were compared with estimates obtained using the sampling-based estimator currently used when reporting population estimates by site. The geostatistical models were applied to survey data of cockle densities across a set of 12 beaches, harbours, and estuaries across northern North Island. Nevertheless, the conclusions are applicable to other studies that attempt to estimate abundance from survey data using a stratified random design for other species and locations.

Because there is no “true” measure of site-wide abundance, the modelling outcomes were compared across methodologies using precision only. This comparison showed that the highest-ranked geostatistical model selected for each site resulted in more precise estimates of population abundance for some sites. Nevertheless, the results were sensitive to model configuration, and some models appeared to predict implausible results. Of note, stratification in all sites is informed by years of sampling and knowledge of boundaries of high-density cockle patches. Sparse or intense sampling in some areas reflects, in a Bayesian sense, a spatio-temporal prior on the expected variance within strata. This knowledge is then used to optimise the distribution of sampling effort in the following year to obtain low CV values for estimates from sampling-based estimators. Because of this aspect, it is relevant to compare population CV values between the spatio-temporal models and the currently-used sampling-based estimators, because the spatio-temporal models effectively incorporate consistency among years to improve estimates.

At the same time, the population estimates for the model-based estimators are derived from the predictive distribution in space, rather than using stratum-level or global mean-densities scaled to stratum size (the approach used for the sampling-based estimators). Because the predictive distribution had higher variance by definition, model-based CV values for population estimates account for more sources of variation at the fine scale. Although they are not strictly comparable to CV values obtained

from sampling-based estimators, model-based CV values for population estimates are expected to be more representative of uncertainty in population estimates at the site under the current sampling protocol.

One of the key steps in developing a geostatistical model under the INLA approach is to design a triangulated “mesh” for which a spatial effect is to be estimated for each vertex, under the assumption of a GRF. Because each of the twelve sites included in this case study had a different spatial configuration, such as overall extent, complexity of the strata shapes, and distance between cockle beds sampled, a set of general rules was trialled to define a mesh design framework that could be applied across sites. These rules focused on the spatial resolution of the mesh as a function of the 5th quantile of the distribution of distances between nearest neighbours, how tightly the shape of the inner mesh area should be constrained by the overall sampling strata shape (i.e., convex versus non-convex hull), and how much buffer around each stratum should be included as part of the inner mesh (i.e., the extension and minimal concave curvature radius).

The current findings showed that it was not possible to define a universal framework for the mesh design that resulted in the highest-ranked model for each site. Instead, model performance for some sites appeared to be robust to mesh configuration, with most mesh configurations resulting in realistic predictions of site-wide abundance with CV values within an acceptable threshold (i.e., below or close to the target CV of 20% for total population estimates from the sampling-based estimator). In contrast, for other sites, only specific mesh configurations achieved a similar result, with the corresponding mesh configuration varying amongst sites. In general, finer meshes appeared more stable (fewer unrealistic predictions) for both convex and non-convex hulls.

Three different performance metrics for model selection were trialled. Two of these metrics balanced improvements in model fit against model complexity (DIC and WAIC); the third was a metric resulting from a cross-validation approach (logCPO). A key concern for fitting the geostatistical models was that some mesh configurations resulted in unrealistic metre-square predictions of cockle abundance (e.g., estimates in excess of five times the maximum density observed in the field since 2013–14). For this reason, a set of criteria was defined for model selection, which accounted for model performance under traditional metrics and omitted models when they failed to meet specific standards for predictions and diagnostics.

Also, for most site-mesh combinations, the included performance metrics did not appear to provide adequate insight into model stability. That is, some models were ranked highest by the metrics, even though they had high uncertainty bounds for some square-metre cells. Once unrealistic models were omitted, all three performance metrics tended to select the same highest-ranked model. This model was usually the model with the closest fit to the observations and the finest mesh. This finding is in contrast to other simulation-based research (also using the INLA framework), which found that the logCPO metric tended to select different, often coarser, mesh configurations than the WAIC and DIC metrics; this previous research also documented that the logCPO-selected meshes were performing “better” overall due to a smaller out-of-sample prediction error (Righetto et al. 2020). Similar findings were found in a separate study by Vehtari et al. (2017). For this reason, the logCPO metric was favoured when selecting the highest-ranked model when there were divergences in model rank amongst metrics.

A key finding of the current study was that, for the same mesh configuration, the spatio-temporal model using data from all surveyed years tended to result in more stable square-metre and site-wide predictions for almost all sites, despite increased model complexity. This outcome indicates that limitations with model stability with single-year models might be due to an insufficient number of observations for adequately fitting the Matérn covariance function.

For Pataua Estuary and Whangateau Harbour, none of the trialled spatial models derived realistic estimates, whereas spatio-temporal models obtained population-wide CV values comparable with values from the sampling-based estimator. The surveys at these two sites extended across large areas with relatively sparse sampling in some strata. With the spatio-temporal model, there were more

observations to inform the spatial effect for each vertex of the mesh than with only a single year of sampling. The resulting spatial coefficients were, therefore, more precise and less likely to result in implausible predictions of site-wide abundance with large CV values. The spatio-temporal models should, therefore, be prioritised in future applications of this research, especially for sites that retain a stable configuration of cockle beds between years. For sites with variable cockle bed locations between years, such as Grahams Beach, single-year models might be more appropriate. Grahams Beach was the one site where all scenarios of the spatio-temporal models derived unrealistic estimates compared with the single-year model. An alternative structure allowing for non-stationarity in the spatio-temporal models could also be used to allow for shifts in the location of cockle beds between years, but the number of observations may be insufficient to inform this more complex model configuration.

Another modelling strategy that was trialled was a multiple mesh approach, whereby spatially disjoint strata for some sites were modelled independently (“split models”). The assumption for this approach was that the Matérn covariance function might differ between the spatially disjoint strata, because they may have been in slightly different habitats. This difference may mean that split models would provide realistic estimates at the strata level. Nevertheless, there were no clear advantages from this approach; the population-wide CV values were similar or slightly smaller than values obtained under the single-mesh approach. For Raglan Harbour, the strata-wide predictions also appeared to more closely match expectations from the sampling-based estimator. Because some strata within sites do occasionally include different habitats (e.g., stratum B in Whangateau Harbour occurs at a slightly lower tidal zone than other strata), the multiple mesh approach might still be valuable when modelling other sites, depending on the strata configuration.

The geostatistical models in this study used total cockle density as a response variable, i.e., included all individuals sampled (all size classes, including juveniles and recruits). An alternative approach would be to only model large-size cockles (>30 mm shell length), because total abundance can be variable due to dynamic patches of newly-settled individuals. Nevertheless, exploration of this aspect suggested that any such subsetting of the sampled population by size would be sensitive to thresholds used. These patches may contribute to the high CV values for site-wide predictions for some of the model configurations.

5. ACKNOWLEDGMENTS

We thank the Shellfish Working Group for feedback on earlier versions of this modelling, and especially Craig Marsh and Darcy Webber for their technical suggestions.

This project was funded by Ministry for Primary Industries, project AKI2018/01.

6. REFERENCES

- Akroyd, J.M.; Manly, B.F.J.; Walshe, K.A.R. (2000). Distribution, abundance and size frequency of pipi (*Paphies australis*), cockles (*Austrovenus stutchburyi*) and tuatua (*Paphies subtriangulata*) at eleven beaches during the 1999/2000 fishing year. Final report to the Ministry of Fisheries, project AKI 1999/01. (Unpublished report held by Fisheries New Zealand, Wellington.)
- Bachl, F.E.; Lindgren, F.; Borchers, D.L.; Illian, J.B. (2019). Inlabru: an R package for Bayesian spatial modelling from ecological survey data. *Methods in Ecology and Evolution* 10 (6): 760–766.
- Berkenbusch, K.; Abraham, E.; Neubauer, P. (2015). Intertidal shellfish monitoring in the northern North Island region, 2013–14. *New Zealand Fisheries Assessment Report 2015/15*. 83 p. Retrieved from <https://fs.fish.govt.nz/Page.aspx?pk=113&dk=23774>.
- Berkenbusch, K.; Neubauer, P. (2016). Intertidal shellfish monitoring in the northern North Island region, 2015–16. *New Zealand Fisheries Assessment Report 2016/49*. 108 p. Retrieved from <https://fs.fish.govt.nz/Page.aspx?pk=113&dk=24186>.
- Berkenbusch, K.; Neubauer, P. (2020). Intertidal shellfish monitoring in the northern North Island region, 2019–20. *New Zealand Fisheries Assessment Report 2020/38*. 103 p. Retrieved from <https://fs.fish.govt.nz/Page.aspx?pk=113&dk=24836>.

- Blangiardo, M.; Cameletti, M.; Baio, G.; avard Rue, H. (2013). Spatial and spatio-temporal models with R-INLA. *Spatial and Spatio-temporal Epidemiology* 7: 39–55.
- Hartill, B.; Morrison, M.A.; Cryer, M. (2005). Estimates of biomass, sustainable yield and harvest: Neither necessary nor sufficient for the management of amateur intertidal fisheries. *Fisheries Research* 71: 209–222.
- King, N.; Lake, R. (2013). Bivalve shellfish harvesting and consumption in New Zealand, 2011: data for exposure assessment. *New Zealand Journal of Marine and Freshwater Research* 47: 62–72.
- Lindgren, F.; Rue, H. (2015). Bayesian spatial modelling with R-INLA. *Journal of Statistical Software* 63 (19): 1–25.
- Lindgren, F.; Rue, H.; Lindström, J. (2011). An explicit link between Gaussian fields and Gaussian Markov random fields: the stochastic partial differential equation approach. *Journal of the Royal Statistical Society: Series B (Statistical Methodology)* 73 (4): 423–498.
- Pawley, M.D.M.; Ford, R. (2007). Report for AKI2006/01. Final Research Report for Ministry of Fisheries Project AKI2006/01. (Unpublished report held by Fisheries New Zealand, Wellington.)
- Piironen, J.; Vehtari, A. (2017). Comparison of bayesian predictive methods for model selection. *Statistics and Computing* 27 (3): 711–735.
- R Core Team (2021). R: A language and environment for statistical computing. R Foundation for Statistical Computing. Vienna, Austria. Retrieved from <https://www.R-project.org/>.
- Righetto, A.J.; Faes, C.; Vandendijck, Y.; Ribeiro Jr, P.J. (2020). On the choice of the mesh for the analysis of geostatistical data using R-INLA. *Communications in Statistics - Theory and Methods* 49 (1): 203–220.
- Vehtari, A.; Gelman, A.; Gabry, J. (2017). Practical Bayesian model evaluation using leave-one-out cross-validation and WAIC. *Statistics and Computing* 27: 1413–1432.

APPENDIX A: SINGLE-YEAR MODELS—MESH SCENARIOS

A.1 Bowentown Beach

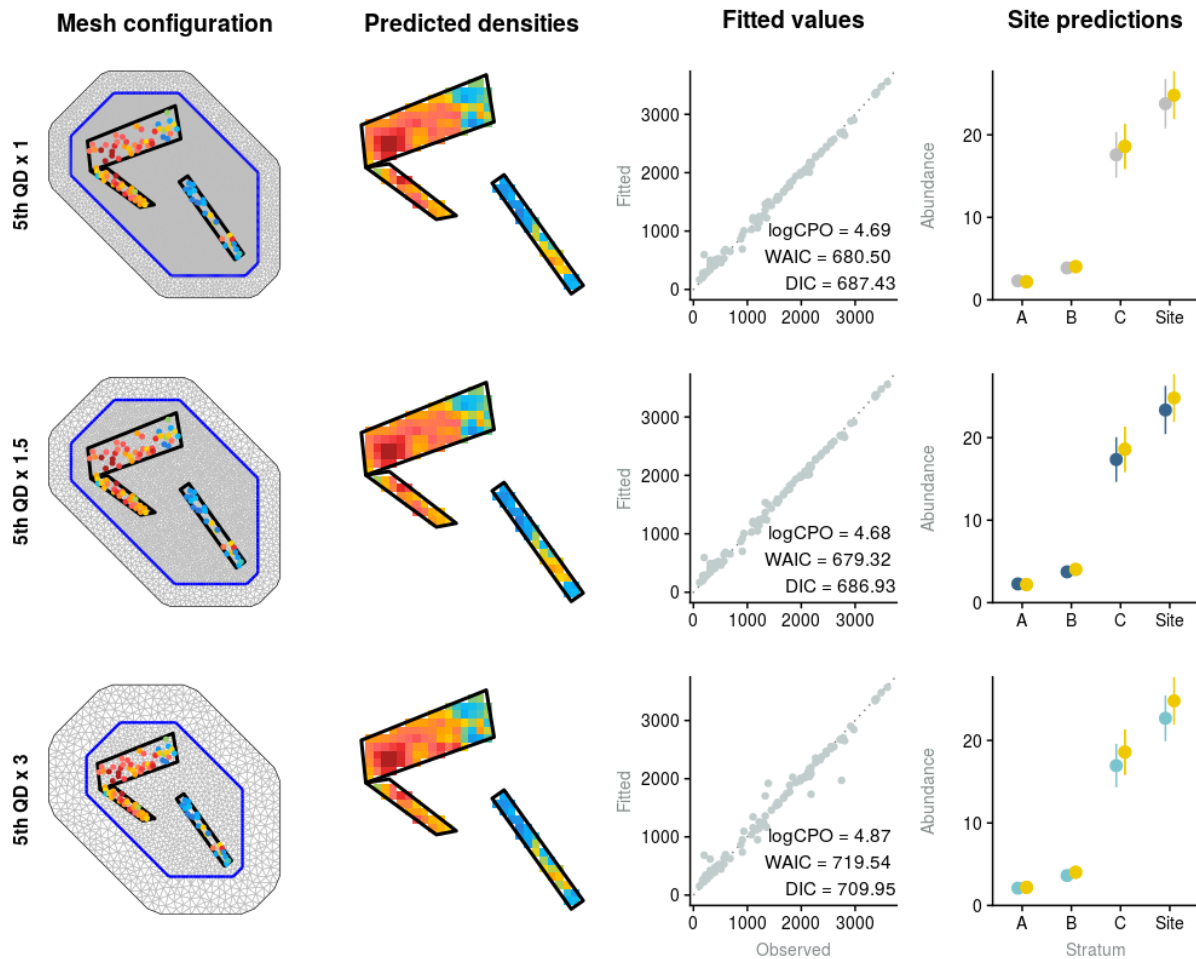


Figure A-1: Model fit and diagnostics for mesh scenarios (in rows) using a convex hull for Bowentown Beach. First column: mesh configuration with the strata highlighted in black and inner mesh area highlighted in blue. Points denote observations for the site, with cockle density scaling from blue to red. Second column: predictions at the square-metre scale resulting from the model; colours scale from 0 to the 97.5th quantile predicted across all scenarios for the site, cells exceeding this threshold are shown in dark red, the colour scale is site-specific. Third column: comparison of observed (X) against predicted densities (Y) for each mesh scenario, with the value of performance metrics for the scenario included in the bottom-right corner (logCPO, conditional predictive ordinate; WAIC, Watanabe-Akaike information criterion; and DIC, Deviance Information Criteria). Fourth column: Stratum-specific and site-wide predictions of cockle abundance (million of individuals) for the mesh scenario, with the corresponding sampling-based estimator shown in yellow.

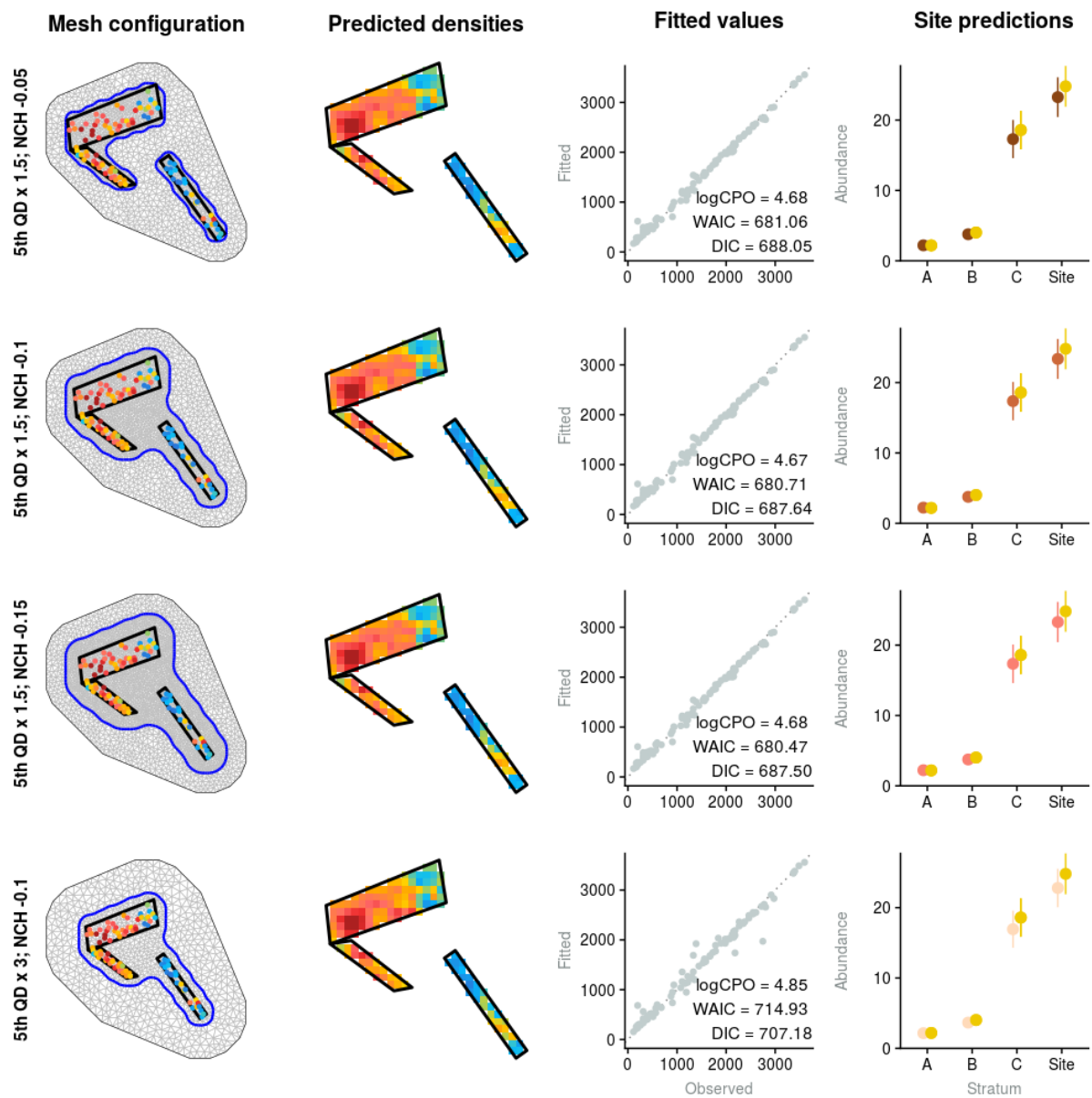


Figure A-2: Model fit and diagnostics for mesh scenarios (in rows) using a non-convex hull for Bowentown Beach. First column: mesh configuration with the strata highlighted in black and inner mesh area highlighted in blue. Points denote observations for the site, with cockle density scaling from blue to red. Second column: predictions at the square-metre scale resulting from the model; colours scale from 0 to the 97.5th quantile predicted across all scenarios for the site, the colour scale is site-specific. Third column: comparison of observed (X) against predicted densities (Y) for each mesh scenario, with the value of performance metrics for the scenario included in the bottom-right corner (logCPO, conditional predictive ordinate; WAIC, Watanabe-Akaike information criterion; and DIC, Deviance Information Criteria). Fourth column: Stratum-specific and site-wide predictions of cockle abundance (million of individuals) for the mesh scenario, with the corresponding sampling-based estimator shown in yellow.

A.2 Cockle Bay

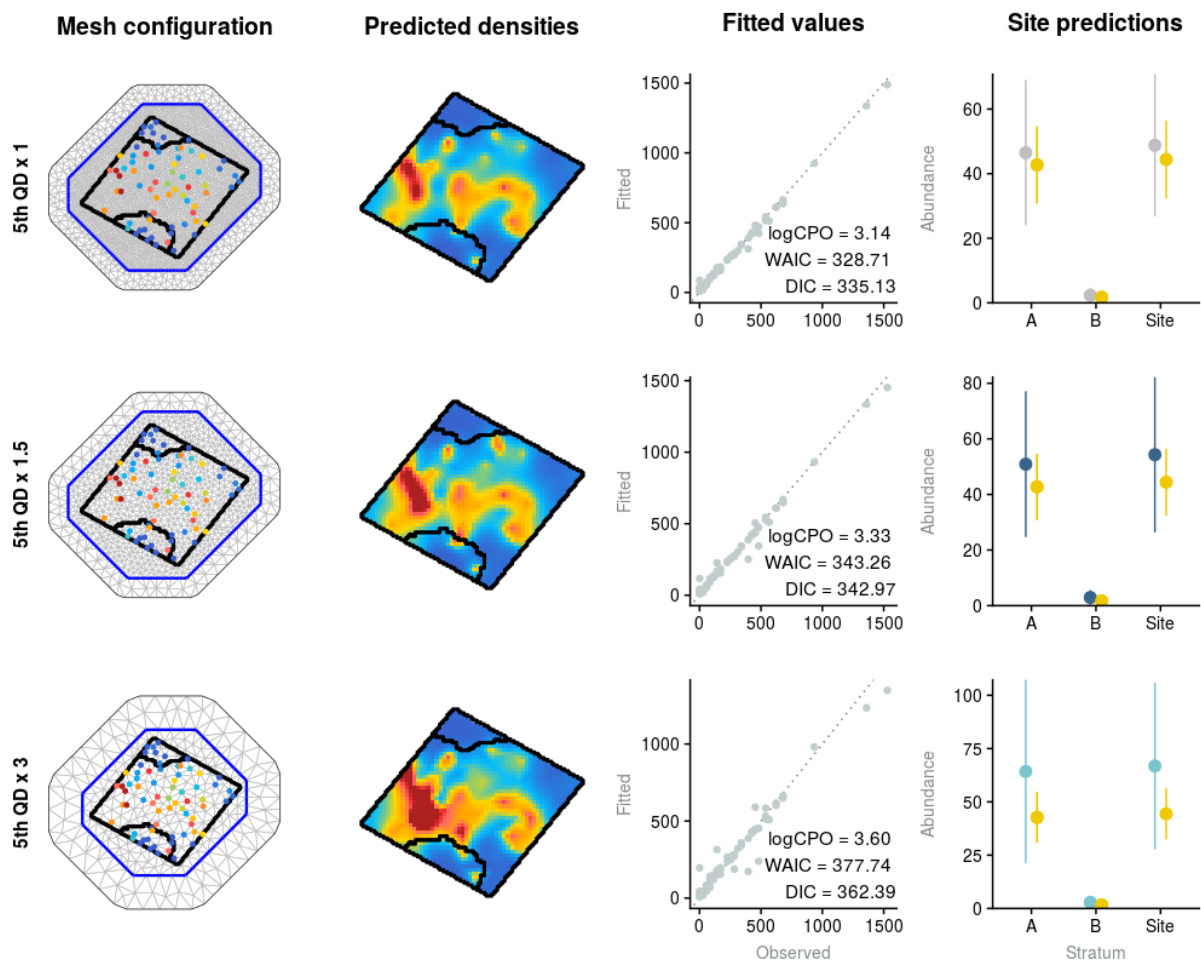


Figure A-3: Model fit and diagnostics for mesh scenarios (in rows) using a convex hull for Cockle Bay. First column: mesh configuration with the strata highlighted in black and inner mesh area highlighted in blue. Points denote observations for the site, with cockle density scaling from blue to red. Second column: predictions at the square-metre scale resulting from the model; colours scale from 0 to the 97.5th quantile predicted across all scenarios for the site, cells exceeding this threshold are shown in dark red, the colour scale is site-specific. Third column: comparison of observed (X) against predicted densities (Y) for each mesh scenario, with the value of performance metrics for the scenario included in the bottom-right corner (logCPO, conditional predictive ordinate; WAIC, Watanabe-Akaike information criterion; and DIC, Deviance Information Criteria). Fourth column: Stratum-specific and site-wide predictions of cockle abundance (million of individuals) for the mesh scenario, with the corresponding sampling-based estimator shown in yellow.

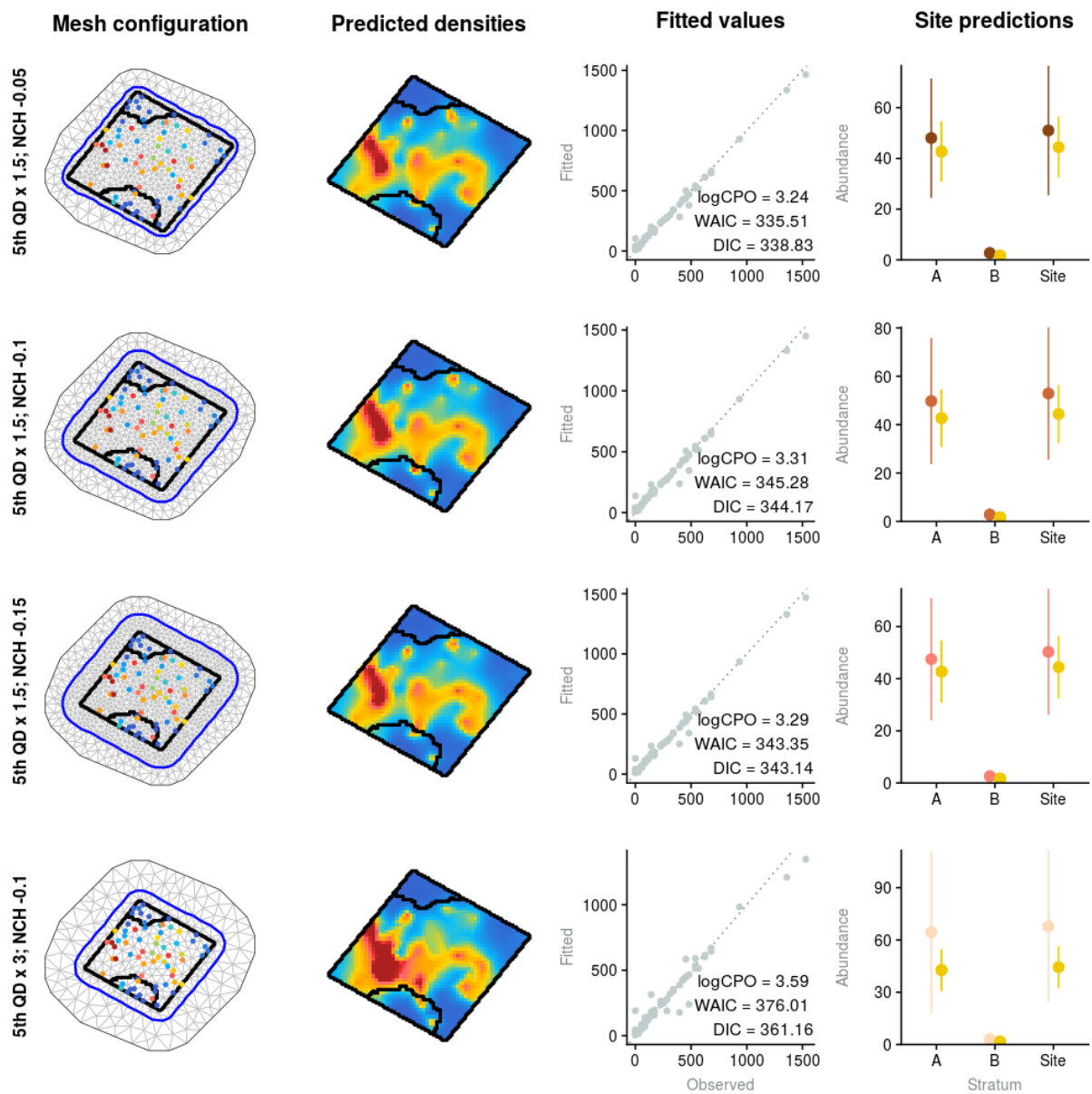


Figure A-4: Model fit and diagnostics for mesh scenarios (in rows) using a non-convex hull for Cockle Bay. First column: mesh configuration with the strata highlighted in black and inner mesh area highlighted in blue. Points denote observations for the site, with cockle density scaling from blue to red. Second column: predictions at the square-metre scale resulting from the model; colours scale from 0 to the 97.5th quantile predicted across all scenarios for the site, cells exceeding that threshold are shown in dark red, the colour scale is site-specific. Third column: comparison of observed (X) against predicted densities (Y) for each mesh scenario, with the value of performance metrics for the scenario included in the bottom-right corner (logCPO, conditional predictive ordinate; WAIC, Watanabe-Akaike information criterion; and DIC, Deviance Information Criteria). Fourth column: Stratum-specific and site-wide predictions of cockle abundance (million of individuals) for the mesh scenario, with the corresponding sampling-based estimator shown in yellow.

A.3 Eastern Beach

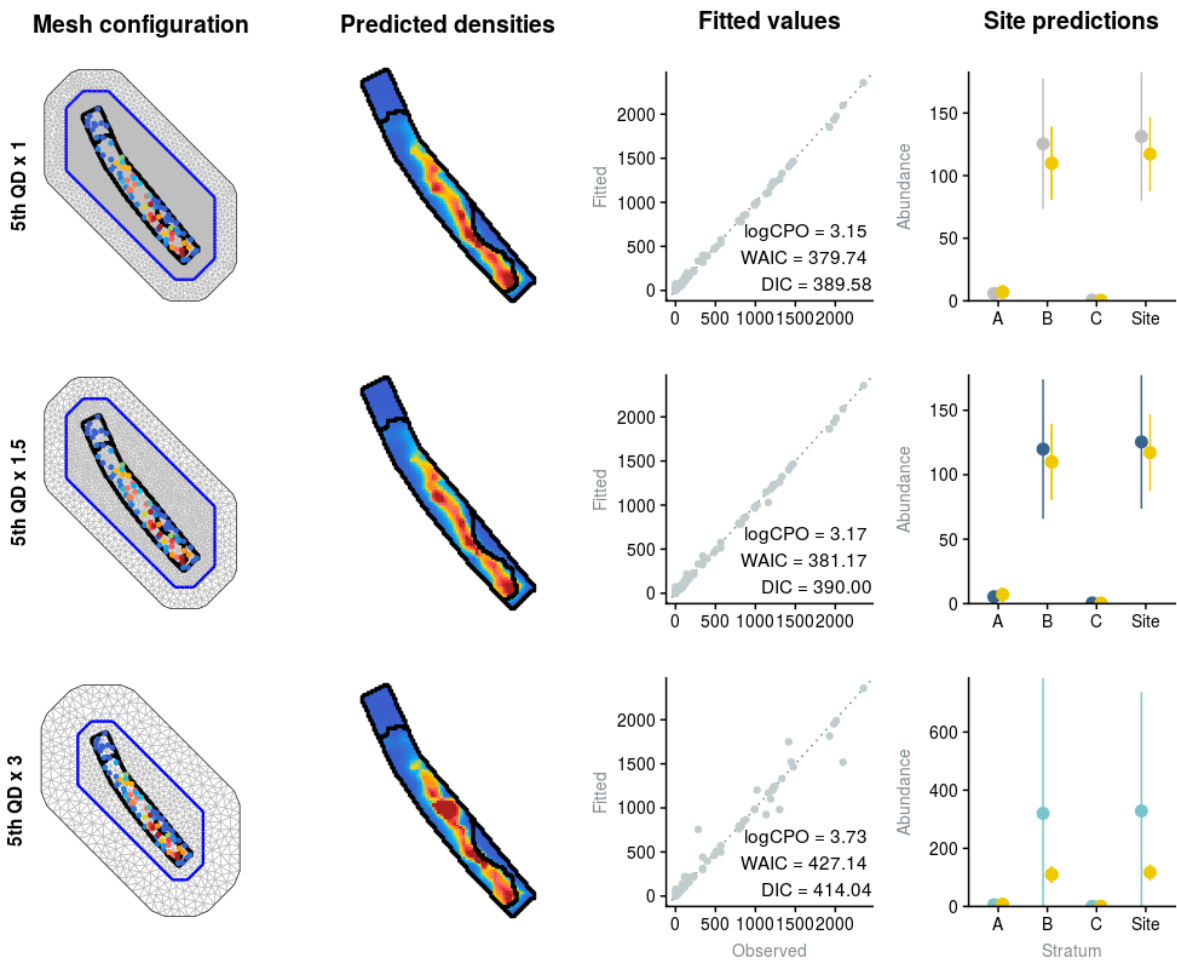


Figure A-5: Model fit and diagnostics for mesh scenarios (in rows) using a convex hull for Eastern Beach. First column: mesh configuration with the strata highlighted in black and inner mesh area highlighted in blue. Points denote observations for the site, with cockle density scaling from blue to red. Second column: predictions at the square-metre scale resulting from the model; colours scale from 0 to the 97.5th quantile predicted across all scenarios for the site, cells exceeding this threshold are shown in dark red, the colour scale is site-specific. Third column: comparison of observed (X) against predicted densities (Y) for each mesh scenario, with the value of performance metrics for the scenario included in the bottom-right corner (logCPO, conditional predictive ordinate; WAIC, Watanabe-Akaike information criterion; and DIC, Deviance Information Criteria). Fourth column: Stratum-specific and site-wide predictions of cockle abundance (million of individuals) for the mesh scenario, with the corresponding sampling-based estimator shown in yellow.

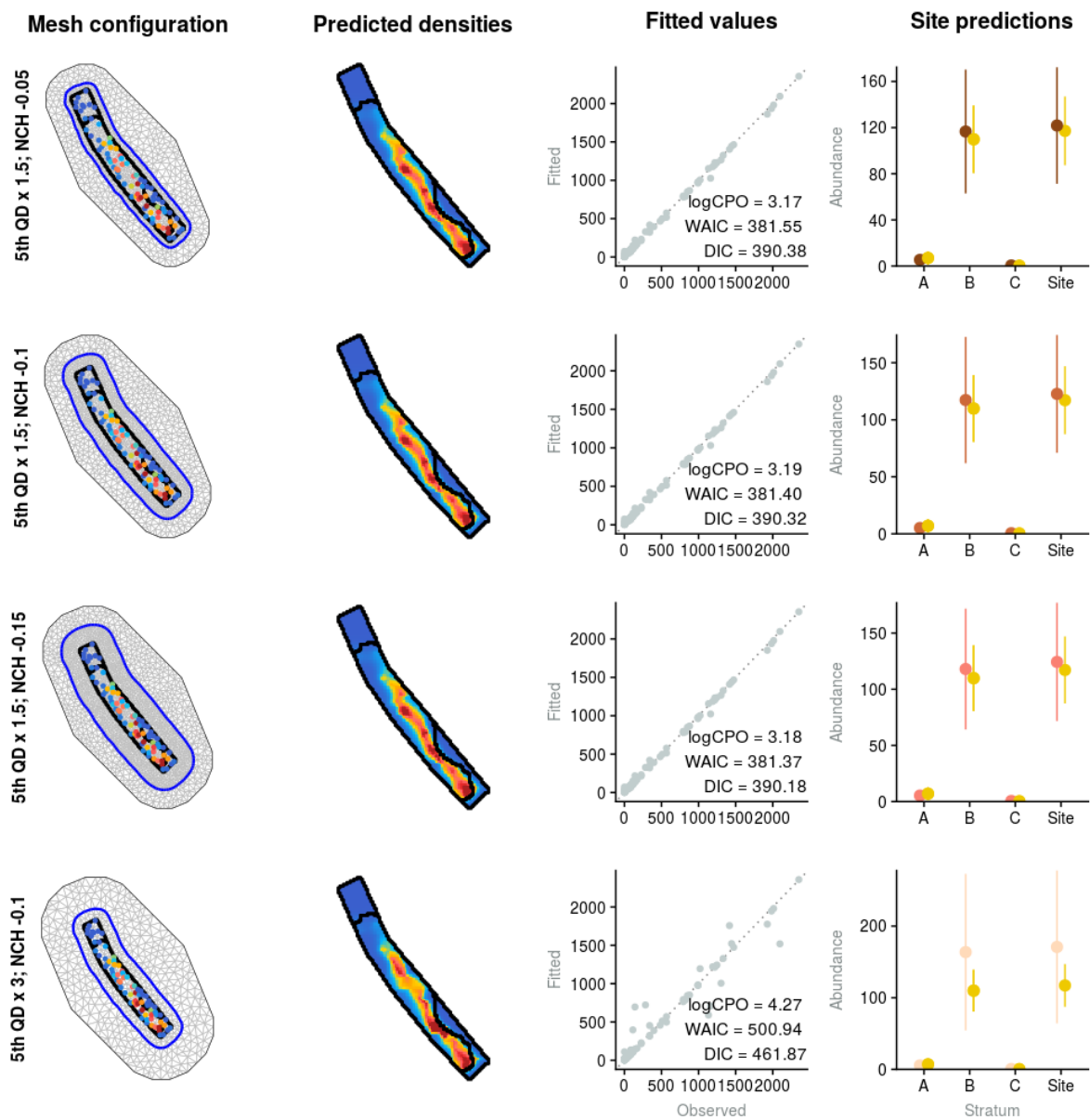


Figure A-6: Model fit and diagnostics for mesh scenarios (in rows) using a non-convex hull for Eastern Beach. First column: mesh configuration with the strata highlighted in black and inner mesh area highlighted in blue. Points denote observations for the site, with cockle density scaling from blue to red. Second column: predictions at the square-metre scale resulting from the model; colours scale from 0 to the 97.5th quantile predicted across all scenarios for the site, cells exceeding that threshold are shown in dark red, the colour scale is site-specific. Third column: comparison of observed (X) against predicted densities (Y) for each mesh scenario, with the value of performance metrics for the scenario included in the bottom-right corner (logCPO, conditional predictive ordinate; WAIC, Watanabe-Akaike information criterion; and DIC, Deviance Information Criteria). Fourth column: Stratum-specific and site-wide predictions of cockle abundance (million of individuals) for the mesh scenario, with the corresponding sampling-based estimator shown in yellow.

A.4 Grahams Beach

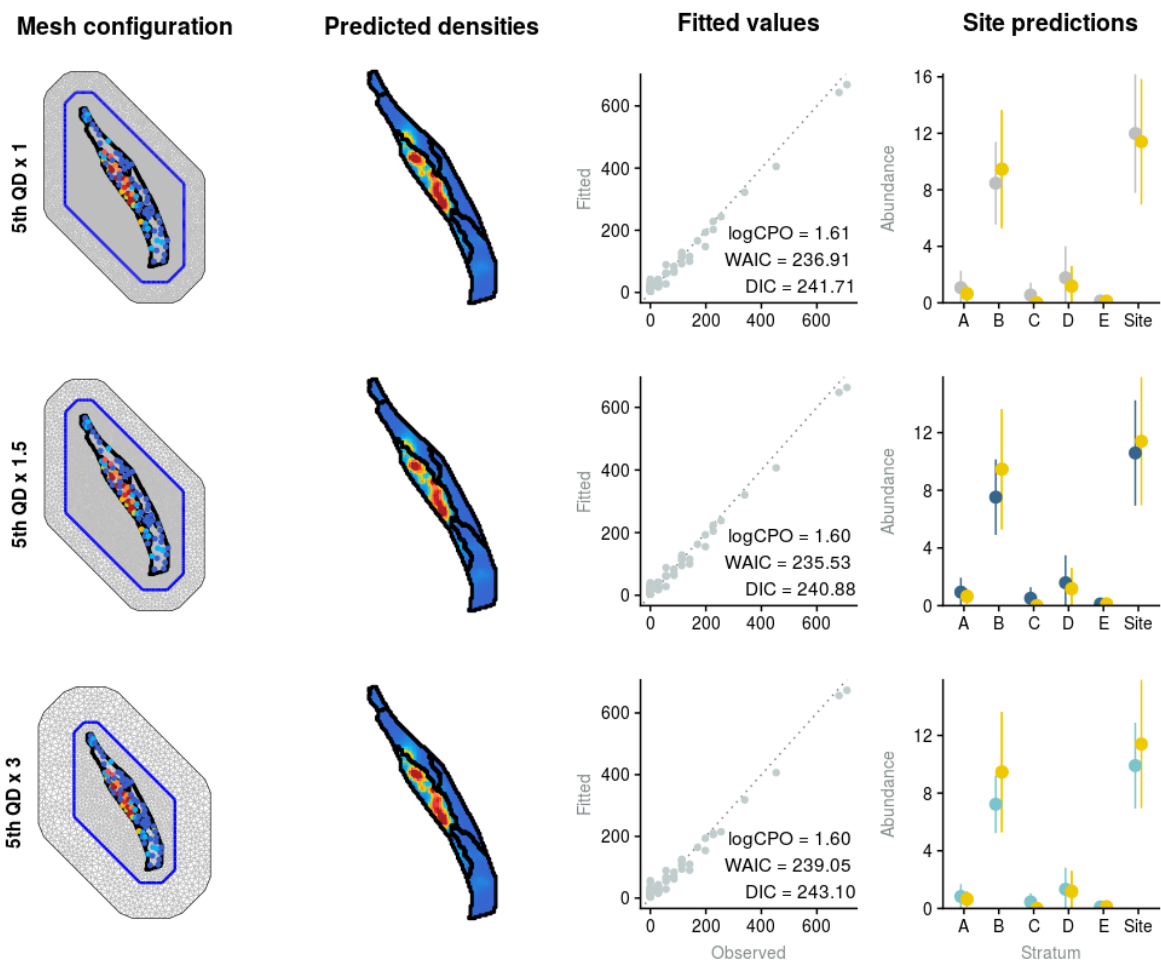


Figure A-7: Model fit and diagnostics for mesh scenarios (in rows) using a convex hull for Grahams Beach. First column: mesh configuration with the strata highlighted in black and inner mesh area highlighted in blue. Points denote observations for the site, with cockle density scaling from blue to red. Second column: predictions at the square-metre scale resulting from the model; colours scale from 0 to the 97.5th quantile predicted across all scenarios for the site, cells exceeding this threshold are shown in dark red, the colour scale is site-specific. Third column: comparison of observed (X) against predicted densities (Y) for each mesh scenario, with the value of performance metrics for the scenario included in the bottom-right corner (logCPO, conditional predictive ordinate; WAIC, Watanabe-Akaike information criterion; and DIC, Deviance Information Criteria). Fourth column: Stratum-specific and site-wide predictions of cockle abundance (million of individuals) for the mesh scenario, with the corresponding sampling-based estimator shown in yellow.

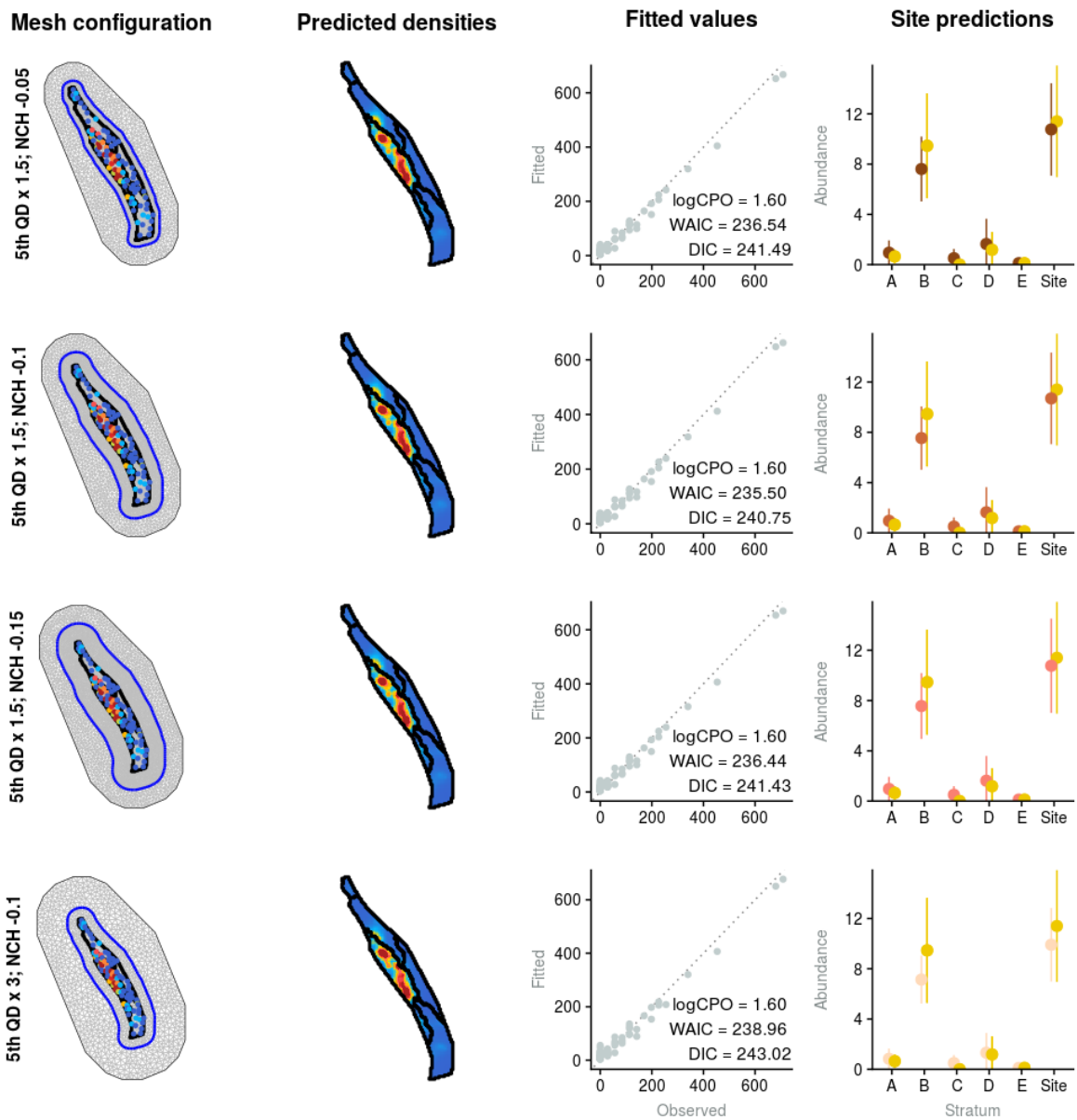


Figure A-8: Model fit and diagnostics for mesh scenarios (in rows) using a non-convex hull for Grahams Beach. First column: mesh configuration with the strata highlighted in black and inner mesh area highlighted in blue. Points denote observations for the site, with cockle density scaling from blue to red. Second column: predictions at the square-metre scale resulting from the model; colours scale from 0 to the 97.5th quantile predicted across all scenarios for the site, cells exceeding that threshold are shown in dark red, the colour scale is site-specific. Third column: comparison of observed (X) against predicted densities (Y) for each mesh scenario, with the value of performance metrics for the scenario included in the bottom-right corner (logCPO, conditional predictive ordinate; WAIC, Watanabe-Akaike information criterion; and DIC, Deviance Information Criteria). Fourth column: Stratum-specific and site-wide predictions of cockle abundance (million of individuals) for the mesh scenario, with the corresponding sampling-based estimator shown in yellow.

A.5 Little Waihi Estuary

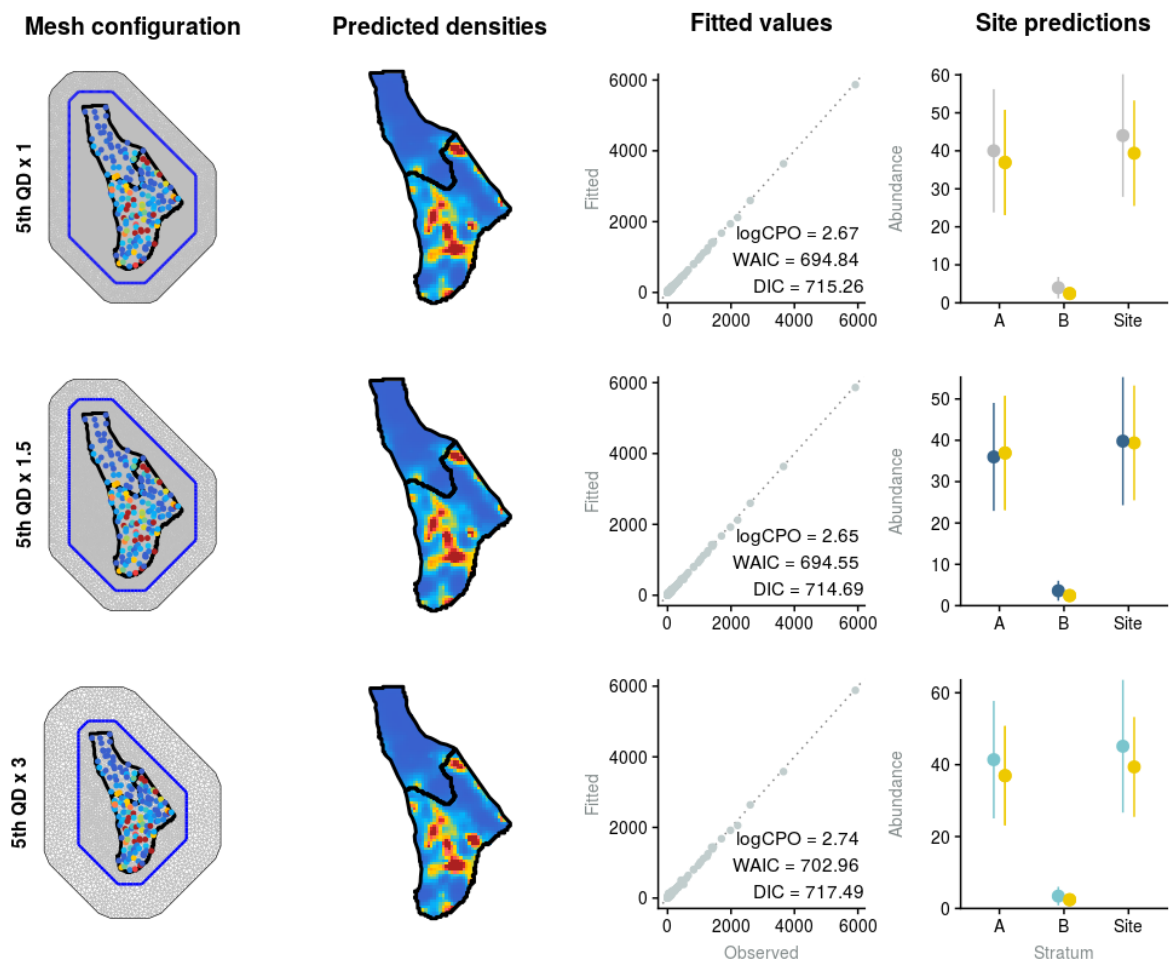


Figure A-9: Model fit and diagnostics for mesh scenarios (in rows) using a convex hull for Little Waihi Estuary. First column: mesh configuration with the strata highlighted in black and inner mesh area highlighted in blue. Points denote observations for the site, with cockle density scaling from blue to red. Second column: predictions at the square-metre scale resulting from the model; colours scale from 0 to the 97.5th quantile predicted across all scenarios for the site, cells exceeding this threshold are shown in dark red, the colour scale is site-specific. Third column: comparison of observed (X) against predicted densities (Y) for each mesh scenario, with the value of performance metrics for the scenario included in the bottom-right corner (logCPO, conditional predictive ordinate; WAIC, Watanabe-Akaike information criterion; and DIC, Deviance Information Criteria). Fourth column: Stratum-specific and site-wide predictions of cockle abundance (million of individuals) for the mesh scenario, with the corresponding sampling-based estimator shown in yellow.

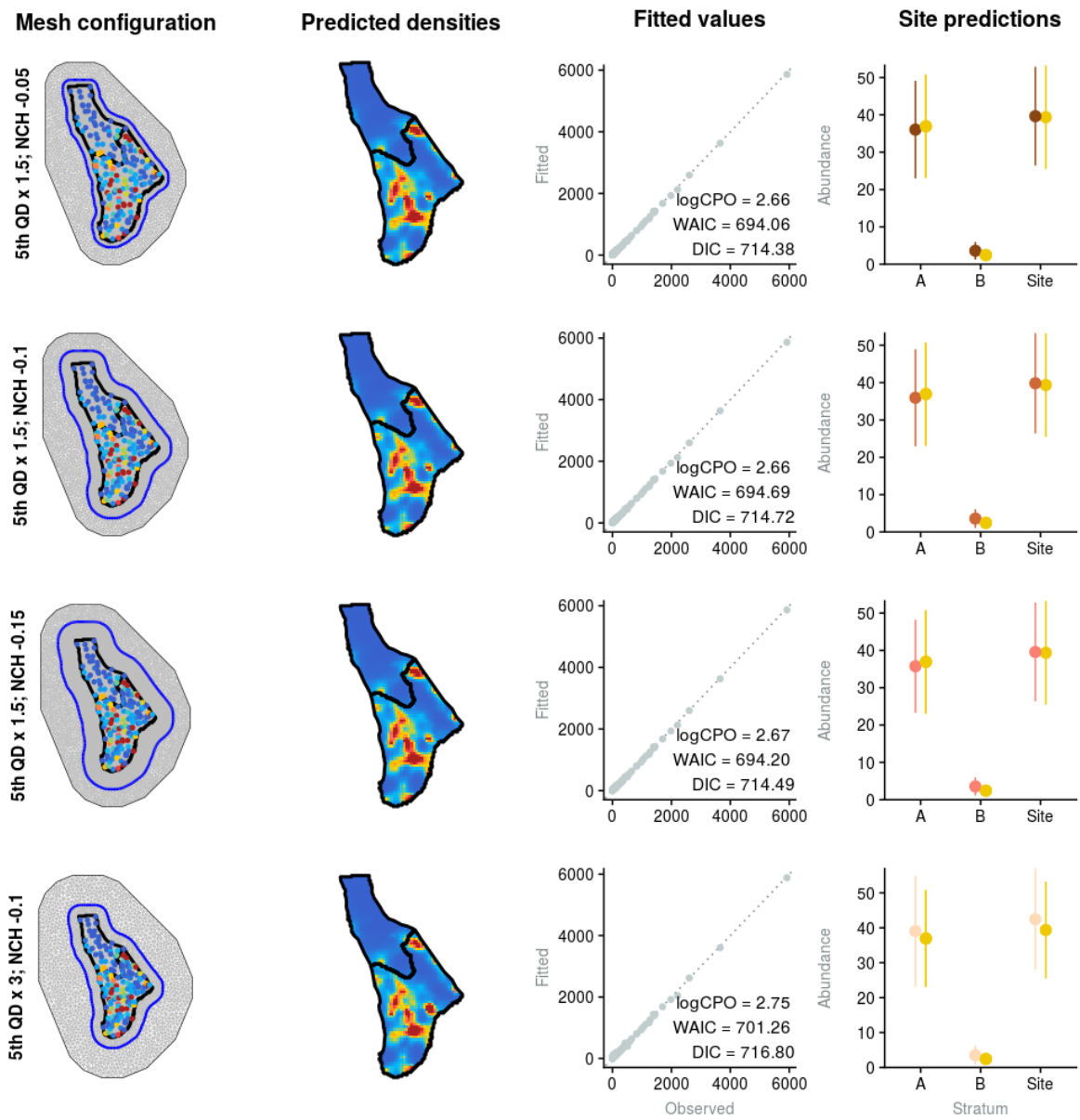


Figure A-10: Model fit and diagnostics for mesh scenarios (in rows) using a non-convex hull for Little Waihi Estuary. First column: mesh configuration with the strata highlighted in black and inner mesh area highlighted in blue. Points denote observations for the site, with cockle density scaling from blue to red. Second column: predictions at the square-metre scale resulting from the model; colours scale from 0 to the 97.5th quantile predicted across all scenarios for the site, cells exceeding that threshold are shown in dark red, the colour scale is site-specific. Third column: comparison of observed (X) against predicted densities (Y) for each mesh scenario, with the value of performance metrics for the scenario included in the bottom-right corner (logCPO, conditional predictive ordinate; WAIC, Watanabe-Akaike information criterion; and DIC, Deviance Information Criteria). Fourth column: Stratum-specific and site-wide predictions of cockle abundance (million of individuals) for the mesh scenario, with the corresponding sampling-based estimator shown in yellow.

A.6 Pataua Estuary

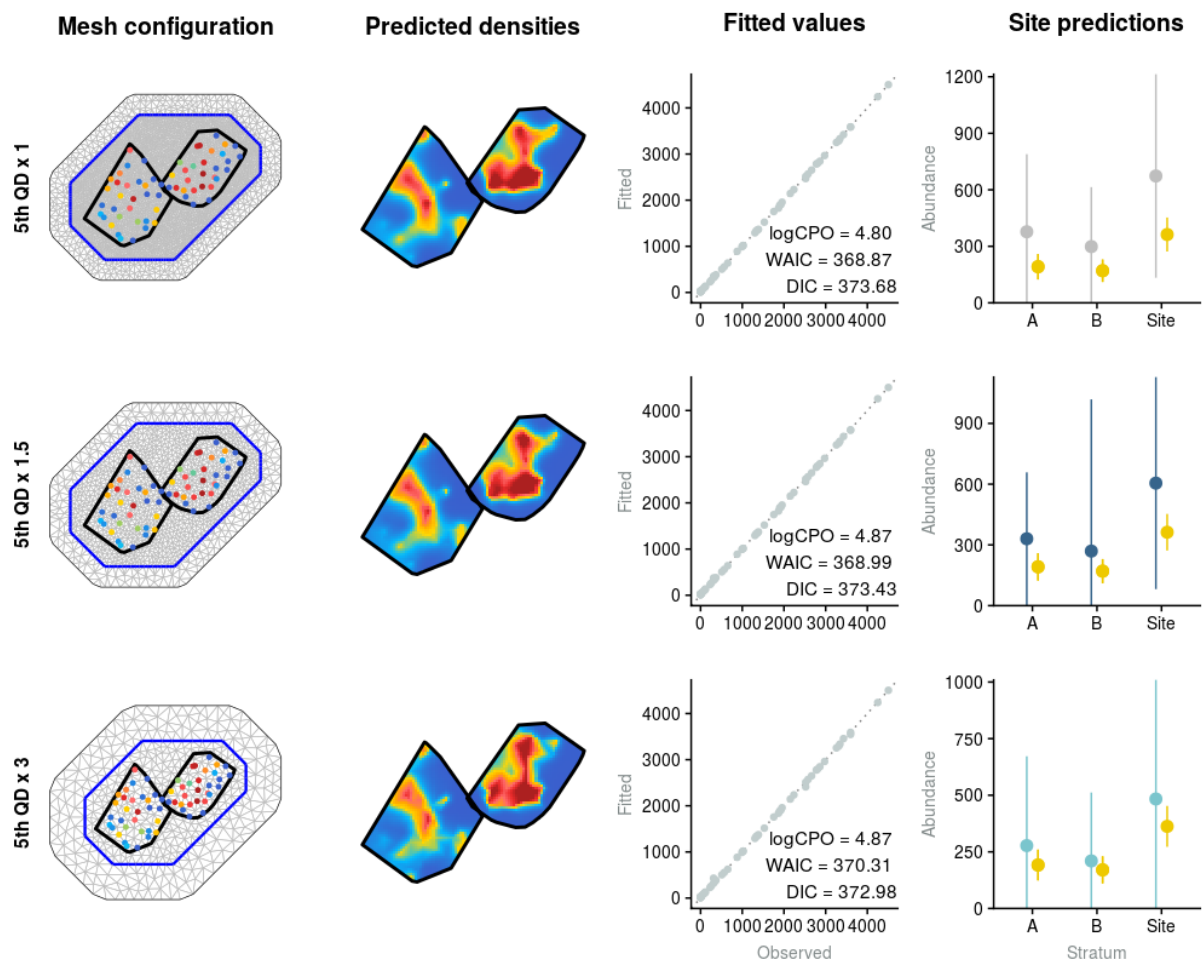


Figure A-11: Model fit and diagnostics for mesh scenarios (in rows) using a convex hull for Pataua Estuary. First column: mesh configuration with the strata highlighted in black and inner mesh area highlighted in blue. Points denote observations for the site, with cockle density scaling from blue to red. Second column: predictions at the square-metre scale resulting from the model; colours scale from 0 to the 97.5th quantile predicted across all scenarios for the site, cells exceeding this threshold are shown in dark red, the colour scale is site-specific. Third column: comparison of observed (X) against predicted densities (Y) for each mesh scenario, with the value of performance metrics for the scenario included in the bottom-right corner (logCPO, conditional predictive ordinate; WAIC, Watanabe-Akaike information criterion; and DIC, Deviance Information Criteria). Fourth column: Stratum-specific and site-wide predictions of cockle abundance (million of individuals) for the mesh scenario, with the corresponding sampling-based estimator shown in yellow.

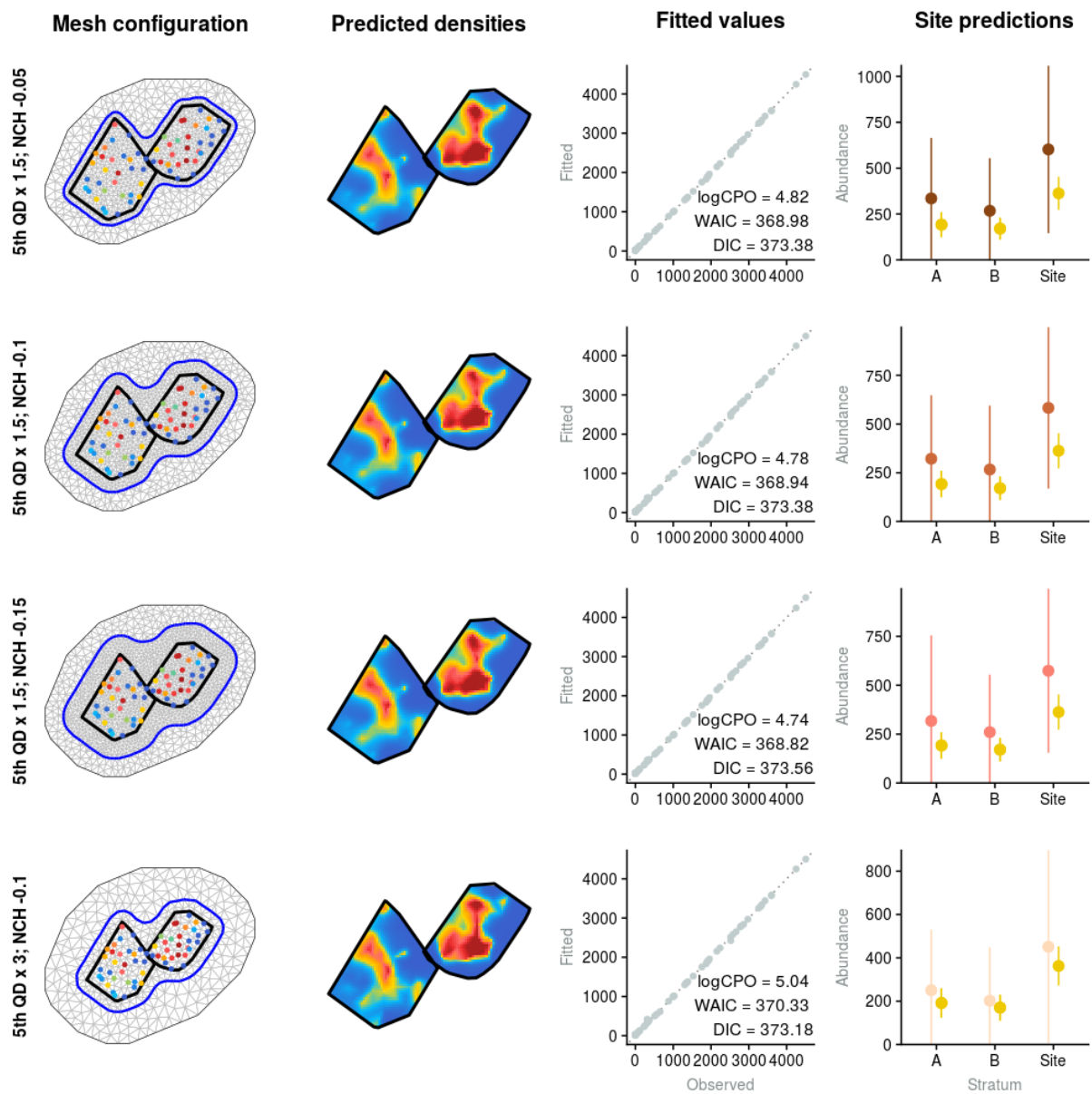


Figure A-12: Model fit and diagnostics for mesh scenarios (in rows) using a non-convex hull for Pataua Estuary. First column: mesh configuration with the strata highlighted in black and inner mesh area highlighted in blue. Points denote observations for the site, with cockle density scaling from blue to red. Second column: predictions at the square-metre scale resulting from the model; colours scale from 0 to the 97.5th quantile predicted across all scenarios for the site, the cells exceeding that threshold are shown in dark red, the colour scale is site-specific. Third column: comparison of observed (X) against predicted densities (Y) for each mesh scenario, with the value of performance metrics for the scenario included in the bottom-right corner (logCPO, conditional predictive ordinate; WAIC, Watanabe-Akaike information criterion; and DIC, Deviance Information Criteria). Fourth column: Stratum-specific and site-wide predictions of cockle abundance (million of individuals) for the mesh scenario, with the corresponding sampling-based estimator shown in yellow.

A.7 Raglan Harbour

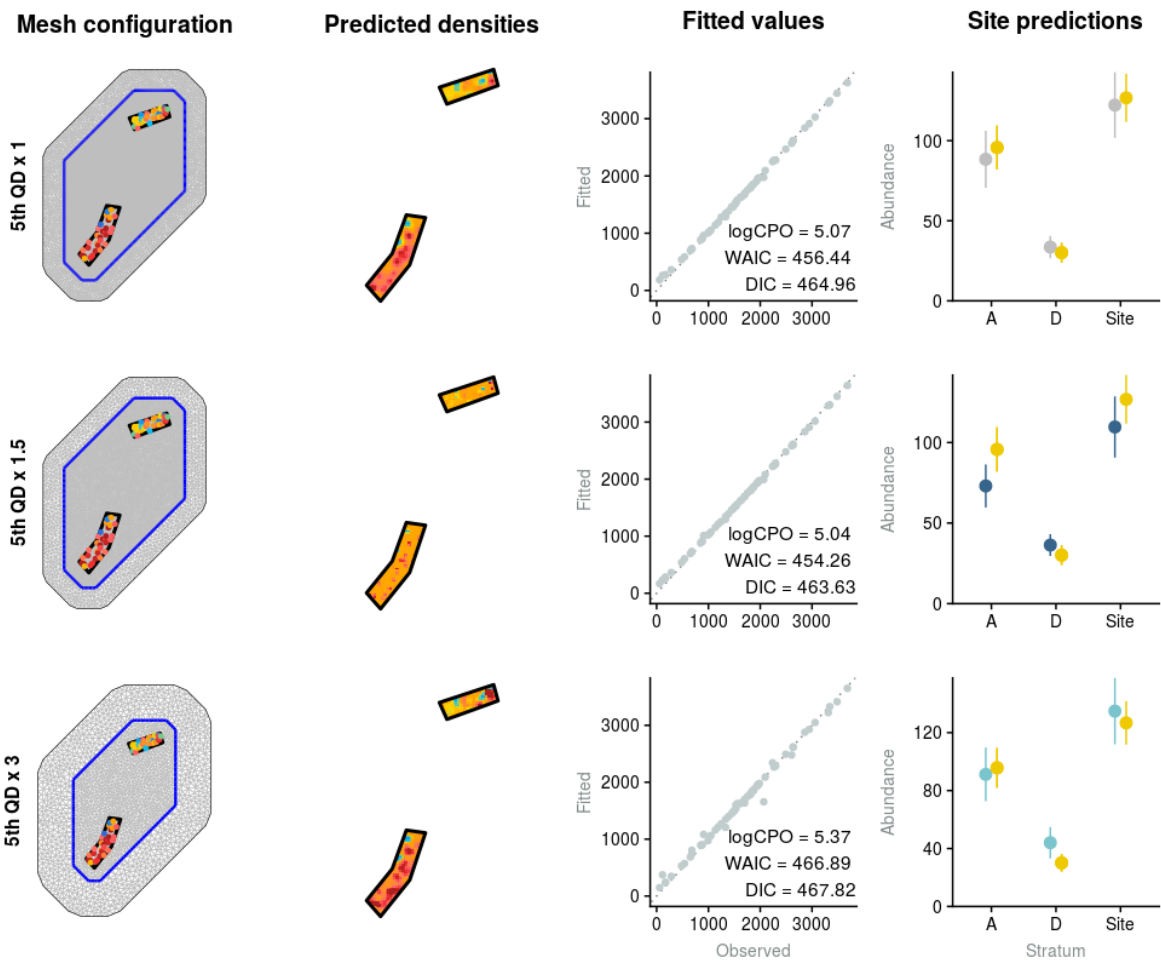


Figure A-13: Model fit and diagnostics for mesh scenarios (in rows) using a convex hull for Raglan Harbour. First column: mesh configuration with the strata highlighted in black and inner mesh area highlighted in blue. Points denote observations for the site, with cockle density scaling from blue to red. Second column: predictions at the square-metre scale resulting from the model; colours scale from 0 to the 97.5th quantile predicted across all scenarios for the site, cells exceeding this threshold are shown in dark red, the colour scale is site-specific. Third column: comparison of observed (X) against predicted densities (Y) for each mesh scenario, with the value of performance metrics for the scenario included in the bottom-right corner (logCPO, conditional predictive ordinate; WAIC, Watanabe-Akaike information criterion; and DIC, Deviance Information Criteria). Fourth column: Stratum-specific and site-wide predictions of cockle abundance (million of individuals) for the mesh scenario, with the corresponding sampling-based estimator shown in yellow.

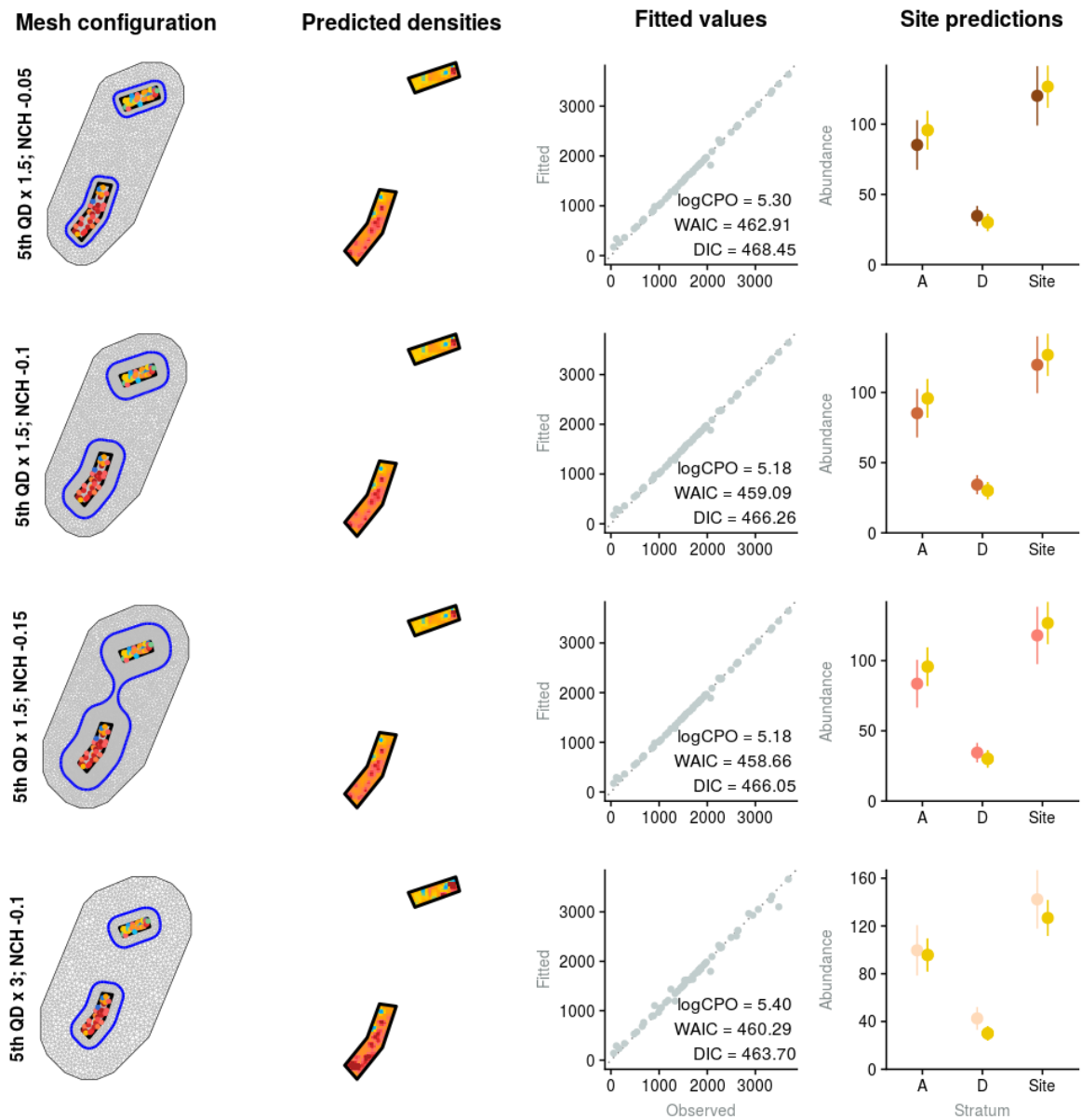


Figure A-14: Model fit and diagnostics for mesh scenarios (in rows) using a non-convex hull for Raglan Harbour. First column: mesh configuration with the strata highlighted in black and inner mesh area highlighted in blue. Points denote observations for the site, with cockle density scaling from blue to red. Second column: predictions at the square-metre scale resulting from the model; colours scale from 0 to the 97.5th quantile predicted across all scenarios for the site, the colour scale is site-specific. Third column: comparison of observed (X) against predicted densities (Y) for each mesh scenario, with the value of performance metrics for the scenario included in the bottom-right corner (logCPO, conditional predictive ordinate; WAIC, Watanabe-Akaike information criterion; and DIC, Deviance Information Criteria). Fourth column: Stratum-specific and site-wide predictions of cockle abundance (million of individuals) for the mesh scenario, with the corresponding sampling-based estimator shown in yellow.

A.8 Tairua Harbour

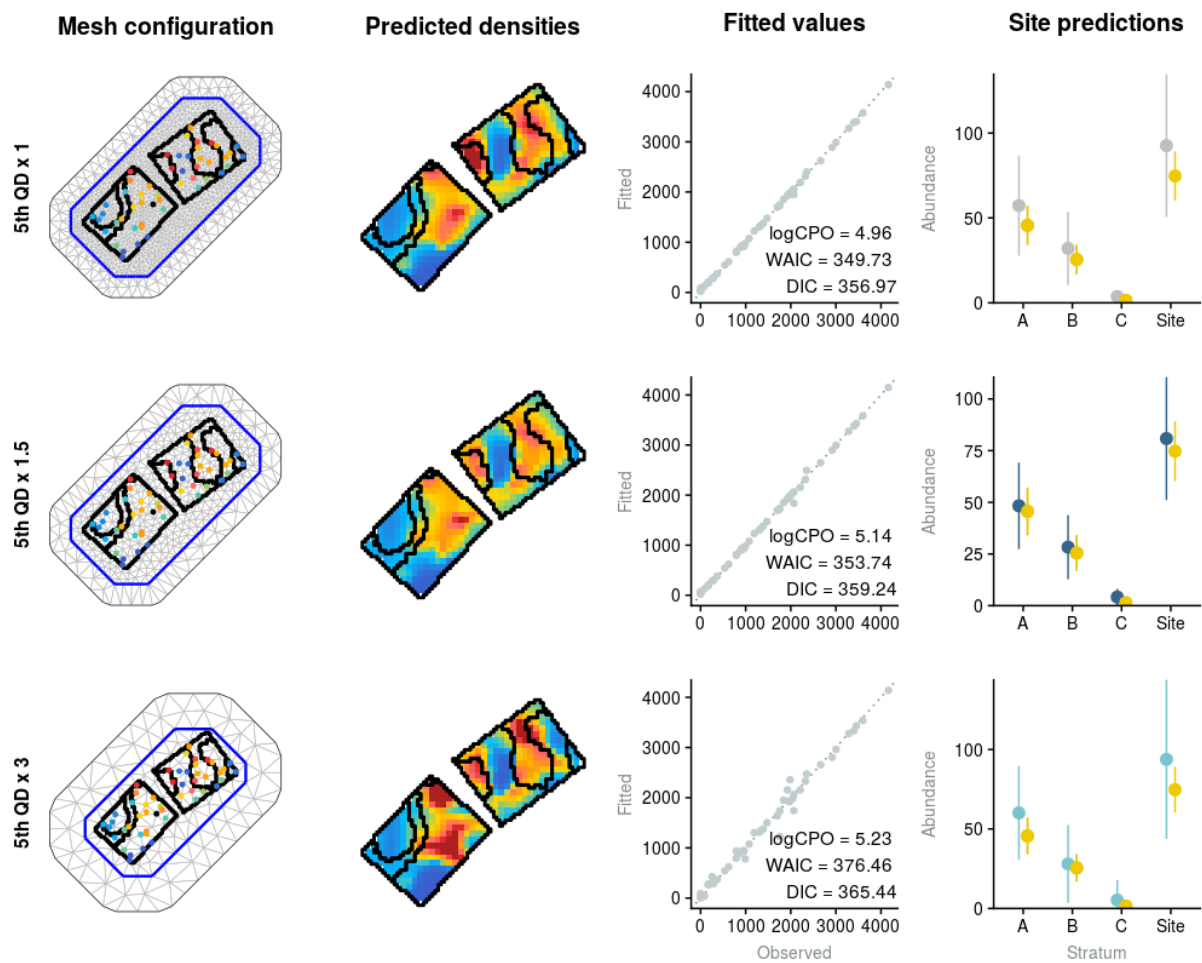


Figure A-15: Model fit and diagnostics for mesh scenarios (in rows) using a convex hull for Tairua Harbour. First column: mesh configuration with the strata highlighted in black and inner mesh area highlighted in blue. Points denote observations for the site, with cockle density scaling from blue to red. Second column: predictions at the square-metre scale resulting from the model; colours scale from 0 to the 97.5th quantile predicted across all scenarios for the site, cells exceeding this threshold are shown in dark red, the colour scale is site-specific. Third column: comparison of observed (X) against predicted densities (Y) for each mesh scenario, with the value of performance metrics for the scenario included in the bottom-right corner (logCPO, conditional predictive ordinate; WAIC, Watanabe-Akaike information criterion; and DIC, Deviance Information Criteria). Fourth column: Stratum-specific and site-wide predictions of cockle abundance (million of individuals) for the mesh scenario, with the corresponding sampling-based estimator shown in yellow.

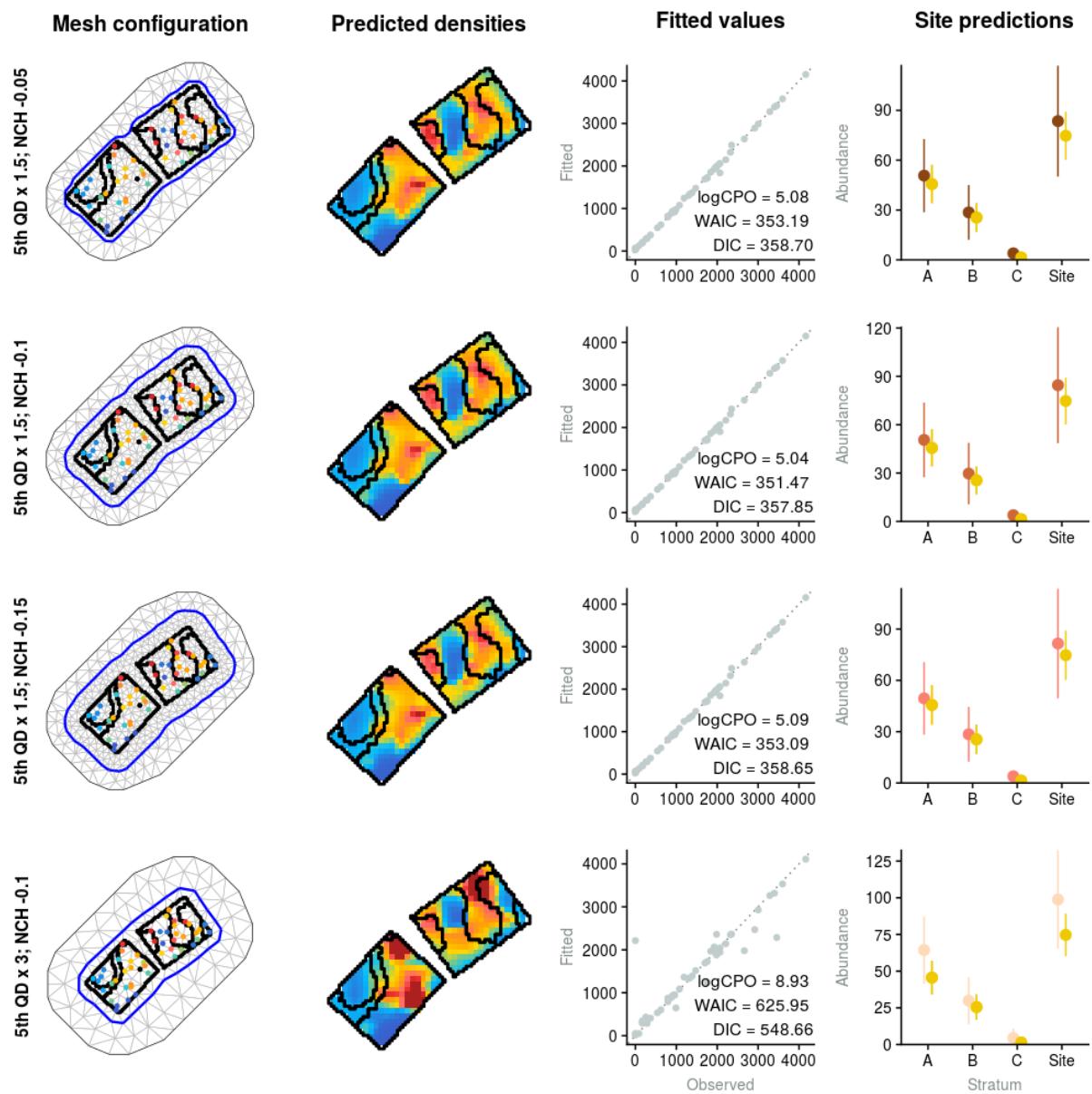


Figure A-16: Model fit and diagnostics for mesh scenarios (in rows) using a non-convex hull for Tairua Harbour. First column: mesh configuration with the strata highlighted in black and inner mesh area highlighted in blue. Points denote observations for the site, with cockle density scaling from blue to red. Second column: predictions at the square-metre scale resulting from the model; colours scale from 0 to the 97.5th quantile predicted across all scenarios for the site, cells exceeding that threshold are shown in dark red, the colour scale is site-specific. Third column: comparison of observed (X) against predicted densities (Y) for each mesh scenario, with the value of performance metrics for the scenario included in the bottom-right corner (logCPO, conditional predictive ordinate; WAIC, Watanabe-Akaike information criterion; and DIC, Deviance Information Criteria). Fourth column: Stratum-specific and site-wide predictions of cockle abundance (million of individuals) for the mesh scenario, with the corresponding sampling-based estimator shown in yellow.

A.9 Umupuia Beach

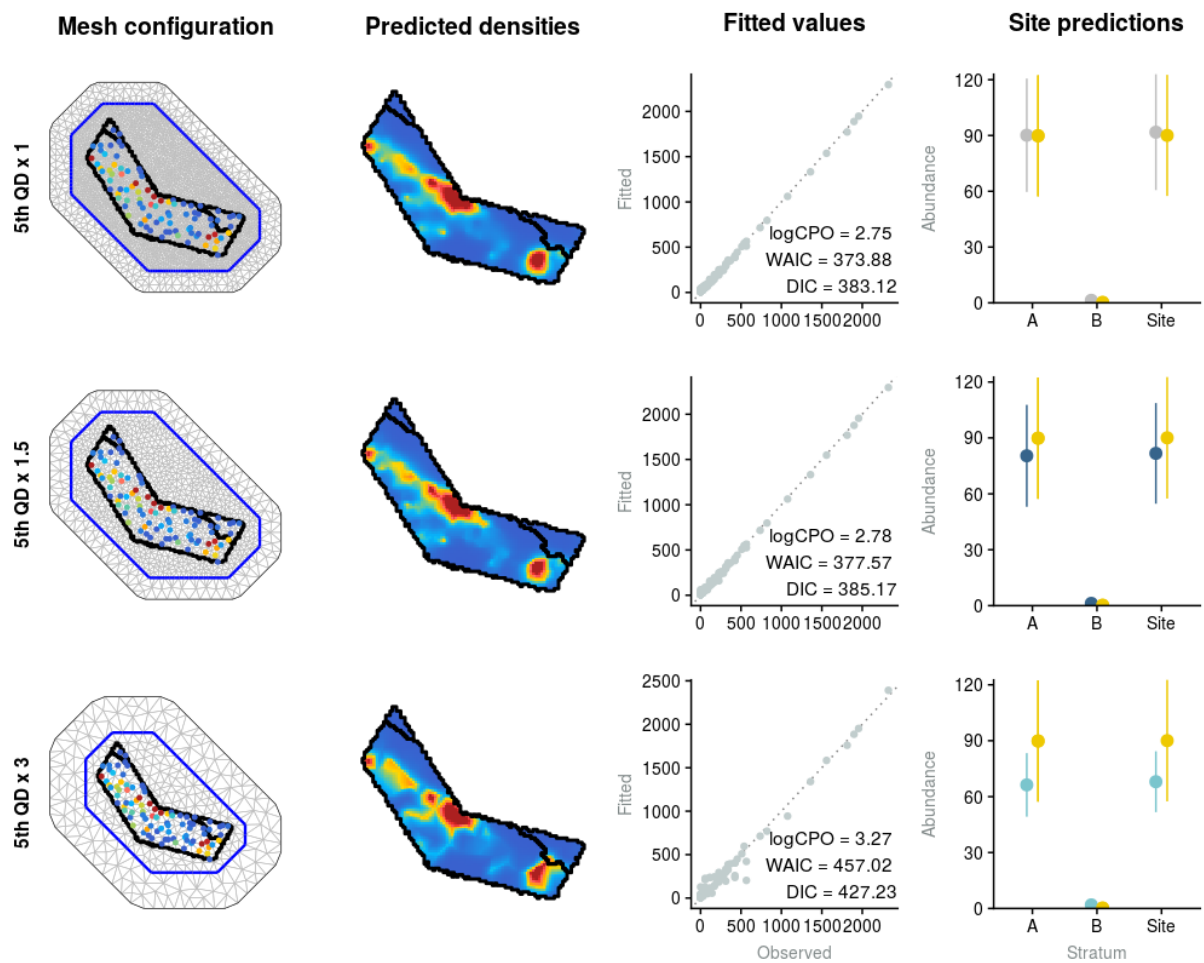


Figure A-17: Model fit and diagnostics for mesh scenarios (in rows) using a convex hull for Umupuia Beach. First column: mesh configuration with the strata highlighted in black and inner mesh area highlighted in blue. Points denote observations for the site, with cockle density scaling from blue to red. Second column: predictions at the square-metre scale resulting from the model; colours scale from 0 to the 97.5th quantile predicted across all scenarios for the site, cells exceeding this threshold are shown in dark red, the colour scale is site-specific. Third column: comparison of observed (X) against predicted densities (Y) for each mesh scenario, with the value of performance metrics for the scenario included in the bottom-right corner (logCPO, conditional predictive ordinate; WAIC, Watanabe-Akaike information criterion; and DIC, Deviance Information Criteria). Fourth column: Stratum-specific and site-wide predictions of cockle abundance (million of individuals) for the mesh scenario, with the corresponding sampling-based estimator shown in yellow.

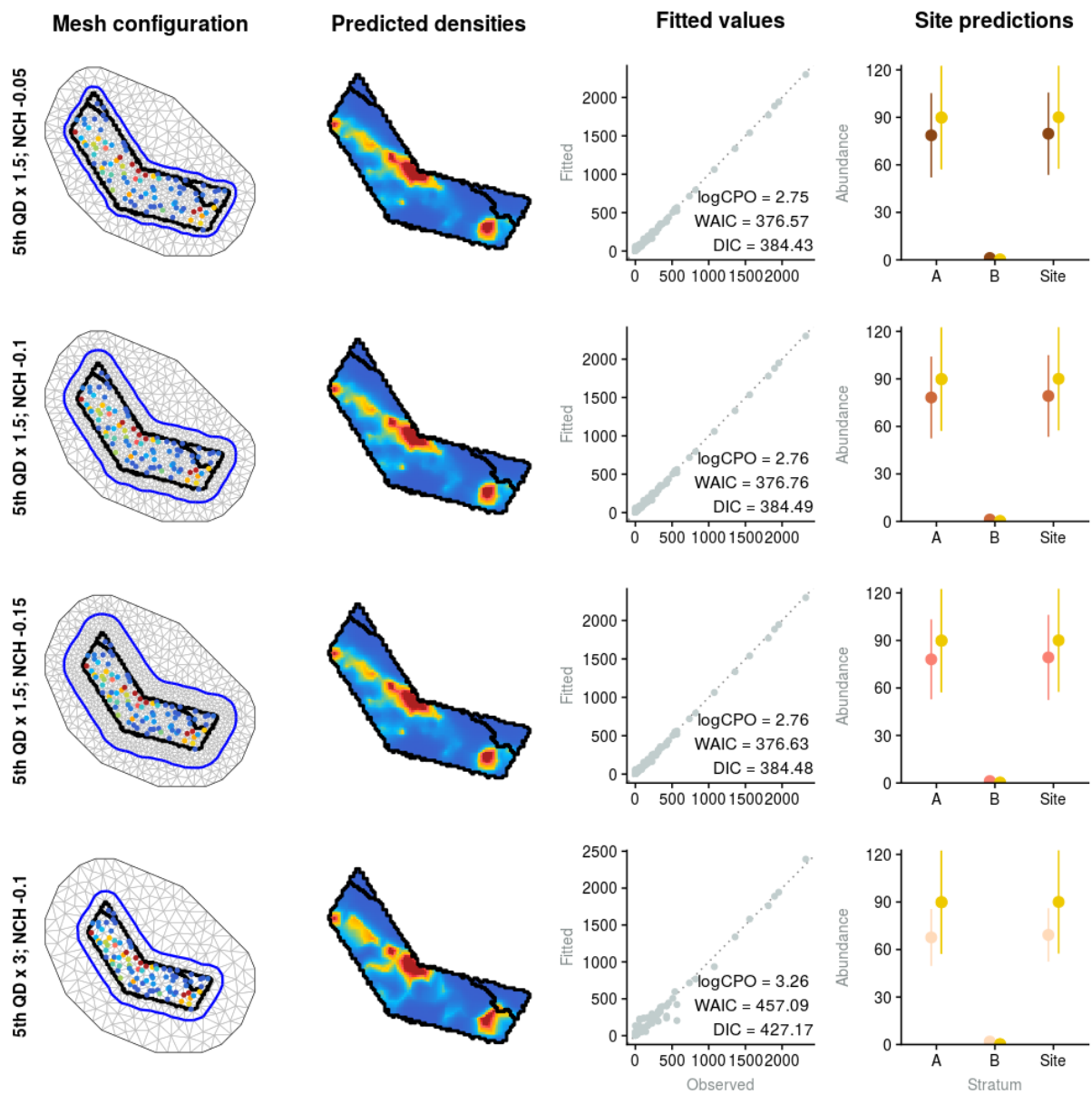


Figure A-18: Model fit and diagnostics for mesh scenarios (in rows) using a non-convex hull for Umupuia Beach. First column: mesh configuration with the strata highlighted in black and inner mesh area highlighted in blue. Points denote observations for the site, with cockle density scaling from blue to red. Second column: predictions at the square-metre scale resulting from the model; colours scale from 0 to the 97th quantile predicted across all scenarios for the site, cells exceeding that threshold are shown in dark red, the colour scale is site-specific. Third column: comparison of observed (X) against predicted densities (Y) for each mesh scenario, with the value of performance metrics for the scenario included in the bottom-right corner (logCPO, conditional predictive ordinate; WAIC, Watanabe-Akaike information criterion; and DIC, Deviance Information Criteria). Fourth column: Stratum-specific and site-wide predictions of cockle abundance (million of individuals) for the mesh scenario, with the corresponding sampling-based estimator shown in yellow.

A.10 Waiotahē Estuary

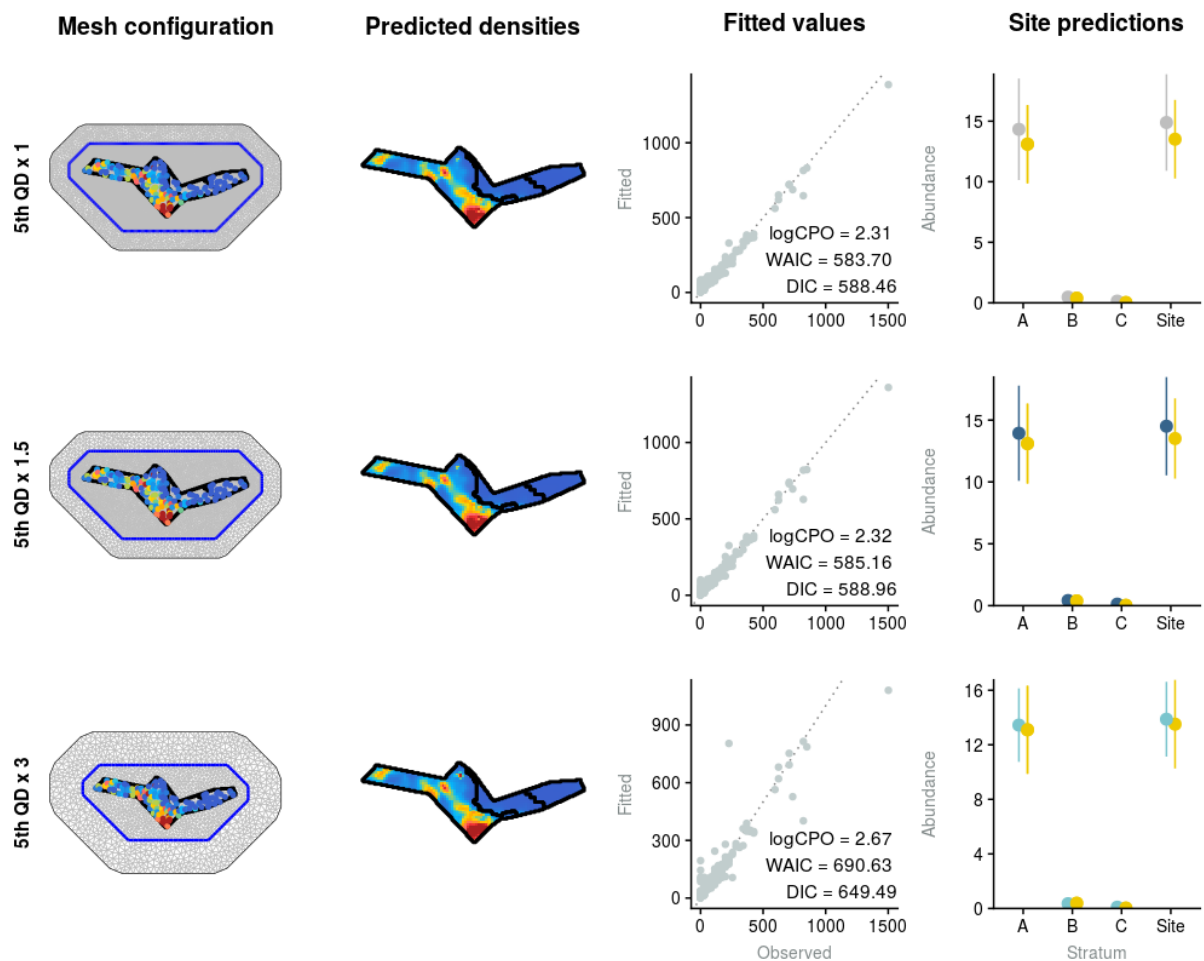


Figure A-19: Model fit and diagnostics for mesh scenarios (in rows) using a convex hull for Waiotahē Estuary. First column: mesh configuration with the strata highlighted in black and inner mesh area highlighted in blue. Points denote observations for the site, with cockle density scaling from blue to red. Second column: predictions at the square-metre scale resulting from the model; colours scale from 0 to the 97.5th quantile predicted across all scenarios for the site, cells exceeding this threshold are shown in dark red, the colour scale is site-specific. Third column: comparison of observed (X) against predicted densities (Y) for each mesh scenario, with the value of performance metrics for the scenario included in the bottom-right corner (logCPO, conditional predictive ordinate; WAIC, Watanabe-Akaike information criterion; and DIC, Deviance Information Criteria). Fourth column: Stratum-specific and site-wide predictions of cockle abundance (million of individuals) for the mesh scenario, with the corresponding sampling-based estimator shown in yellow.

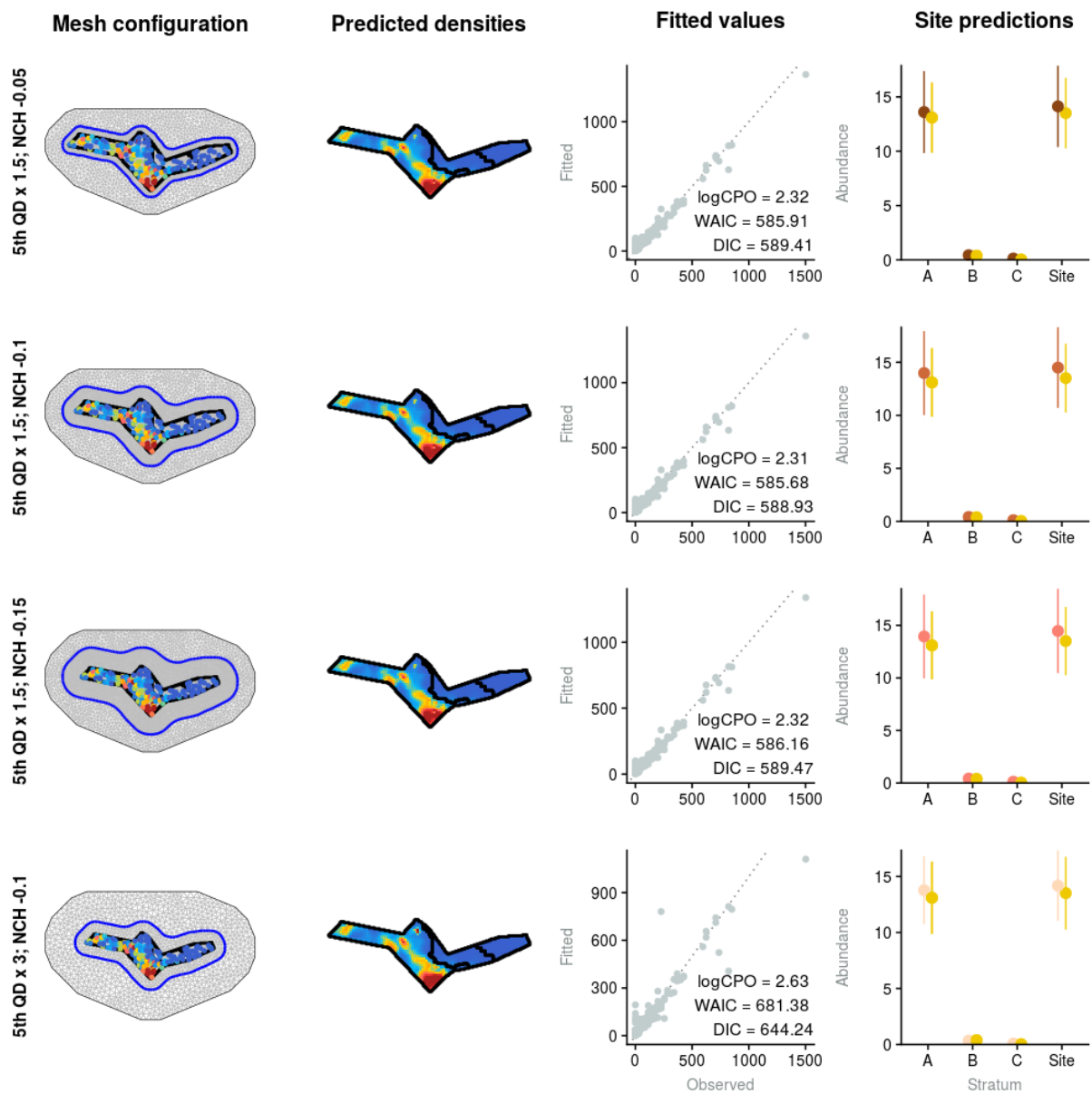


Figure A-20: Model fit and diagnostics for mesh scenarios (in rows) using a non-convex hull for Waiotahi Estuary. First column: mesh configuration with the strata highlighted in black and inner mesh area highlighted in blue. Points denote observations for the site, with cockle density scaling from blue to red. Second column: predictions at the square-metre scale resulting from the model; colours scale from 0 to the 97.5th quantile predicted across all scenarios for the site, cells exceeding that threshold are shown in dark red, the colour scale is site-specific. Third column: comparison of observed (X) against predicted densities (Y) for each mesh scenario, with the value of performance metrics for the scenario included in the bottom-right corner (logCPO, conditional predictive ordinate; WAIC, Watanabe-Akaike information criterion; and DIC, Deviance Information Criteria). Fourth column: Stratum-specific and site-wide predictions of cockle abundance (million of individuals) for the mesh scenario, with the corresponding sampling-based estimator shown in yellow.

A.11 Whangateau Harbour

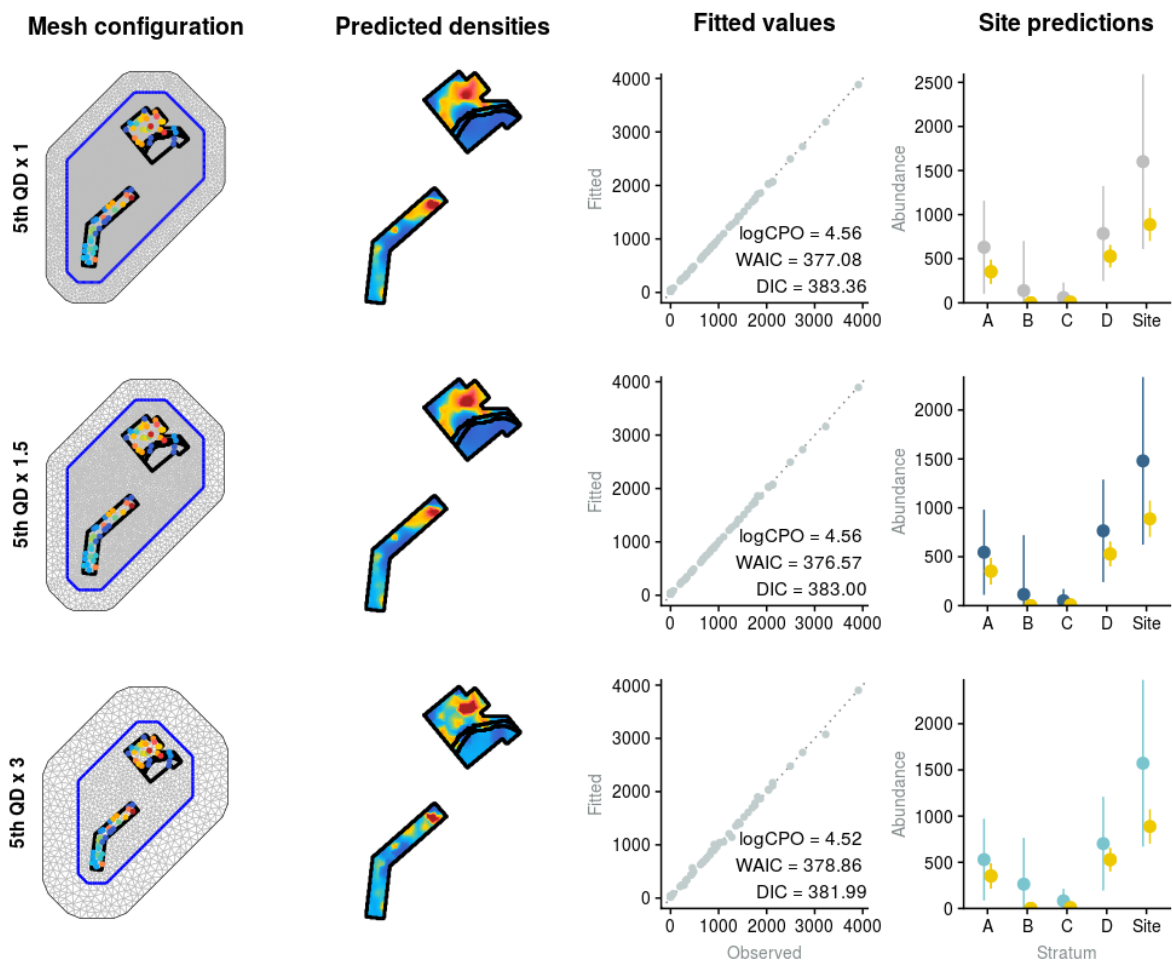


Figure A-21: Model fit and diagnostics for mesh scenarios (in rows) using a convex hull for Whangateau Harbour. First column: mesh configuration with the strata highlighted in black and inner mesh area highlighted in blue. Points denote observations for the site, with cockle density scaling from blue to red. Second column: predictions at the square-metre scale resulting from the model; colours scale from 0 to the 97.5th quantile predicted across all scenarios for the site, cells exceeding this threshold are shown in dark red, the colour scale is site-specific. Third column: comparison of observed (X) against predicted densities (Y) for each mesh scenario, with the value of performance metrics for the scenario included in the bottom-right corner (logCPO, conditional predictive ordinate; WAIC, Watanabe-Akaike information criterion; and DIC, Deviance Information Criteria). Fourth column: Stratum-specific and site-wide predictions of cockle abundance (million of individuals) for the mesh scenario, with the corresponding sampling-based estimator shown in yellow.

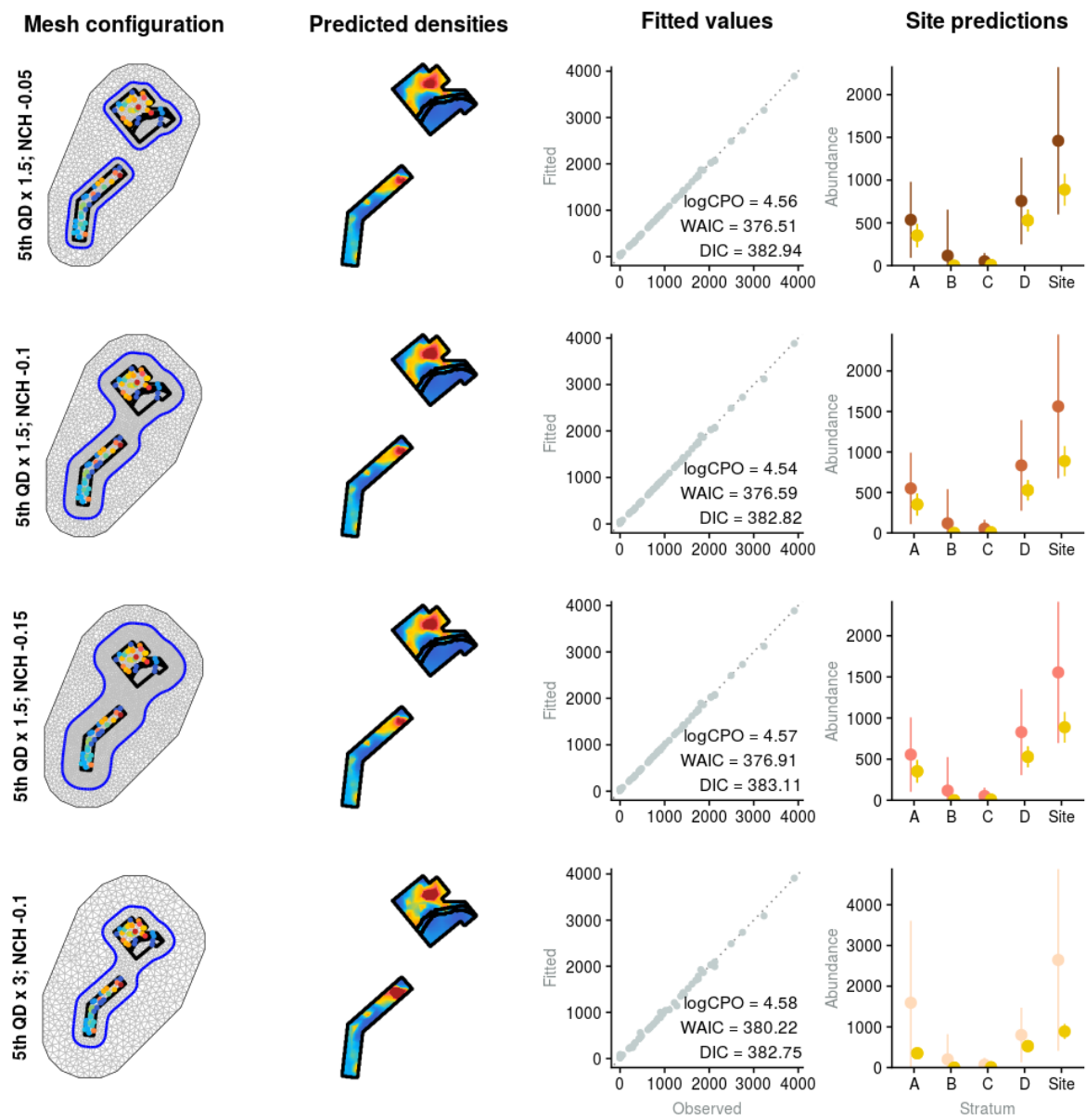


Figure A-22: Model fit and diagnostics for mesh scenarios (in rows) using a non-convex hull for Whangateau Harbour. First column: mesh configuration with the strata highlighted in black and inner mesh area highlighted in blue. Points denote observations for the site, with cockle density scaling from blue to red. Second column: predictions at the square-metre scale resulting from the model; colours scale from 0 to the 97.5th quantile predicted across all scenarios for the site, the colour scale is site-specific. Third column: comparison of observed (X) against predicted densities (Y) for each mesh scenario, with the value of performance metrics for the scenario included in the bottom-right corner (logCPO, conditional predictive ordinate; WAIC, Watanabe-Akaike information criterion; and DIC, Deviance Information Criteria). Fourth column: Stratum-specific and site-wide predictions of cockle abundance (million of individuals) for the mesh scenario, with the corresponding sampling-based estimator shown in yellow.

A.12 Whitianga Harbour

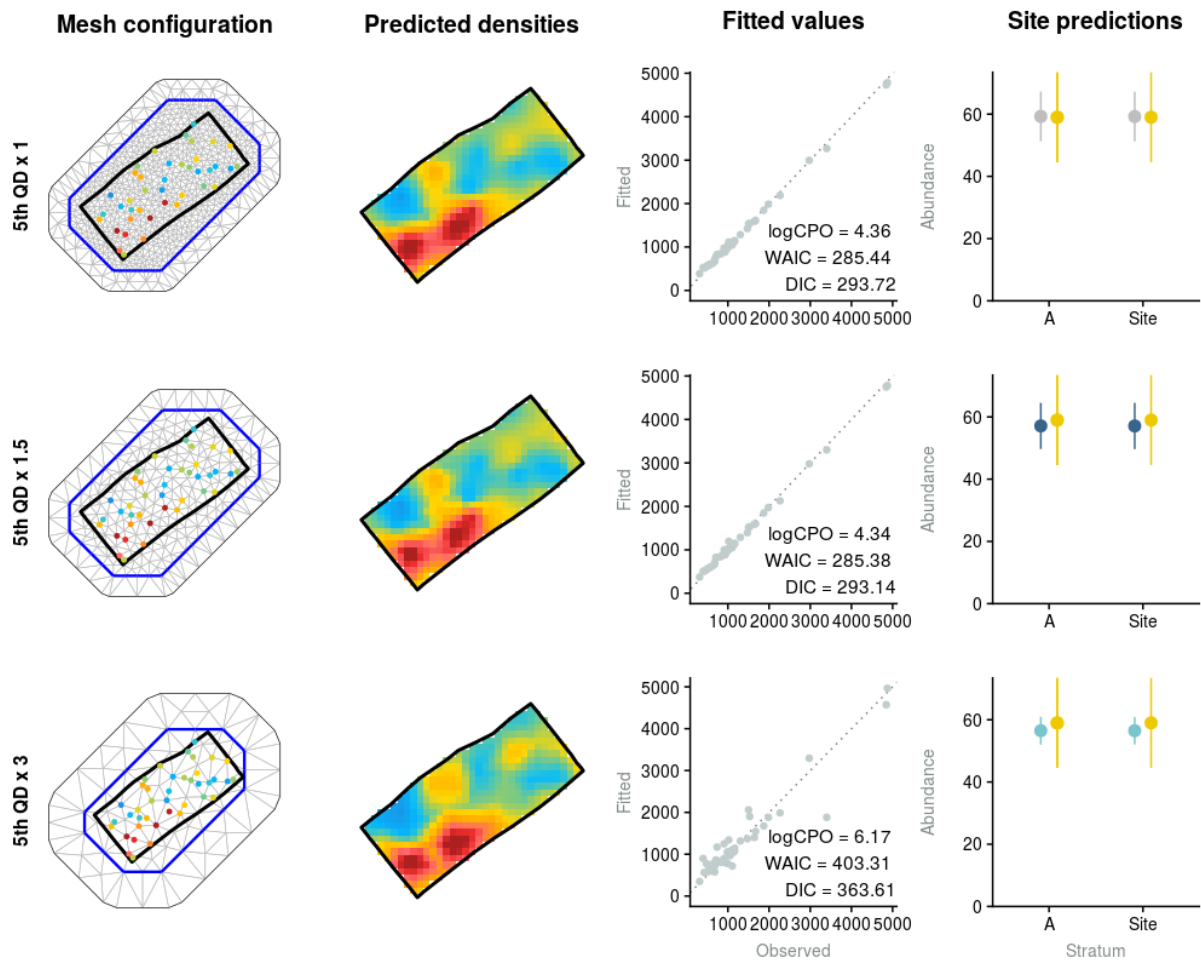


Figure A-23: Model fit and diagnostics for mesh scenarios (in rows) using a convex hull for Whitianga Harbour. First column: mesh configuration with the strata highlighted in black and inner mesh area highlighted in blue. Points denote observations for the site, with cockle density scaling from blue to red. Second column: predictions at the square-metre scale resulting from the model; colours scale from 0 to the 97.5th quantile predicted across all scenarios for the site, cells exceeding this threshold are shown in dark red, the colour scale is site-specific. Third column: comparison of observed (X) against predicted densities (Y) for each mesh scenario, with the value of performance metrics for the scenario included in the bottom-right corner (logCPO, conditional predictive ordinate; WAIC, Watanabe-Akaike information criterion; and DIC, Deviance Information Criteria). Fourth column: Stratum-specific and site-wide predictions of cockle abundance (million of individuals) for the mesh scenario, with the corresponding sampling-based estimator shown in yellow.

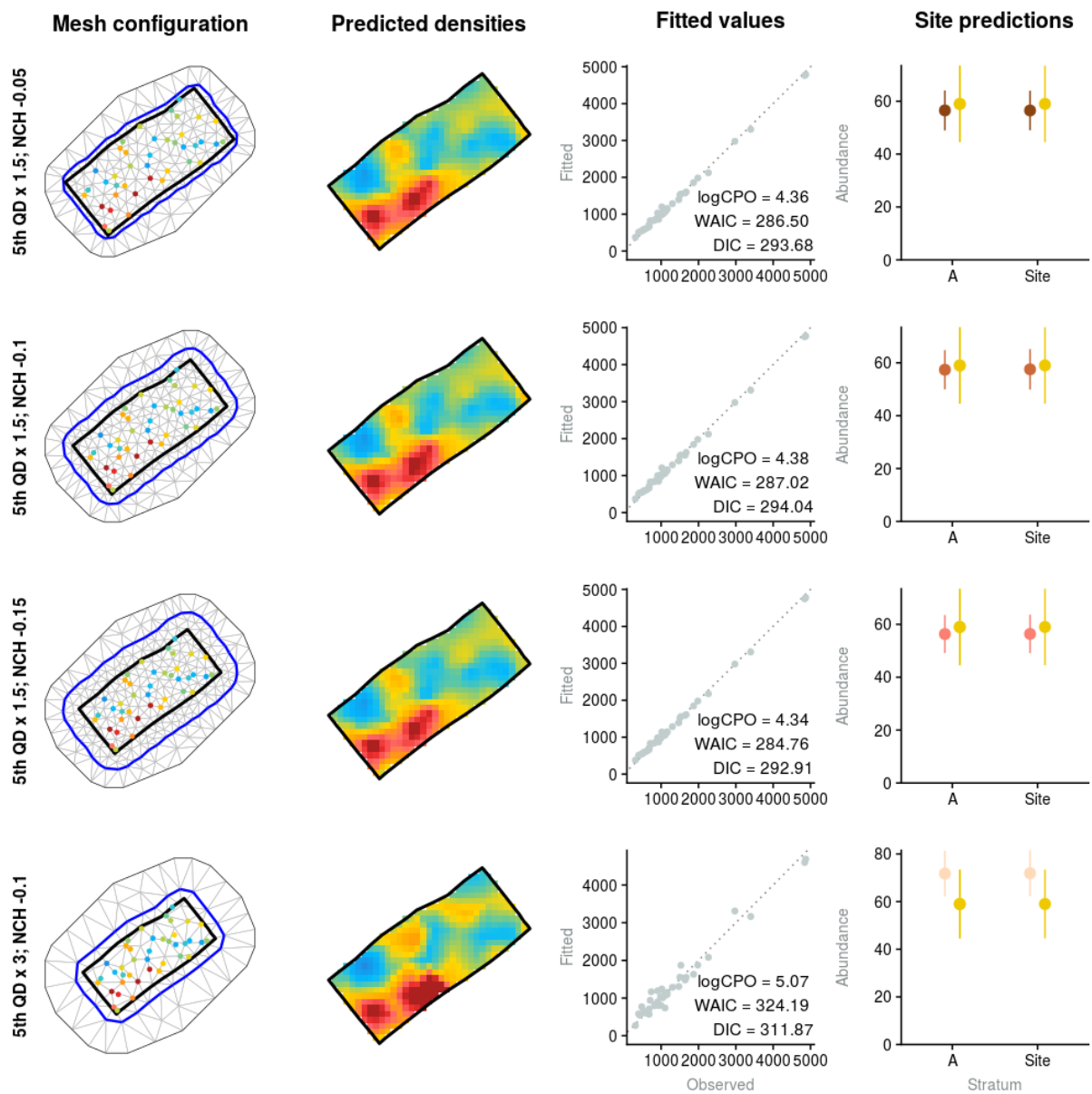


Figure A-24: Model fit and diagnostics for mesh scenarios (in rows) using a non-convex hull for Whitianga Harbour. First column: mesh configuration with the strata highlighted in black and inner mesh area highlighted in blue. Points denote observations for the site, with cockle density scaling from blue to red. Second column: predictions at the square-metre scale resulting from the model; colours scale from 0 to the 97.5th quantile predicted across all scenarios for the site, cells exceeding that threshold are shown in dark red, the colour scale is site-specific. Third column: comparison of observed (X) against predicted densities (Y) for each mesh scenario, with the value of performance metrics for the scenario included in the bottom-right corner (logCPO, conditional predictive ordinate; WAIC, Watanabe-Akaike information criterion; and DIC, Deviance Information Criteria). Fourth column: Stratum-specific and site-wide predictions of cockle abundance (million of individuals) for the mesh scenario, with the corresponding sampling-based estimator shown in yellow.

APPENDIX B: SPATIO-TEMPORAL MODELS

B.1 Bowentown Beach

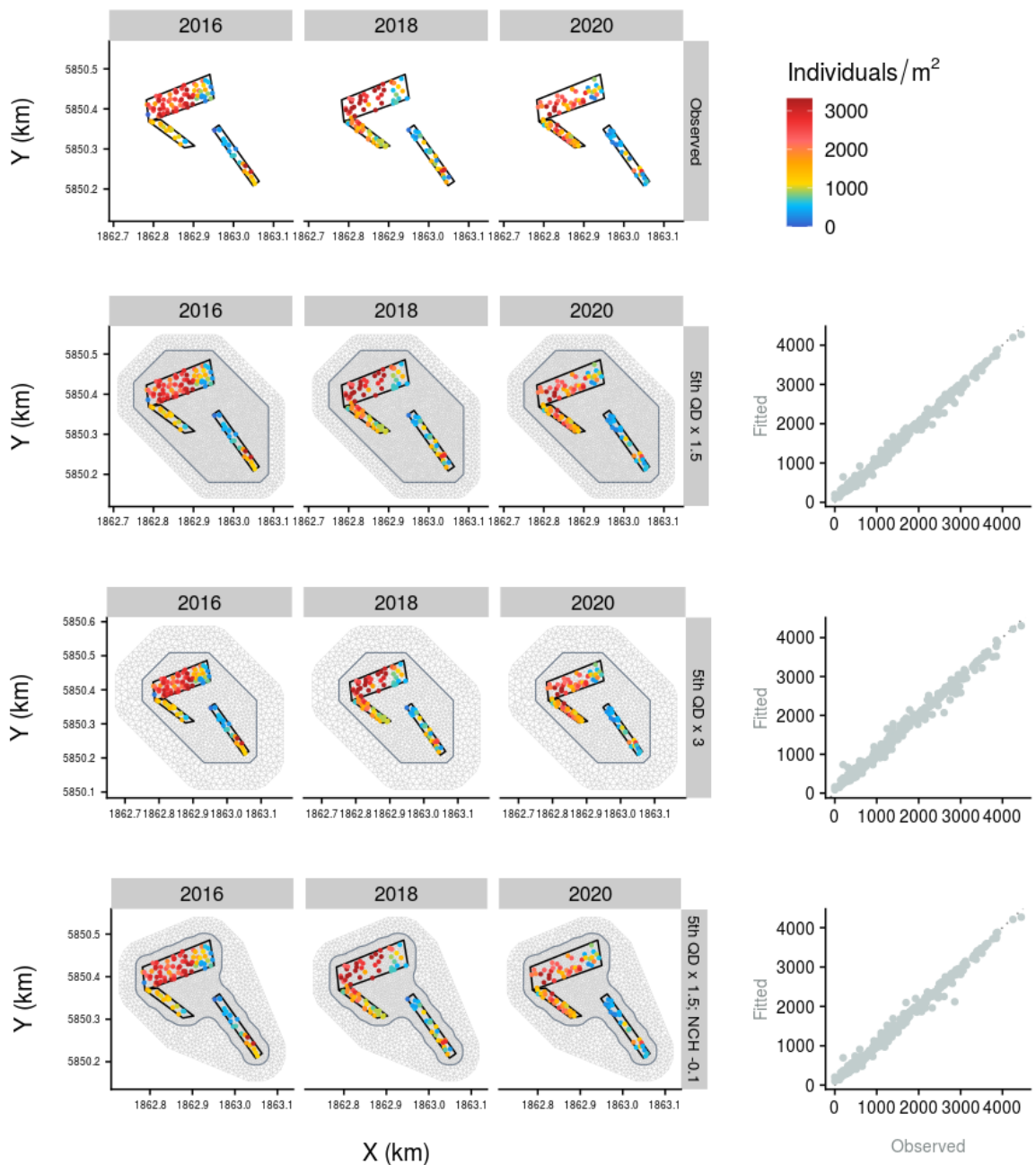


Figure B-1: Comparison of observed (top row) and predicted (rows 2 to 4) densities from blue to dark red for the spatio-temporal model of cockle abundance for Bowentown Beach across different mesh configurations. Mesh structure is shown in grey, inner mesh region in blue and strata are highlighted in black. Colours scale from 0 (blue) to the 97.5th quantile predicted across all spatial scenarios for the site, cells exceeding that threshold are shown in dark red; the colour scale is site-specific. The right-most column compares the fitted against observed values for each observation.

B.2 Cockle Bay

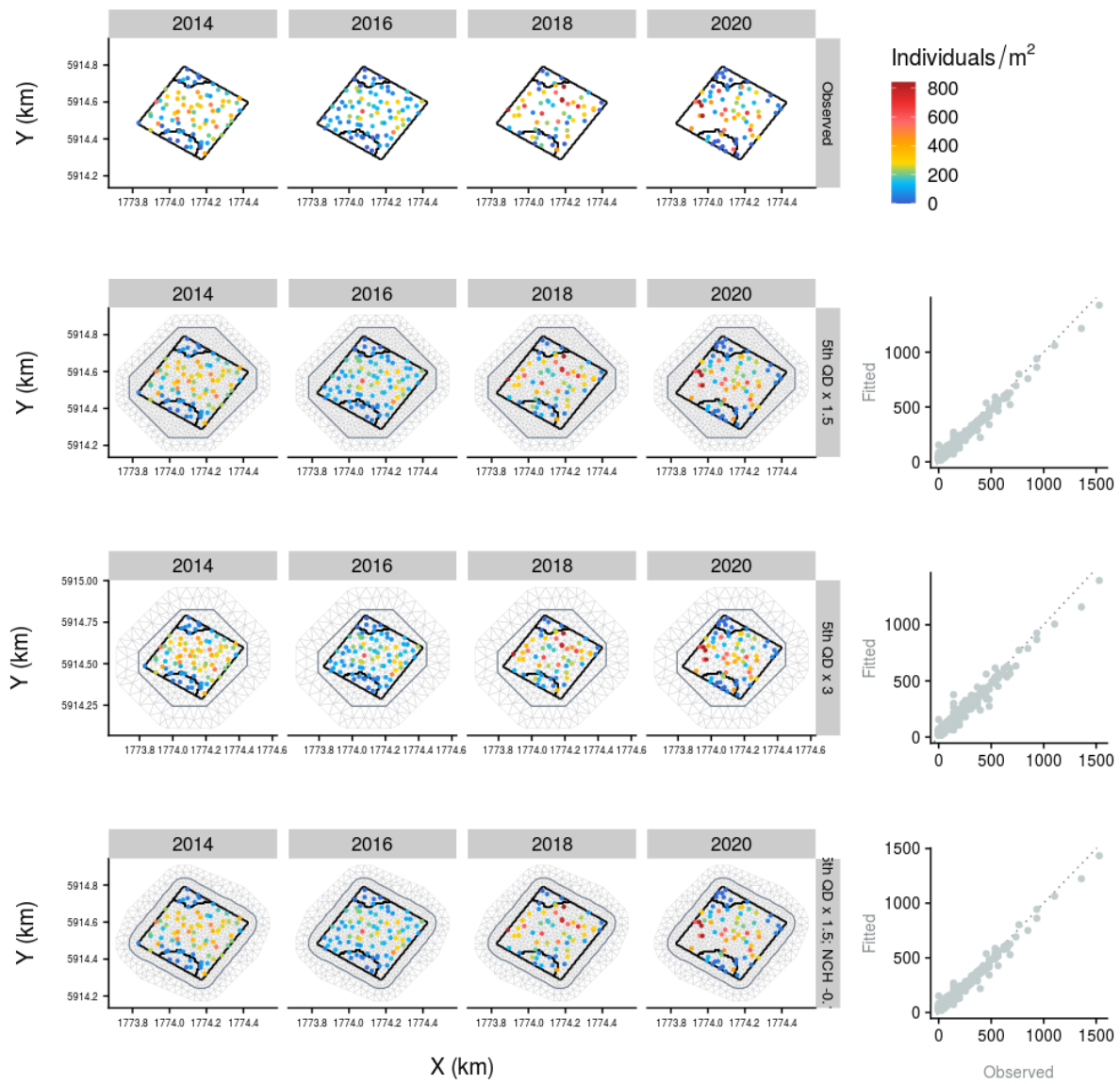


Figure B-2: Comparison of observed (top row) and predicted (rows 2 to 4) densities from blue to dark red for the spatio-temporal model of cockle abundance for Cockle Bay across different mesh configurations. Mesh structure is shown in grey, inner mesh region in blue and strata are highlighted in black. Colours scale from 0 (blue) to the 97.5th quantile predicted across all spatial scenarios for the site, cells exceeding that threshold are shown in dark red; the colour scale is site-specific. The right-most column compares the fitted against observed values for each observation.

B.3 Eastern Beach

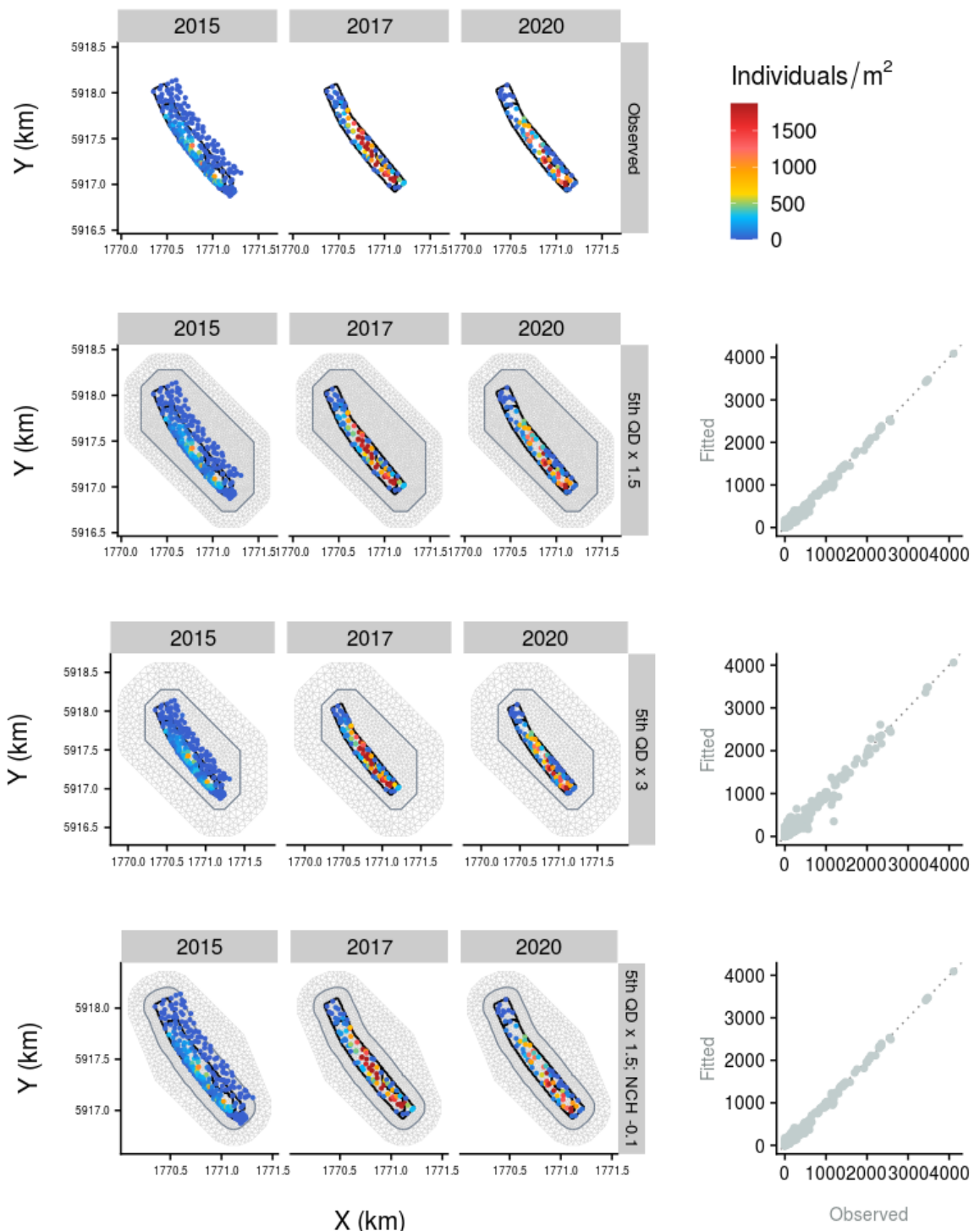


Figure B-3: Comparison of observed (top row) and predicted (rows 2 to 4) densities from blue to dark red for the spatio-temporal model of cockle abundance for Eastern Beach across different mesh configurations. Mesh structure is shown in grey, inner mesh region in blue and strata are highlighted in black. Colours scale from 0 (blue) to the 97.5th quantile predicted across all spatial scenarios for the site, cells exceeding that threshold are shown in dark red; the colour scale is site-specific. The right-most column compares the fitted against observed values for each observation.

B.4 Grahams Beach

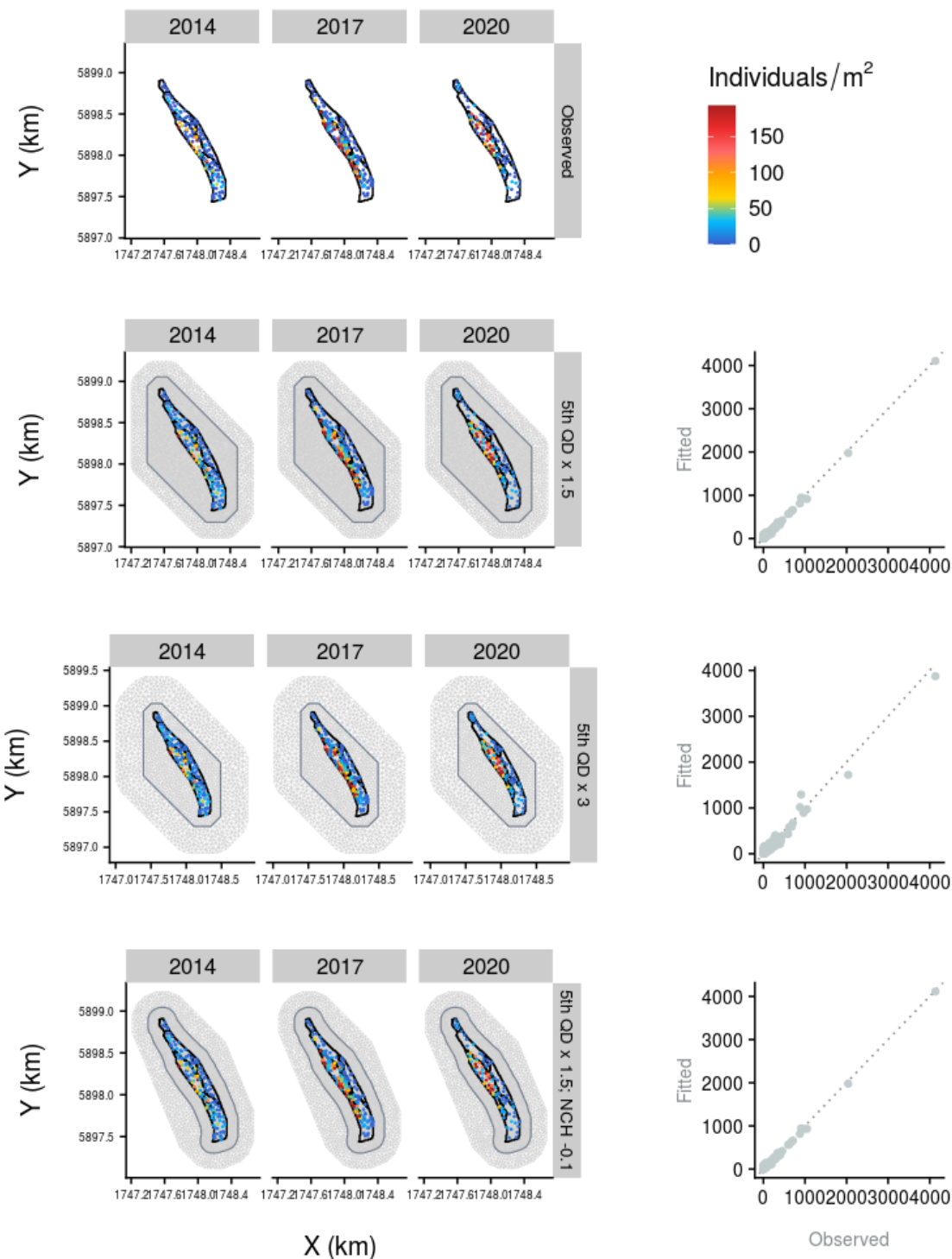


Figure B-4: Comparison of observed (top row) and predicted (rows 2 to 4) densities from blue to dark red for the spatio-temporal model of cockle abundance for Grahams Beach across different mesh configurations. Mesh structure is shown in grey, inner mesh region in blue and strata are highlighted in black. Colours scale from 0 (blue) to the 97.5th quantile predicted across all spatial scenarios for the site, cells exceeding that threshold are shown in dark red; the colour scale is site-specific. The right-most column compares the fitted against observed values for each observation.

B.5 Little Waihi Estuary

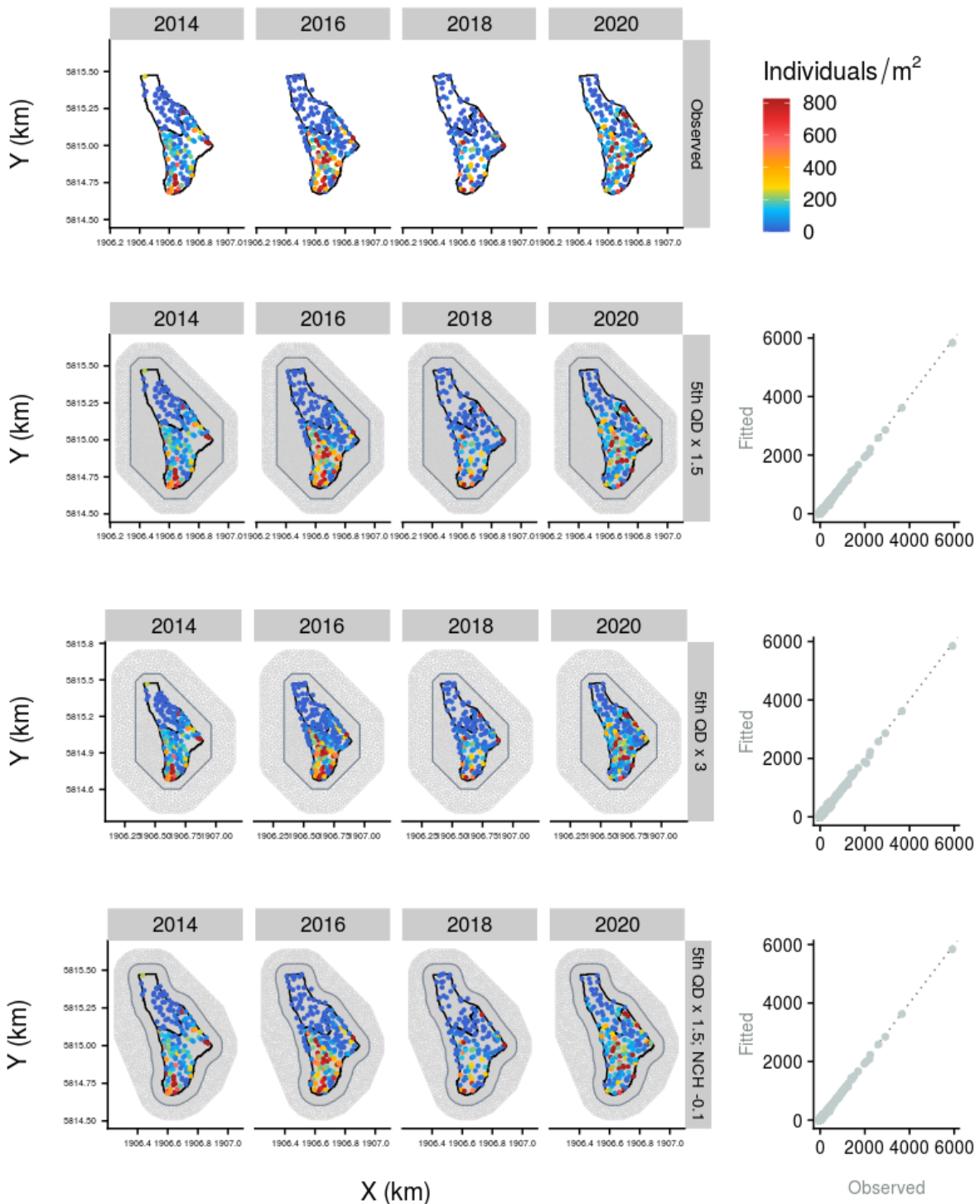


Figure B-5: Comparison of observed (top row) and predicted (rows 2 to 4) densities from blue to dark red for the spatio-temporal model of cockle abundance for Little Waihi Estuary across different mesh configurations. Mesh structure is shown in grey, inner mesh region in blue and strata are highlighted in black. Colours scale from 0 (blue) to the 97.5th quantile predicted across all spatial scenarios for the site, cells exceeding that threshold are shown in dark red; the colour scale is site-specific. The right-most column compares the fitted against observed values for each observation.

B.6 Pataua Estuary

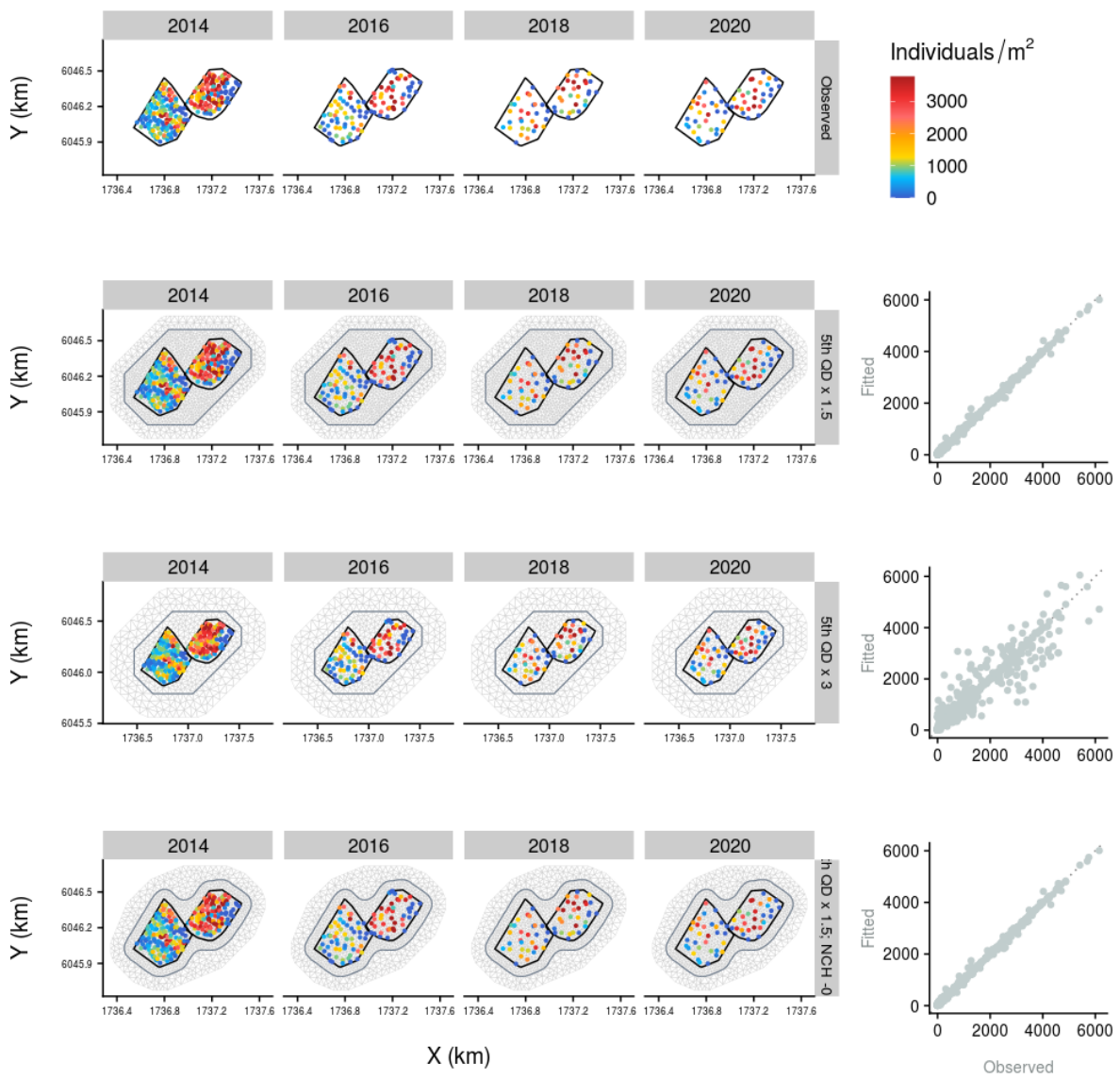


Figure B-6: Comparison of observed (top row) and predicted (rows 2 to 4) densities from blue to dark red for the spatio-temporal model of cockle abundance for Pataua Estuary across different mesh configurations. Mesh structure is shown in grey, inner mesh region in blue and strata are highlighted in black. Colours scale from 0 (blue) to the 97.5th quantile predicted across all spatial scenarios for the site, cells exceeding that threshold are shown in dark red; the colour scale is site-specific. The right-most column compares the fitted against observed values for each observation.

B.7 Raglan Harbour

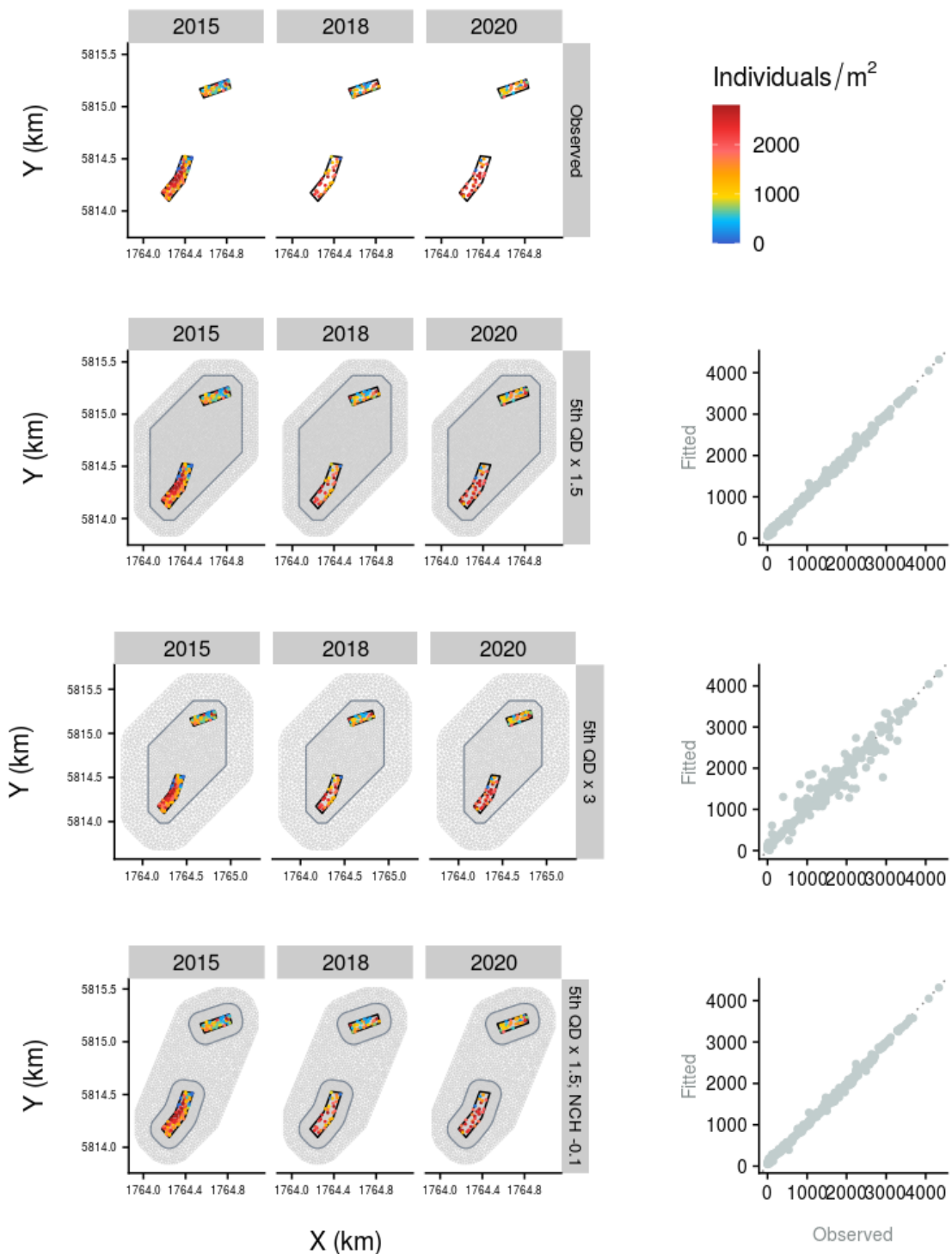


Figure B-7: Comparison of observed (top row) and predicted (rows 2 to 4) densities from blue to dark red for the spatio-temporal model of cockle abundance for Raglan Harbour across different mesh configurations. Mesh structure is shown in grey, inner mesh region in blue and strata are highlighted in black. Colours scale from 0 (blue) to the 97.5th quantile predicted across all spatial scenarios for the site, cells exceeding that threshold are shown in dark red; the colour scale is site-specific. The right-most column compares the fitted against observed values for each observation.

B.8 Tairua Harbour

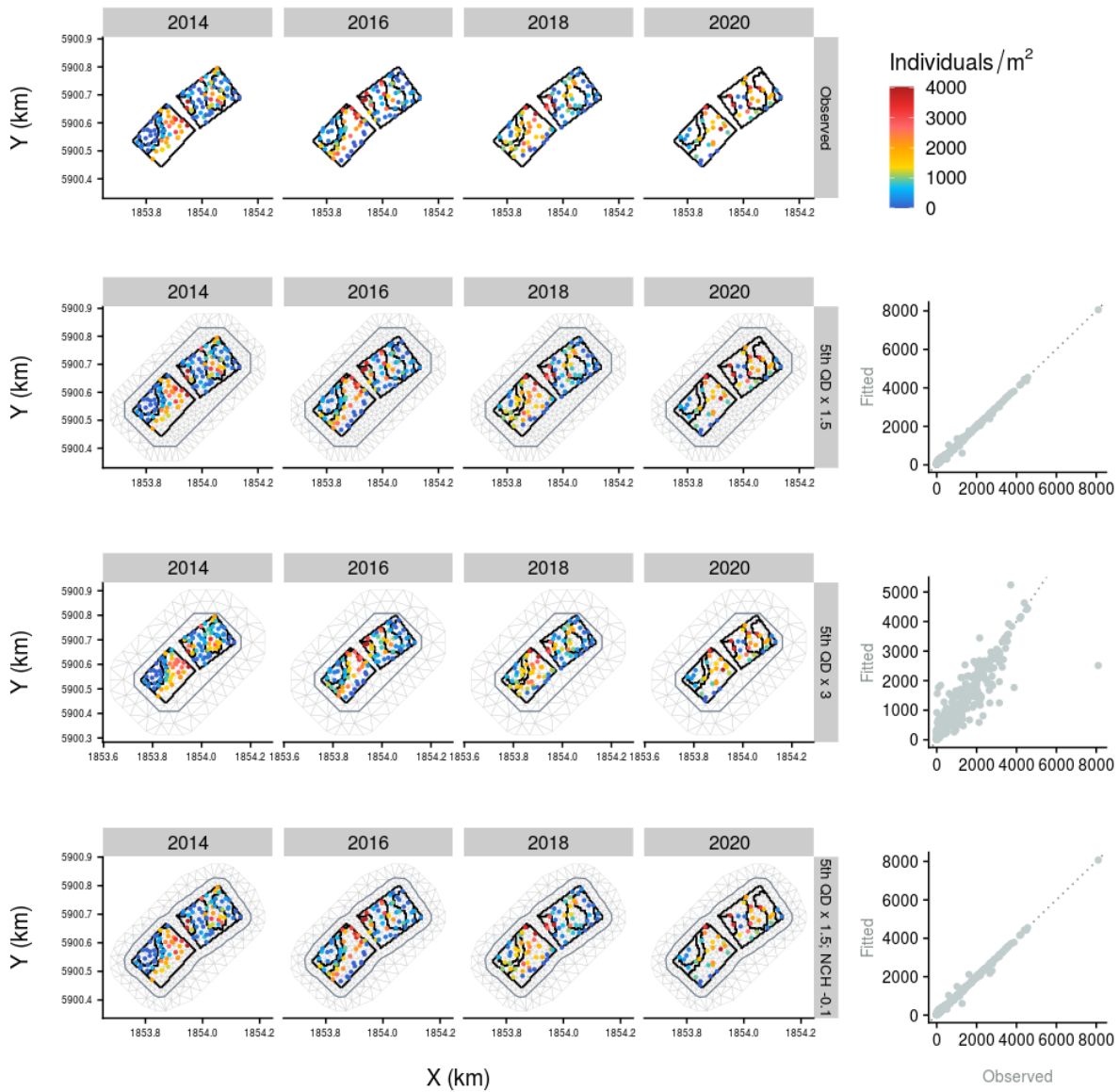


Figure B-8: Comparison of observed (top row) and predicted (rows 2 to 4) densities from blue to dark red for the spatio-temporal model of cockle abundance for Tairua Harbour across different mesh configurations. Mesh structure is shown in grey, inner mesh region in blue and strata are highlighted in black. Colours scale from 0 (blue) to the 97.5th quantile predicted across all spatial scenarios for the site, cells exceeding that threshold are shown in dark red; the colour scale is site-specific. The right-most column compares the fitted against observed values for each observation.

B.9 Umupuia Beach

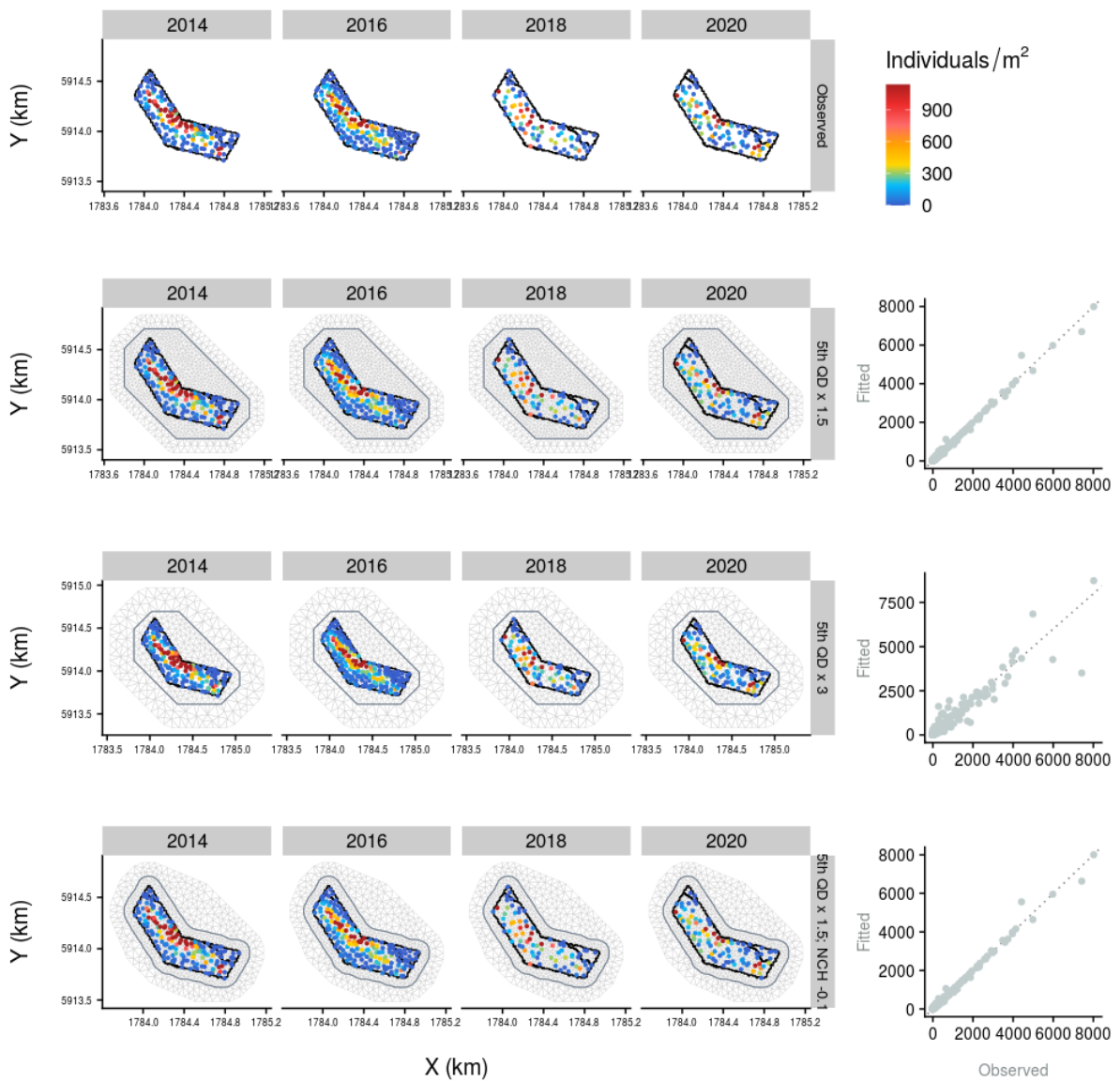


Figure B-9: Comparison of observed (top row) and predicted (rows 2 to 4) densities from blue to dark red for the spatio-temporal model of cockle abundance for Umupuia Beach across different mesh configurations. Mesh structure is shown in grey, inner mesh region in blue and strata are highlighted in black. Colours scale from 0 (blue) to the 97.5th quantile predicted across all spatial scenarios for the site, cells exceeding that threshold are shown in dark red; the colour scale is site-specific. The right-most column compares the fitted against observed values for each observation.

B.10 Waiotahi Estuary

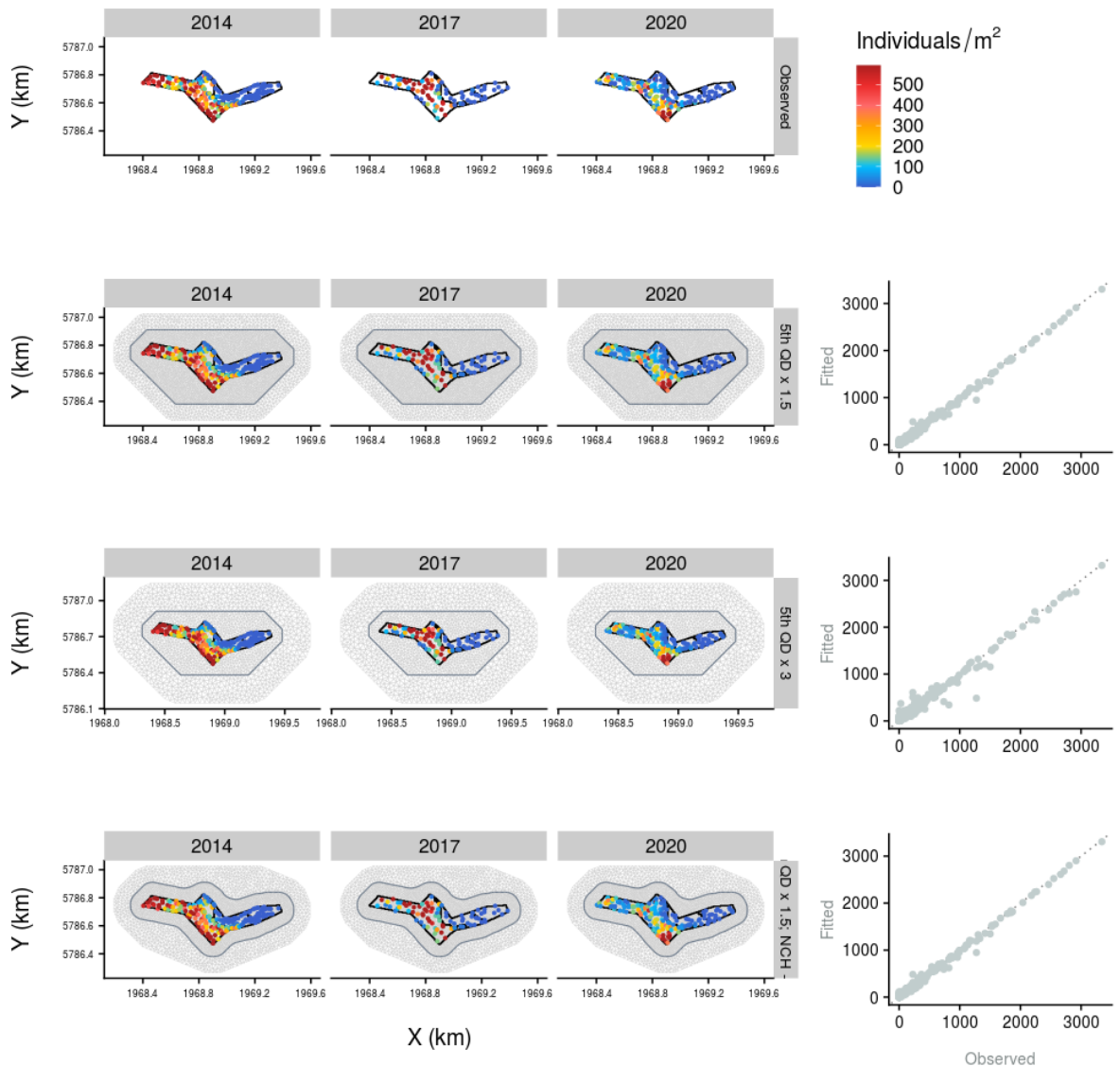


Figure B-10: Comparison of observed (top row) and predicted (rows 2 to 4) densities from blue to dark red for the spatio-temporal model of cockle abundance for Waiotahi Estuary across different mesh configurations. Mesh structure is shown in grey, inner mesh region in blue and strata are highlighted in black. Colours scale from 0 (blue) to the 97.5th quantile predicted across all spatial scenarios for the site, cells exceeding that threshold are shown in dark red; the colour scale is site-specific. The right-most column compares the fitted against observed values for each observation.

B.11 Whangateau Harbour

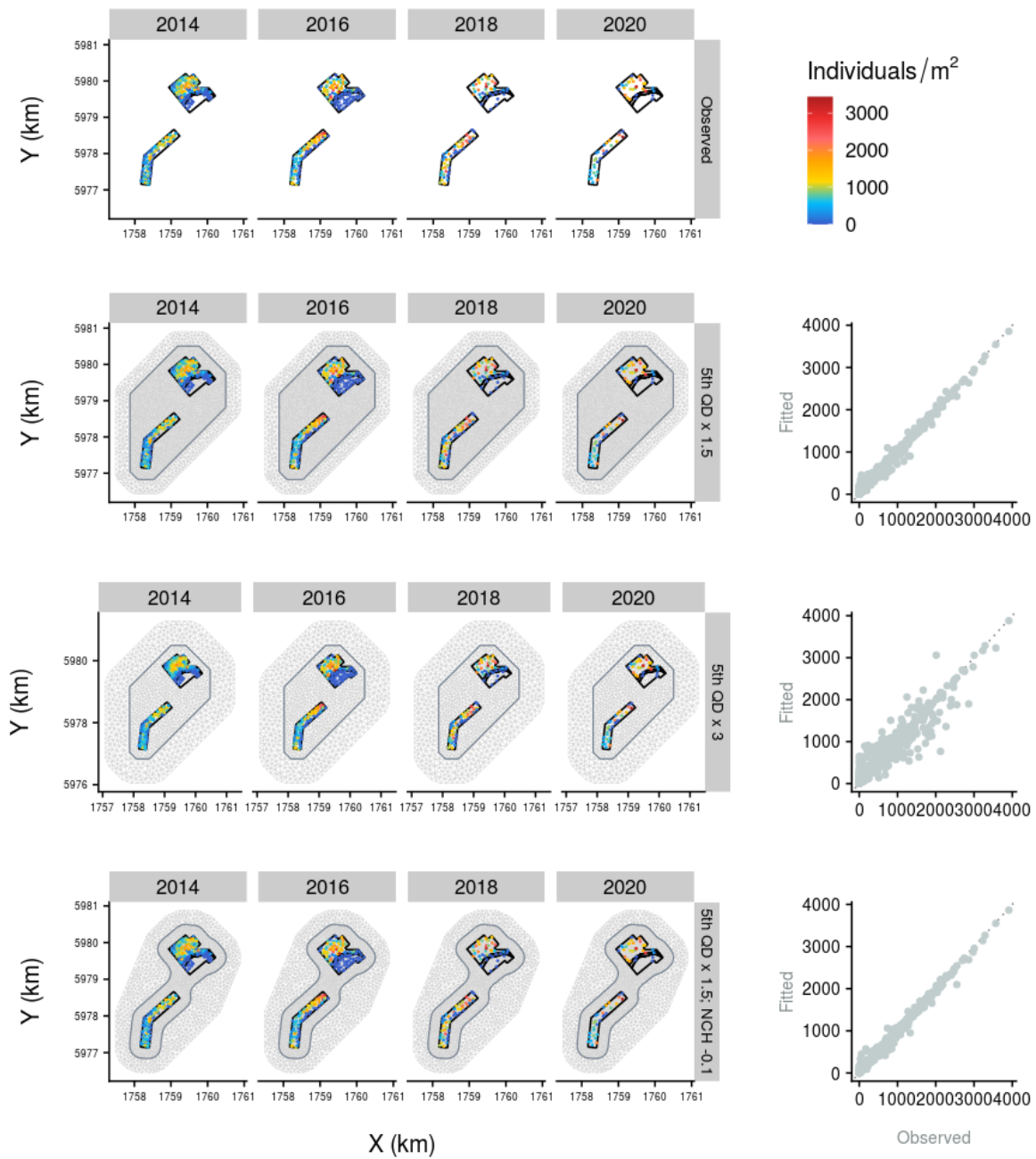


Figure B-11: Comparison of observed (top row) and predicted (rows 2 to 4) densities from blue to dark red for the spatio-temporal model of cockle abundance for Whangateau Harbour across different mesh configurations. Mesh structure is shown in grey, inner mesh region in blue and strata are highlighted in black. Colours scale from 0 (blue) to the 97.5th quantile predicted across all spatial scenarios for the site, cells exceeding that threshold are shown in dark red; the colour scale is site-specific. The right-most column compares the fitted against observed values for each observation.

B.12 Whitianga Harbour

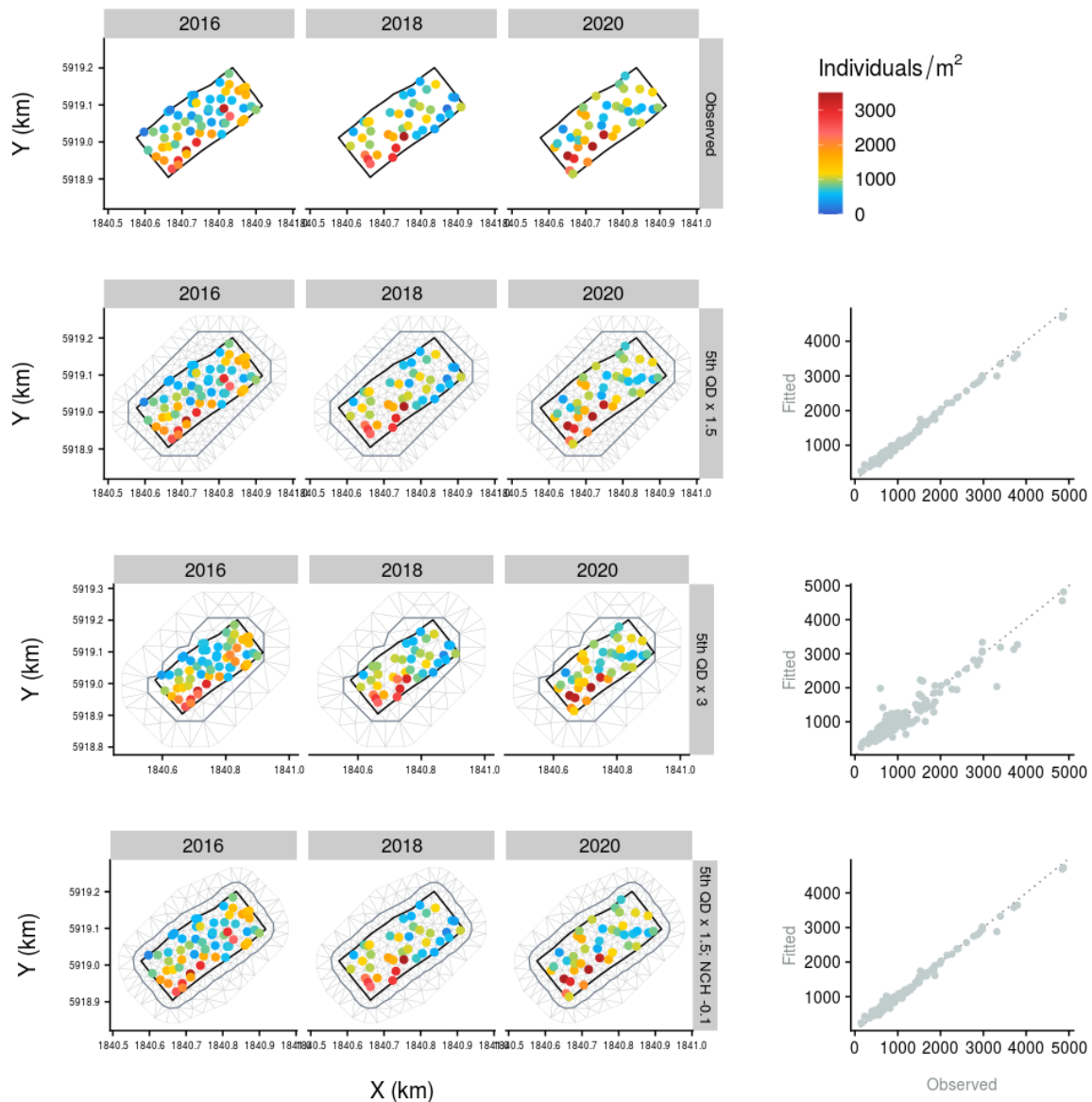


Figure B-12: Comparison of observed (top row) and predicted (rows 2 to 4) densities from blue to dark red for the spatio-temporal model of cockle abundance for Whitianga Harbour across different mesh configurations. Mesh structure is shown in grey, inner mesh region in blue and strata are highlighted in black. Colours scale from 0 (blue) to the 97.5th quantile predicted across all spatial scenarios for the site, cells exceeding that threshold are shown in dark red; the colour scale is site-specific. The right-most column compares the fitted against observed values for each observation.

APPENDIX C: SPLIT MODELS BY SITE

C.1 Bowentown Beach

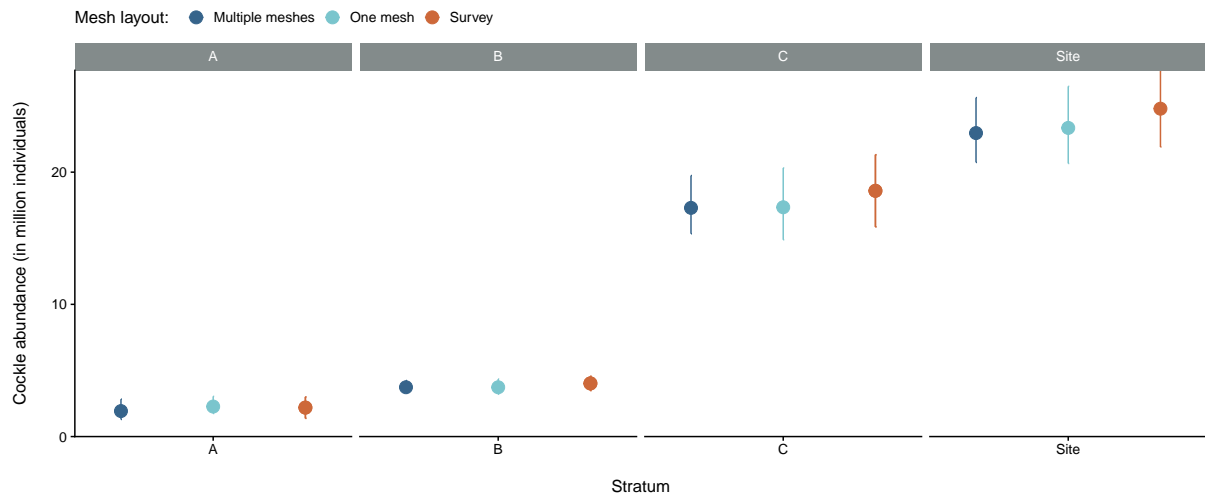


Figure C-1: Comparison of stratum-specific and site-wide predictions of cockle abundance (mean and 95% confidence interval) under different approaches to defining the mesh across distanced strata for Bowentown Beach (blue shades), against the corresponding estimate from the sampling-based estimator (orange). The dark blue point denotes the “multiple mesh” approach whereby separate models were developed for distanced strata within the site, whereas the light blue point denotes the default approach of using a single model to fit all strata within the site.

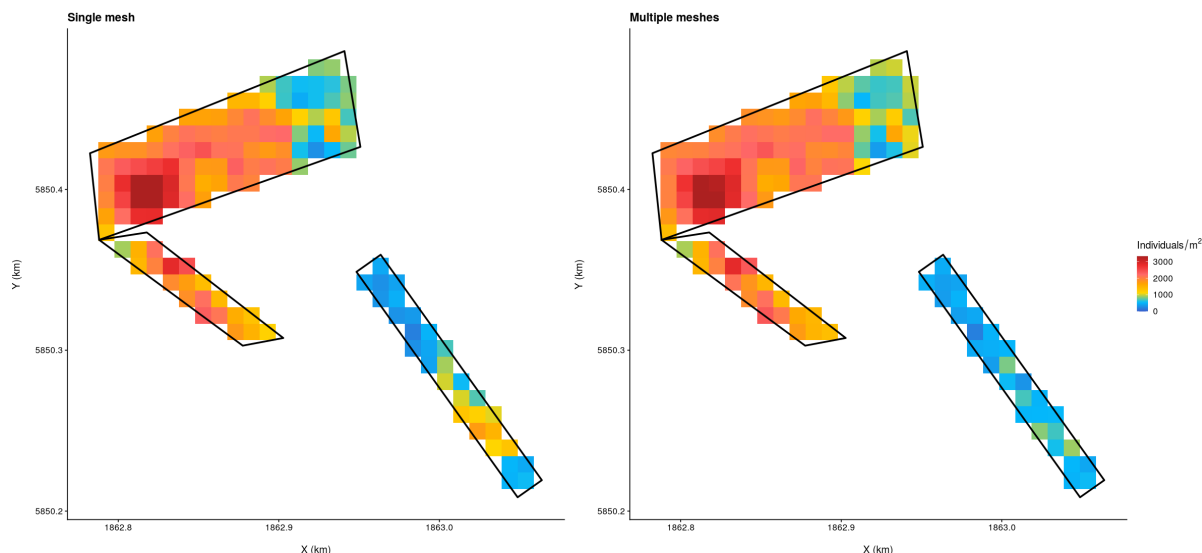


Figure C-2: Comparison of predictions of cockle density at the square-metre scale for Bowentown Beach, using the single-mesh approach (left) and the multiple-mesh approach (right); mesh scenarios for both use a convex hull with $1.5 \times 5^{\text{th}}$ quantile distance between nearest observations. Colours scale from 0 (blue) to the 97.5th quantile predicted across all spatial scenarios for the site, cells exceeding that threshold are shown in dark red.

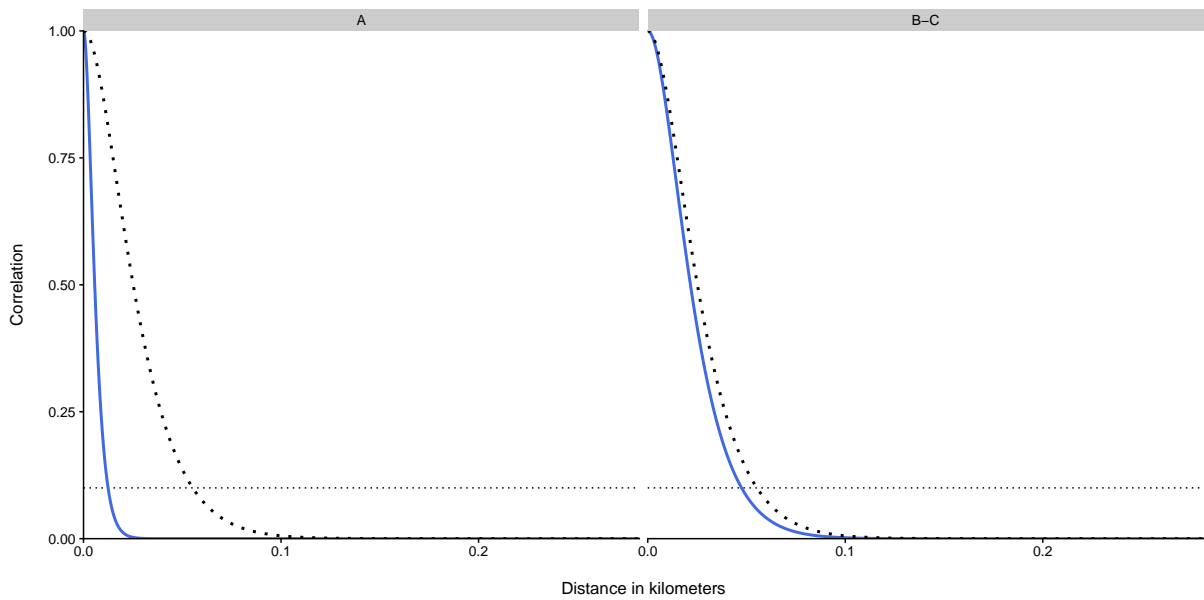


Figure C-3: Comparison of the Matérn covariance relationship estimated for each group of strata at Bowentown Beach under the multiple-mesh approach, with the single Matérn covariance relationship estimated under the single-model approach across all strata shown with a dotted line.

C.2 Raglan Harbour

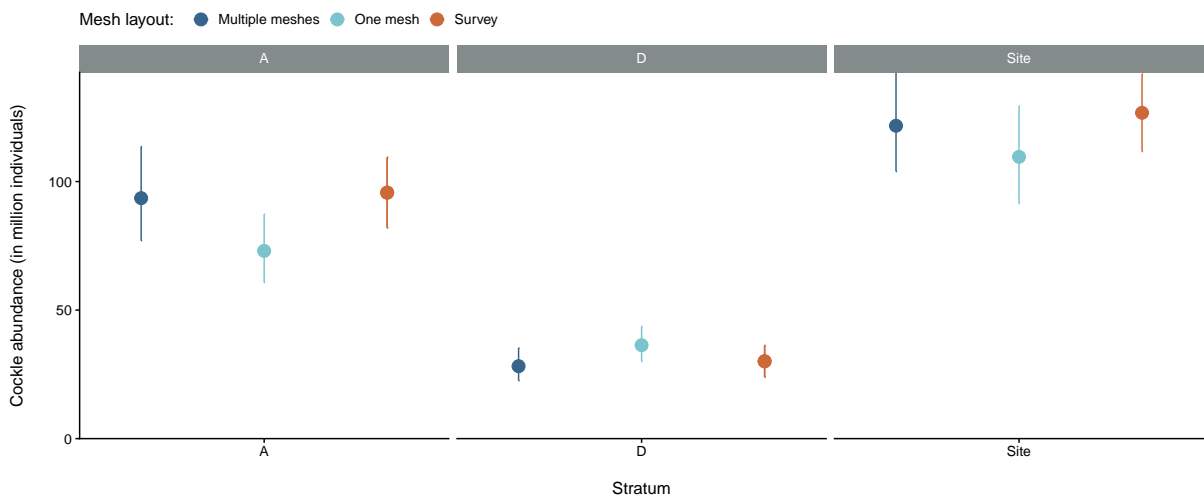


Figure C-4: Comparison of stratum-specific and site-wide predictions of cockle abundance (mean and 95% confidence interval) under different approaches to defining the mesh across distanced strata for Raglan Harbour (blue shades), against the corresponding estimate from the sampling-based estimator (orange). The dark blue point denotes the “multiple mesh” approach whereby separate models were developed for distanced strata within the site, whereas the light blue point denotes the default approach of using a single model to fit all strata within the site.

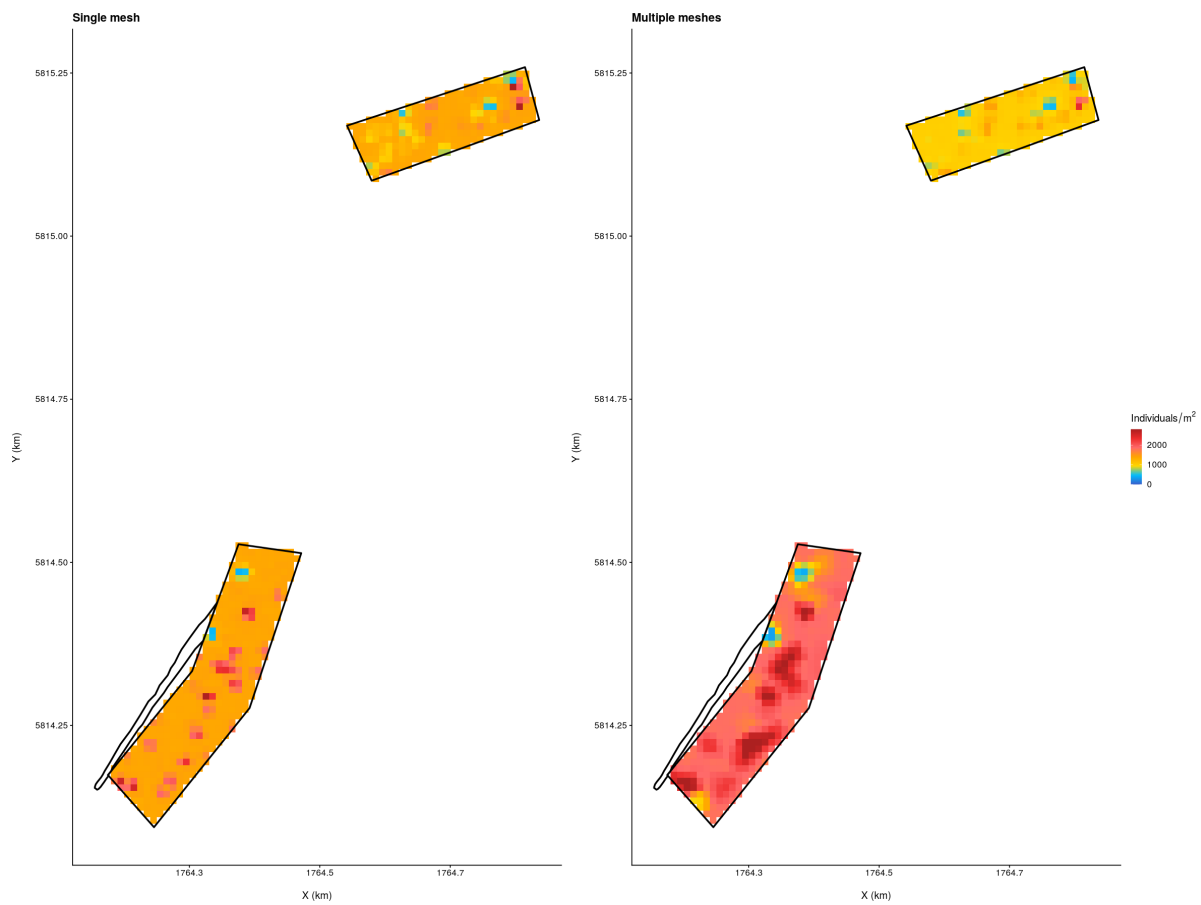


Figure C-5: Comparison of predictions of cockle density at the square-metre scale for Raglan Harbour, using the single-mesh approach (left) and the multiple-mesh approach (right); mesh scenarios for both use a convex hull with $1.5 \times 5^{\text{th}}$ quantile distance between nearest observations. Colours scale from 0 (blue) to the 97.5th quantile predicted across all spatial scenarios for the site, cells exceeding that threshold are shown in dark red.

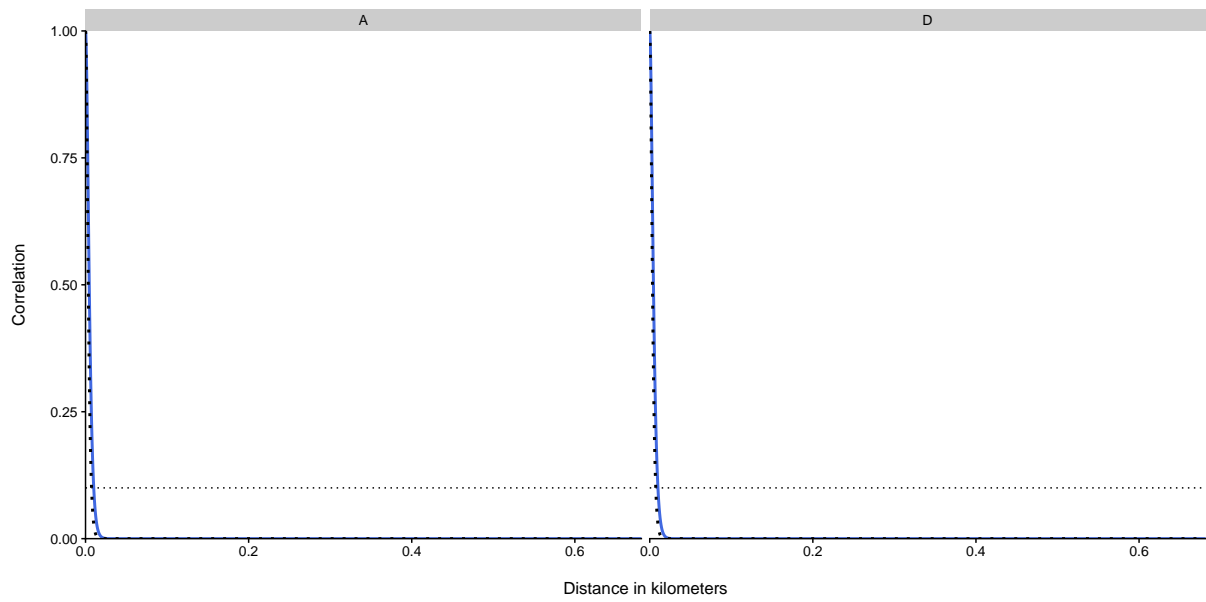


Figure C-6: Comparison of the Matérn covariance relationship estimated for each group of strata at Raglan Harbour under the multiple-mesh approach, with the single Matérn covariance relationship estimated under the single-model approach across all strata shown with a dotted line.

C.3 Whangateau Harbour

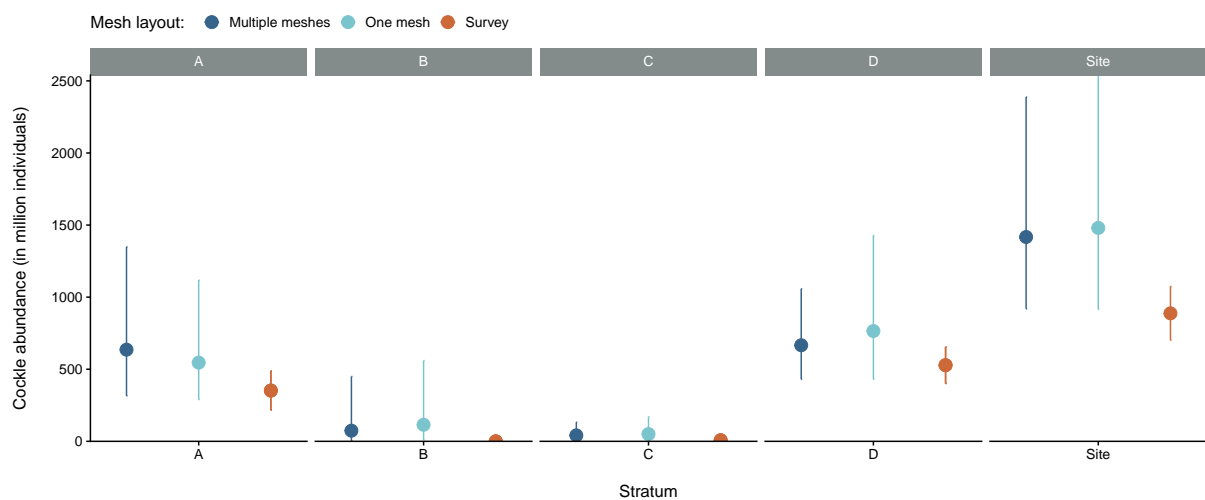


Figure C-7: Comparison of stratum-specific and site-wide predictions of cockle abundance (mean and 95% confidence interval) under different approaches to defining the mesh across distanced strata for Whangateau Harbour (blue shades), against the corresponding estimate from the sampling-based estimator (orange). The dark blue point denotes the “multiple mesh” approach whereby separate models were developed for distanced strata within the site, whereas the light blue point denotes the default approach of using a single model to fit all strata within the site.

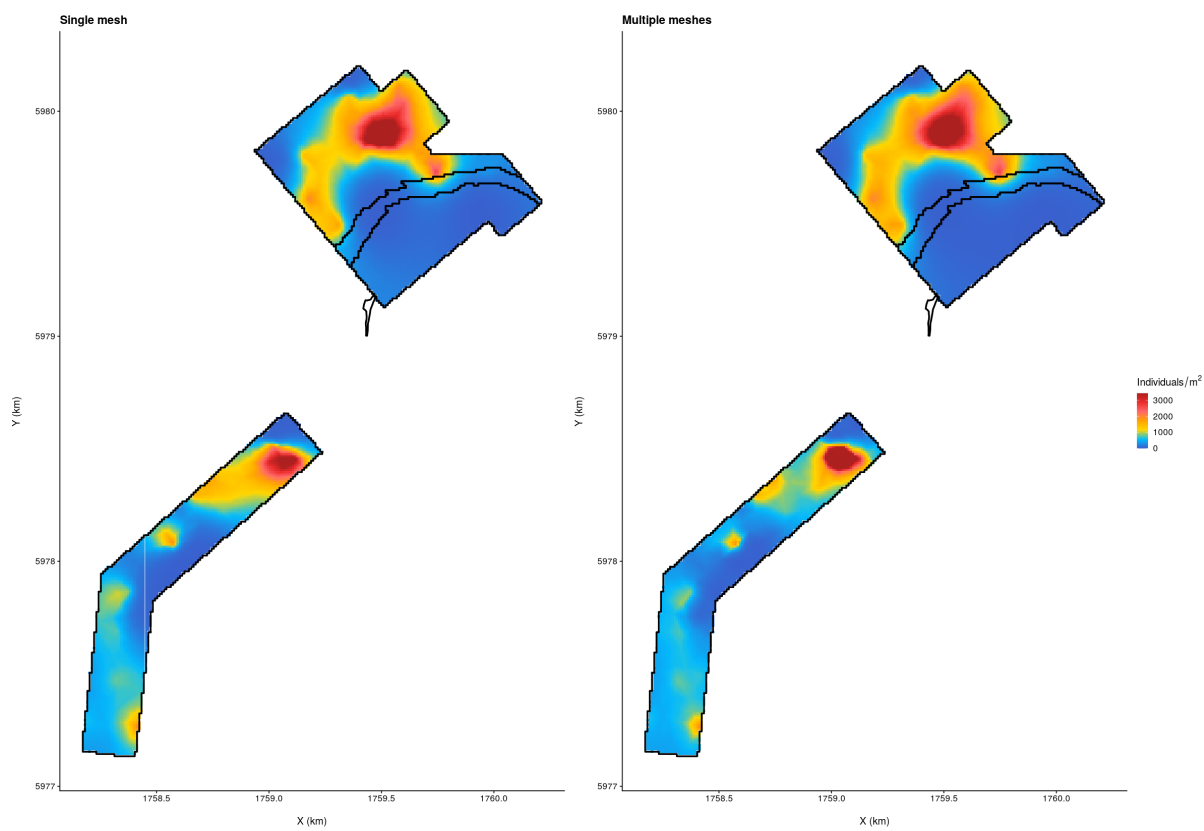


Figure C-8: Comparison of predictions of cockle density at the square-metre scale for Whangateau Harbour, using the single-mesh approach (left) and the multiple-mesh approach (right); mesh scenarios for both use a convex hull with $1.5 \times 5^{\text{th}}$ quantile distance between nearest observations. Colours scale from 0 (blue) to the 97.5th quantile predicted across all spatial scenarios for the site, cells exceeding that threshold are shown in dark red.

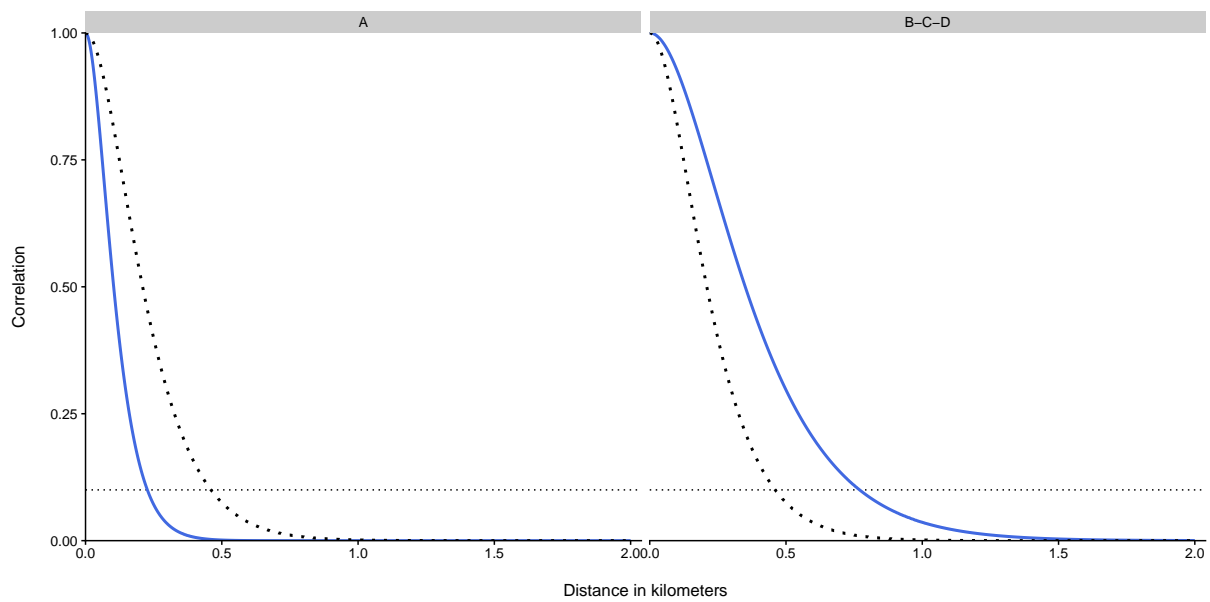


Figure C-9: Comparison of the Matérn covariance relationship estimated for each group of strata at Whangateau Harbour under the multiple-mesh approach, with the single Matérn covariance relationship estimated under the single-model approach across all strata shown with a dotted line.